

# Theory and simulations of singly resonant optical parametric oscillators

---

Domenico Cuozzo

A thesis submitted for the degree of  
Doctor of Philosophy

Computational Non Linear and Quantum Optics Group  
Department of Physics  
University of Strathclyde  
Glasgow

2014

## Declaration

This thesis is the result of the author's original research. It has been composed by the author and has not been previously submitted for examination which has led to the award of a degree.

The copyright of this thesis belongs to the author under the terms of the United Kingdom Copyright Acts as qualified by University of Strathclyde Regulation 3.50. Due acknowledgement must always be made of the use of any material contained in, or derived from, this thesis.

Domenico Cuzzo

August 24, 2014

# Contents

<b>1</b>	<b>Introduction</b>	<b>1</b>
1.1	Parametric down-conversion and optical parametric oscillators . . . . .	1
1.2	Squeezed states of light in OPOs . . . . .	2
1.3	Pulsed OPOs . . . . .	3
1.4	Transverse pattern formation, cavity solitons, optical turbulence . . . . .	3
1.5	Outline of the thesis . . . . .	4
<b>2</b>	<b>Squeezed States of Light and the Parametric Amplifier</b>	<b>10</b>
2.1	Introduction to Nonlinear Optics . . . . .	10
2.1.1	Linear Response . . . . .	10
2.1.2	Nonlinear Response . . . . .	11
2.2	Definition of Squeezed States of Light . . . . .	12
2.2.1	Quantum nature of the squeezed state . . . . .	14
2.3	Single Mode Quadrature Squeezed States . . . . .	15
2.3.1	Squeezing for a two-photon coherent state . . . . .	17
2.3.2	Ideal squeezed states or displaced squeezed states . . . . .	18
2.4	Two-Mode Quadrature Squeezed States . . . . .	20
2.5	Quantum Entanglement . . . . .	21
2.5.1	Bipartite separability . . . . .	23
2.5.2	Separability criterion for mixed states . . . . .	25
2.5.3	Separability criterion for continuous variables. . . . .	25
2.6	Introduction to Parametric Amplifiers . . . . .	26
2.6.1	Degenerate Parametric Amplifier . . . . .	27
2.6.2	Non Degenerate Parametric Amplifier . . . . .	30
2.7	Conclusions . . . . .	31
<b>3</b>	<b>Measuring Squeezing in Optical Parametric Oscillators</b>	<b>33</b>
3.1	Introduction to Optical Parametric Oscillators . . . . .	33
3.2	Photo-Electric Detection of Squeezed Light . . . . .	34
3.2.1	Ordinary Homodyne Detection . . . . .	35
3.2.2	Balanced Homodyne Detection . . . . .	37
3.3	Input-Output Formulation of Optical Cavities . . . . .	38

3.4	Heisenberg-Langevin Treatment for a TROPO . . . . .	42
3.4.1	The Below-Threshold Degenerate Case . . . . .	43
3.4.2	The Below-Threshold Non-Degenerate Case . . . . .	44
3.5	Master Equation Approach to Optical Cavities . . . . .	46
3.5.1	Master Equation Approach for a TROPO . . . . .	46
3.6	Conclusions . . . . .	49
<b>4</b>	<b>Squeezing and Quantum Entanglement in a SROPO Below Threshold</b>	<b>51</b>
4.1	Introduction . . . . .	51
4.2	The Langevin Equation . . . . .	52
4.3	Two-Time Correlation Functions . . . . .	55
4.4	Intensity Difference Correlation . . . . .	58
4.5	Quadrature Correlations . . . . .	62
4.6	Quantum Entanglement in SROPO . . . . .	67
4.7	Numerical Results for Intensity Difference Spectra . . . . .	67
4.8	Conclusions . . . . .	70
<b>5</b>	<b>Short pulse generation in the synchronously pumped SROPO</b>	<b>73</b>
5.1	Introduction . . . . .	73
5.2	Mathematical Overview of Non-Normal Operators . . . . .	74
5.2.1	The Case of Optical Resonator Eigenmodes . . . . .	75
5.3	Overview Of the Concept Of Pseudo-Spectra . . . . .	77
5.4	The Synchronously Pumped Optical Parametric Model . . . . .	80
5.4.1	The SPOPO Model . . . . .	80
5.5	Giant Noise Amplification in SPOPO . . . . .	84
5.5.1	The Singly Resonant Case . . . . .	84
5.5.2	High finesse singly resonant case . . . . .	88
5.5.3	The Doubly Resonant and Degenerate Cases . . . . .	88
5.5.4	Conditions for Giant Noise Amplification in SPOPO . . . . .	88
5.6	Giant Amplification of Quantum Noise . . . . .	93
5.6.1	Nondegenerate OPO in the time domain . . . . .	93
5.6.2	Propagation inside the crystal . . . . .	93
5.6.3	The Langevin Equation . . . . .	95
5.6.4	Propagation in the empty part of the cavity . . . . .	97
5.6.5	Application of Ito calculus . . . . .	98
5.7	Conclusions . . . . .	99
<b>6</b>	<b>Self-organization, Pattern Formation, Cavity Solitons and Rogue Waves in SRO- POs</b>	<b>101</b>
6.1	Introduction. . . . .	101
6.2	Mean-field models. . . . .	102
6.2.1	The close-to-threshold approximation. . . . .	107
6.3	Plane wave steady-states . . . . .	108
6.3.1	Linear stability analysis of the SROPO with seeding. . . . .	110
6.4	Turing instabilities and pattern formation . . . . .	110
6.4.1	Numerical patterns . . . . .	113
6.5	Optical turbulence, rogue waves and cavity solitons . . . . .	115

---

6.6	Conclusions. . . . .	118
<b>7</b>	<b>Conclusions</b>	<b>123</b>
7.0.1	Achievements of the thesis . . . . .	123
7.0.2	Future work . . . . .	124

## Acknowledgments

My deep gratitude is addressed to my Supervisor, Prof. Gian-Luca Oppo for his continuous support in the research work undertaken in this thesis. Continuous, stimulating and lively discussion with him has been very precious to me. Gian-Luca's support has been crucial to me for the realization of this work.

I am grateful to Prof. John Jeffers and Prof. Francesco Papoff for their professional advice and useful discussions. I am also grateful to Strathclyde University which gave me the chance to reach such an important target and European Union commission through the IST network project HIDEAS (Grant No. FP7-ICT-221906) which provided me with financial support.

I am particularly grateful to Ilaria who supported me for the entire duration of this experience and for her constant and patient help in running my bad moods as well my good days. Life without her would have been definitely harder, less colorful and empty.

Eventually, I wish to express my gratitude to my parents and to my sister Roberta who always made me feel at home even from a distance and to all wonderful people I have met.

## Papers and Conferences

- “Two-color continuous-variable quantum entanglement in a singly resonant optical parametric oscillator”, *Phys. Rev. A* **84**, 043810 (2011).
- “Quantum entanglement in strongly non degenerate OPOs: the doubly and singly resonant cases”, in *CLEO/Europe and EQEC 2011 Conference Digest*, OSA Technical Digest (CD) (Optical Society of America, 2011), paper EA5\_3.
- “Self-organization, Pattern Formation, Cavity Solitons and Turbulence in Singly Resonant Optical Parametric Oscillator”, *Phys. Rev. A* **88**, 043813 (2013).
- First year PhD Conference at Ross Priory in Glasgow, Scotland. (2009)
- “High Dimensional Entangled Systems” (HiDEaS) in Leiden, Holland. (2009)
- Second year PhD Conference at Ross Priory in Glasgow, Scotland. (2009)
- “High Dimensional Entangled Systems” (HiDEaS) in Paris, France. (2010)
- CLEO/Europe-EQEC Conference in Munich, Germany. (2011)
- “High Dimensional Entangled Systems” (HiDEaS) in Como, Italy. (2011)

## Abstract

Optical parametric oscillators have been known and used for a long time as efficient sources of non-classical states of light both below threshold of oscillation, where they generate squeezed vacuum states and bi-partite entangled states, and above threshold of oscillation, where they generate intensity correlated twin beams. The singly-resonant cavity, where only one of the three field involved in the parametric amplification process is resonated (signal), is in principle a simpler configuration to realize experimentally but, to the best of our knowledge, theoretical investigations of non-classical features of the light from a singly-resonant OPO (SROPO) are missing. One of the reasons is that SROPOs operate with strongly non-degenerate frequencies while much of the literature on squeezing focuses on the degenerate or close to degeneracy cases. Recent interest in non-classical correlations of the strongly non-degenerate regime of parametric down-conversion makes the study of entanglement in SROPO important for the optimization of coherent sources with fluctuations below the shot-noise level. There are clear technical advantages for SROPO configurations: only resonance of the signal field has to be maintained, continuous temperature tuning and suppression of mode-hopping. As a matter of fact even if the doubly resonant configuration, where both the signal and the idler fields are resonated, has a much lower threshold pump power, the tuning behavior is complicated and is massively affected by changes of the crystal temperature or pump wavelength, causing the signal and idler wavelengths undergoing jumps, and the tuning is generally non-monotonous. This is because the operation wavelengths are determined primarily by the requirement for simultaneous resonance for signal and idler, and not only by a phase-matching condition as in the case of singly resonant configuration.

It is in this spirit that in Chapter 4 we apply the input-output theory of optical cavities to formulate a quantum treatment of a continuous wave singly-resonant optical parametric oscillator. This case is mainly relevant to largely non-degenerate signal and idler modes. We show that both intensity and quadrature squeezing are present and that the maximum noise reduction below the standard quantum limit is the same at the signal and idler frequencies in a way similar to the doubly resonant case. As the threshold of oscillation is approached, however, the intensity-difference and quadrature spectra display a progressive line-narrowing which is absent in the balanced doubly-resonant case. By using the separability criterion for continuous variables, the signal-idler state is found to be entangled over wide ranges of the parameters. We show that attainable levels of squeezing and entanglement make singly-resonant configurations ideal candidates for two-colour quantum information processes because of their ease of tuning in experimental realizations.

Another very interesting feature of SROPOs which, this time, has no counterpart in the doubly-

---

resonant regime is described in Chapter 5 where model equations for the evolution of signal and idler pulses in a synchronously pumped optical parametric oscillator are derived and numerically integrated. A novel regime of giant sub-threshold pulses driven by quantum fluctuations is described through the analysis of stability eigenvalues, growth factors and pseudospectra. Sub-threshold pulses driven by quantum fluctuations are found at various mirror reflectivities in the non degenerate regime where signal and idler have different group velocities. Giant sub-threshold pulses open the possibility of observing macroscopic continuous variable entanglement with non-classical features. This important feature is peculiar to the singly-resonant configuration and has no counterpart in the doubly-resonant regime.

Very interesting classical features of SROPOs light are investigated in Chapter 6 where we show that spatio-temporal dynamics of singly resonant optical parametric oscillators with external seeding displays hexagonal, roll and honeycomb patterns, optical turbulence, rogue waves and cavity solitons. We derive appropriate mean-field equations with a  $\text{sinc}^2$  non-linearity and demonstrate that off-resonance seeding is necessary and responsible for the formation of complex spatial structures via self-organization. We compare this model with those derived close to the threshold of signal generation and find that back-conversion of signal and idler photons is responsible for multiple regions of spatio-temporal self-organization when increasing the power of the pump field.

## 1.1 Parametric down-conversion and optical parametric oscillators

Parametric down conversion is an optical process in which a pump photon of frequency  $\omega_p$  splits in two photons at different frequencies  $\omega_s$  (signal) and  $\omega_i$  (idler) such that  $\omega_p = \omega_s + \omega_i$  by interacting with a second-order nonlinear crystal. In contrast to atomic transitions where two energy levels of the Schrödinger equation are involved, in parametric down-conversion the upper level of the transition is a virtual level that exists for a time smaller than that allowed by the Heisenberg uncertainty principle for time and energy. For this reason, the process is very rare but at the same time incredibly fast. Parametric down-conversion is the complementary process to second harmonic generation where two photons at frequency  $\omega_p$  combine to generate a single photon at frequency  $2\omega_p$ . Second harmonic generation originated the entire field of laser induced nonlinear optics with the seminal experiment of P. Franken and collaborators in 1961 [1].

Spontaneous emission, which is intrinsic in this process, is driven by the vacuum fluctuations of the electromagnetic field and produces two photons which have a strong correlation in energy and momentum. The powers of the signal and idler field can be enhanced by seeding a classical beam of frequency  $\omega_s$  thus stimulating the emission of photons at the frequency of the idler beam. If the active medium is put in an optical cavity the parametric interaction can overcome the effect of losses thus producing oscillation. This device is called an optical parametric oscillator (OPO). OPOs were initially used as laser sources due to their wide tunability properties, particularly useful for applications in spectroscopy [2]. Nowadays there are available OPOs for the down-conversion of pulsed laser beams, used as light sources in the range between 330 and 2000 nm. These devices are used as coherent light sources in regions of the spectra where no effective laser medium is available, converting light of Nd:YAG lasers into the mid infrared region [3]. On the other hand quantum properties of the light emitted from these sources have been investigated and make OPOs among the most used devices for the production of non-classical states of light [4].

The simplest configuration of an OPO is obtained by using a singly resonant cavity (SROPO), in which the cavity is resonant only to the signal field while the pump and idler beams make a single pass interaction in the nonlinear crystal and exit the cavity without any feedback. The doubly resonant configurations (DROPO), in which both signal and idler beams are resonant in the cavity, can be used in order to reduce the oscillation threshold. While the SROPO allows for a broad continuous variation of the signal and idler wavelengths in the phase matching range, the threshold power is much higher when compared with DROPO. On the other hand the doubly

resonant condition and the energy conservation condition of DROPOs have the effect to limit the output modes to a discrete set of values leading to undesirable mode-hopping.

The threshold power for an OPO can be reduced further by using a cavity which is also resonant to the pump beam, thus obtaining a triply resonant OPO (TROPO). This type of configuration reduced the threshold power to 1 mW for CW operation in KTP [5], while the use of new materials reduced the power to  $300 \mu\text{W}$  with quasi phase matched crystal (QPM) [6]. One of the major applications of OPO below threshold of oscillation is for the production of squeezed states of light.

## 1.2 Squeezed states of light in OPOs

Squeezed states of light, where the noise in one quadrature of the fields is reduced below the vacuum level, are important elements in several applications of quantum information processes. These include sub-shot-noise phase measurements [7, 8], interferometric detection of gravitational radiation [9, 10] and quantum information with continuous variables [11]. In the latter case, squeezed states are used to generate continuous variable entanglement and achieve high fidelity in quantum teleportation protocols [11]. To squeeze quantum fluctuations of the electromagnetic field one needs nonlinear optical effects such as parametric down-conversion or four-wave mixing [12].

Squeezed states of light have been realised and utilized in OPO configurations. The first realization was achieved by R.E. Slusher by means of four wave mixing in atomic sodium [13]. Thereafter several realization of squeezed states of light have been obtained. Twins beams generated by above threshold OPOs have been shown to produce non classical noise reduction in intensity difference [14, 15, 16]. Twin beams have been used to enhance performances of optical setup for spectroscopy [17, 18, 19]. The DROPO have been the subject of many experimental and theoretical works [20, 21, 22, 23] where the features of OPO were investigated in relation to several parameters such as cavity dumping coefficients, degree of excitation below threshold, spurious losses, deviation from resonance condition and pump amplitude/phase fluctuations. Interest has been paid also to the transition from below to above threshold regime [24] and to the region close to threshold [25] showing the importance of nonlinear contribution to the dynamic of the system. The singly-resonant cavity of the SROPO is in principle a simpler configuration to realize experimentally but, to the best of our knowledge, theoretical investigations of squeezing and entanglement of the light from a singly-resonant OPO (SROPO) are missing. One of the reasons is that SROPOs operate with strongly non-degenerate frequencies while much of the literature on squeezing focuses on the degenerate or close to degeneracy cases [29, 30]. Recent interest in non-classical correlations of the strongly non-degenerate regime of parametric down-conversion [31] makes the study of entanglement in SROPO important for the optimization of coherent sources with fluctuations below the shot-noise level. There are clear technical advantages for SROPO configurations: only resonance of the signal field has to be maintained, continuous temperature tuning and suppression of mode-hopping. It is part of the aim of this thesis to investigate the squeezing and entanglement properties of SROPO when signal and idler fields have large frequency separations (two-color case). Our approach is similar to what has been used in the case of second harmonic generation [32, 14], namely a two-photon loss model in which a cavity mode is coupled quadratically to a continuum of output modes rather than linearly as usual in the input-output formulation of optical cavities.

## 1.3 Pulsed OPOs

A very interesting feature of OPO can be found in the pulsed-pump regime (synchronously pumped OPO or SPOPO) where under some conditions the device is able to reduce the duration of the input pulses at the frequencies of the signal and idler fields [47]. SPOPOs as sources of ultrashort pulses have been implemented in several experiments [34, 35, 36, 37, 38, 39]. Mode-locked OPOs have been used to generate picosecond pulses squeezed light in a degenerate configuration [40] or in quasi-degenerate configurations [41]. A recent quantum theory of SPOPO have been discussed by Patera et al. [42] while generation and characterization of multimode quantum frequency combs in SPOPO has been realized by Pinel et al. [43]. Furthermore quantum correlations and fluctuations in the pulsed light produced by a SPOPO has been investigated in several works [44, 45, 46]. In this thesis model equations for the evolution of signal and idler pulses in a SPOPO are derived and numerically integrated. A novel regime of giant sub-threshold pulses driven by quantum fluctuations is described through the analysis of stability eigenvalues, growth factors and pseudospectra. Sub-threshold pulses driven by quantum fluctuations are found at various mirror reflectivities in the non-degenerate regime where signal and idler have different group velocities. Giant sub-threshold pulses open the possibility of observing continuous variable entanglement with non-classical features.

## 1.4 Transverse pattern formation, cavity solitons, optical turbulence

Other interesting features that we will investigate in OPO and SROPO models are transverse pattern formation, autosolitons and cavity solitons which have been the subject of intense research in nonlinear optics in the last two decades since their original predictions [48, 49, 50, 51, 52]. Unlike in other fields of science, transverse patterns and dissipative solitons find useful applications in photonics such as optical memories, delay lines and optical registers [53]. Cavity solitons' counterparts in the propagation direction have also been shown to generate passive mode-locking in fiber lasers [54].

The formation of transverse spatial structures in quadratic nonlinear cavities was predicted first in optical parametric oscillators (OPOs) [55, 56] and later extended to second harmonic generation [57, 58]. Early predictions in OPOs were confined to the degenerate case where signal and idler fields have the same frequency. Experimental evidence of pattern formation was indeed found in triply resonant degenerate OPOs close to the confocal cavity configuration [59] and via conical emissions [60]. Confirmation of the predictions of [55] was provided in a broad-aperture degenerate OPOs in a plane-mirror mini-cavity [62]. Degenerate OPOs also display phase domain dynamics and dark-ring cavity solitons [64]. Finally, OPO models for non-degenerate Type-II cases in doubly or triply resonant cavity configurations have also been shown to display self-organization and pattern formation [63, 65, 66, 67, 68].

Transverse instabilities in the case of non-degenerate, SROPOs, have been less discussed in the literature. On the theoretical side pattern formation in SROPOs is expected to replicate results of the complex Ginzburg-Landau laser case [65]. On the experimental side cw SROPO configurations are notoriously difficult to operate because of high oscillation thresholds (typically several watts) in common birefringent crystals [69]. Quasi-phase matching in periodically poled materials has, however, considerably reduced operation thresholds of cw SROPOs [70] allowing for diode [71] and fiber [72] laser pumping for spectroscopy applications. A major advantage of cw SROPOs is that

their wide tunability is monotonic and not affected by mode jumps typical of doubly or triply resonant configurations.

In this thesis we investigate the formation and dynamics of transverse structures in SROPOs. We first derive a mean-field model in section 6.2 where the nonlinearity is of  $\text{sinc}^2$  form in agreement with early studies of SROPO steady states emissions [73, 74, 75]. The analysis builds on approaches that describe and integrate the propagation equations inside the OPO crystal [76, 77] by considering transverse effects and by carefully separating the mean-field and close-to-threshold approximations. The final model equations are capable of describing transverse pattern formation in the presence of pump depletion, signal-idler recombination and external seeding close to the signal frequency. External seeding proves to be of fundamental importance for transverse structures in SROPOs since, in its absence, changes of the cavity length are compensated by changes in the signal (and idler) frequency thus nullifying the common mechanism of Turing pattern formation in off-resonant optical systems [48, 78].

Plane-wave steady states and their stability are then analyzed in the SROPO models with external seeding, close to and far from threshold. These studies confirm that no pattern formation should be expected without a detuned external seed. Analytical expressions for the location in the parameter space of the loss of stability of homogeneous solutions to spatially modulated structures are discussed. The thresholds for pattern formation when changing the seeding intensity are then compared with those obtained from numerical integration of the SROPO dynamical equations with excellent agreement. Optical turbulence is demonstrated to be the mechanism which generates rogue waves in the spatio-temporal evolution of the output fields. Finally, bright and dark cavity solitons are found in multistable configurations with localized hexagonal and honeycomb patterns.

## 1.5 Outline of the thesis

This thesis is organized as follows:

Chapter 2 is dedicated to an overview of nonlinear optics and to the related argument of quantum squeezing. Quantum entanglement and its connection to quantum squeezing will also be introduced and will be useful for the understanding of the rest of this thesis. The last part of the chapter deals with optical parametric amplifiers (OPA) and their squeezing properties, in both the degenerate and non-degenerate case.

Chapter 3 is dedicated to the problem of the detection of squeezed light through the ordinary and balanced homodyne detection schemes. The input-output formulation of optical cavities will be explained and both the Heisenberg-Langevin and master equation approaches to the optical cavities problem will be analyzed. Then the last part of the chapter will deal with application of these theoretical approaches to the case of a triply resonant OPO (TROPO) in the below threshold degenerate and non-degenerate cases.

Chapter 4 is dedicated to the analysis of squeezing properties and entanglement of a singly resonant optical parametric oscillator (SROPO) in the cw-regime. It will be shown that squeezing and entanglement are both present in this regime of singly resonant operation and for different experimental configurations. Since the singly resonant regime is easier to achieve than the doubly and triply resonant case where the idler, the signal and the pump must be resonated inside the optical cavity, it seems the case that it should be preferred to the multi-resonant cases for the

---

production of squeezed states of light. The necessity of a more powerful pump source to achieve the threshold for oscillation is not an impossible issue with nowadays available laser sources.

Chapter 5 is dedicated to the issue of short pulse generation and giant noise amplification in synchronously pumped SROPO. An introduction to non-normal operators and pseudospectra is provided which is essential for the understanding of the chapter. Since under appropriate conditions the SROPO system is capable to show sustained, noise driven oscillation, even below threshold of oscillation, we will address the question of whether quantum noise can drive those oscillation and hence if quantum properties, such as squeezing and entanglement survive this regime of operation. In this case we would have a demonstration of the possibility of macroscopic quantum entanglement of bright beams in SROPO below threshold.

In Chapter 6 we derive appropriate mean-field equations with a  $\text{sinc}^2$  nonlinearity and demonstrate that off-resonance seeding is necessary and is responsible for the formation of complex spatial structures via self-organization. We compare this model with those derived close to the threshold of signal generation and find that back-conversion of signal and idler photons is responsible for multiple regions of spatiotemporal self-organization when increasing the power of the pump field. It will be shown that the spatiotemporal dynamics of SROPO with external seeding display hexagonal, roll and honeycombs patterns, optical turbulence, rogue waves and cavity solitons.

Conclusions and future work are provided in Chapter 7.

## Bibliography

- [1] P. A. Franken, A. E. Hill, C. W. Peters, and G. Weinreich, *Phys. Rev. Lett.* **7**, 118 (1961).
- [2] J. A. Giordmaine and R. C. Miller, *Phys. Rev. Lett.* **14**, 973 (1965).
- [3] Special edition on Optical Parametric Oscillation and Amplification of *J. Opt. Soc. Am. B* **10**, Robert L. Byer and Algis Piskarskas eds. (1993).
- [4] R. Loudon, *The quantum theory of light*, Third Edition (Oxford University Press, Oxford, 2000).
- [5] K. Kasay, G. Jiangrui and C. Fabre, *Europhys. Lett.* **40**, 25 (1997).
- [6] M. Martinelli, K. S. Zhang, T. Coudreau, A. Maitre, C. Fabre, *J. Opt. A: Pure Appl. Opt.* **3**, 300 (2001).
- [7] P. Grangier, R. E. Slusher, B. Yurke and A. La Porta, *Phys. Rev. Lett.* **59**, 2153 (1987).
- [8] M. Xiao, L. A. Wu and H. J. Kimble, *Phys. Rev. Lett.* **59**, 278 (1987).
- [9] C. M. Caves, *Phys. Rev. Lett.* **45**, 75 (1980).
- [10] A. F. Pace, M. J. Collett, D. F. Walls, *Phys. Rev. A* **47**, 3173 (1993).
- [11] S. L. Braunstein, P. Van Loock, *Reviews of Modern Physics* **77**, 513 (2005).
- [12] L. Mandel and E. Wolf, *Optical Coherence and Quantum Optics* (Cambridge University Press, Cambridge, 1995).
- [13] R.E. Slusher, L.W. Hollberg, B. Yurke, J.C. Mertz, J.F. Valley, *Phys. Rev. Lett.* **55**, 2409 (1985).
- [14] A.S. Lane, M.D. Reid and D. Walls, *Phys. Rev. A* **38**, 788 (1998).
- [15] P-R- Tapster, S.F. Seward and J.G. Rarity, *Phys. Rev. A* **44**, 3266 (1991).
- [16] A. Porzio, F. Sciarino, A. Chiummo, M. Fiorentino and S. Solimeno, *Optics Communications* **194**, 373 (2001).

- 
- [17] C.D. Nabors and R.M. Shelby, *Phys. Rev. A* **42**, 556 (1990);
- [18] J.J. Snyder, E. Giacobino, C. Fabre, A. Heidmann and M. Duchoy, *JOSA B* **7**, 2132 (1990).
- [19] A. Porzio, C. Altucci, M. Autiero, A. Chiummo, C. de Lisio and S. Solimeno, *Appl. Phys. B* **73**, 763 (2001).
- [20] M.J. Collet and C. W. Gardiner, *Phys. Rev. A* **30**, 1386 (1984).
- [21] M.J. Collet and D.F. Walls, *Phys. Rev. A* **32**, 2887 (1985).
- [22] M.J. Collet and R. Loudon, *J. Opt. Soc. Am. B* **4**, 1525 (1987).
- [23] L. Wu, H. Kimble, J. Hall and H. Wu, *Phys. Rev. Lett.* **57**, 2520 (1986).
- [24] P. Kinsler and P.D. Drummond, *Phys. Rev. A* **43**, 6194 (1991).
- [25] S. Chaturvedi, K. Dechoum and P.D. Drummond, *Phys. Rev. A* **65**, 033805 (2002).
- [26] C. Fabre, E. Giacobino, A. Heidmann and S. Reynaud, *J. Phys. France* **50** 1209 (1989).
- [27] C. Schori, J. L. Sorensen and E. S. Polzik, *Phys. Rev. A* **66**, 033802 (2002).
- [28] J. Laurat, T. Coudreau, G. Keller, N. Treps, and C. Fabre, *Phys. Rev. A* **71**, 022313 (2005).
- [29] C. W. Gardiner and P. Zoller, *Quantum Noise*, (Springer, Berlin, 2004).
- [30] D. F. Walls and Gerard J. Milburn, *Quantum Optics*, (Springer, Berlin, 2008).
- [31] I. N. Agafonov, M. V. Chekhova and G. Leuchs, *Phys. Rev. A* **82**, 011801(R) (2010).
- [32] M. J. Collett and R. B. Levien, *Phys. Rev. A* **43**, 5068 (1991).
- [33] R. Paschotta, M. Collett, P. Kürz, K. Fiedler, H. A. Bachor and J. Mlynek, *Phys. Rev. Lett.* **72**, 3807 (1994).
- [34] M. Ebrahimzadeh, G. J. Hall and A. I. Ferguson, *Opt. Lett.* **16**, 1744 (1991).
- [35] D. C. Edelstein, E. S. Wachman, C. L. Tang, *Appl. Phys. Lett.* **54**, 1728 (1989).
- [36] G. Mak, Q. Fu, H. van Driel, *Appl. Phys. Lett.* **60**, 542 (1992).
- [37] G. T. Maker and A. I. Ferguson, *Appl. Phys. Lett.* **56**, 1614 (1990).
- [38] M. J. McCarty and D. C. Hanna, *Opt. Lett.* **17**, 402 (1992).
- [39] A. Piskarskas, V. J. Smil'gyavichyus and A. Umbrasas, *Sov. Quantum Electron.* **18**, 155 (1988).
- [40] R. M. Shelby and M. Rosenbluh, *Appl. Phys. B* **55**, 226 (1992).
- [41] N. Forget, S. Bahbah, C. Drag, F. Bretenaker, M. Lefèbvre and E. Rosencher, *Opt. Lett.* **31**, 972 (2006).
- [42] G. Patera, G. De Valcarcel, N. Treps, C. Fabre, *Eur. Phys. Journal D* **56**, 123 (2010).

- 
- [43] O. Pinel, Pu Jian, R. Medeiros, Jinxia Feng, B ; B. Chalopin, C. Fabre, N. Treps, Phys. Rev. Letters **108**, 083601 (2012).
- [44] V.A. Averchenko, Yu.M. Golubev, C. Fabre, N. Treps, Opt. Spectroscopy **110**, 925 (2011).
- [45] V.A. Averchenko, Yu.M. Golubev, C. Fabre, N. Treps, Eur. Phys. Journal D **61**, 207 (2010).
- [46] G. De Valcarcel, G. Patera, N. Treps, C. Fabre, Phys. Rev. A **74**, 061801(R) (2006).
- [47] L. Lefort, K. Puech, S. D. Butterworth, Y. P. Svirko, and D. C. Hanna, Opt. Lett. **24**, 28 (1999).
- [48] L. A. Lugiato and R. Lefever, Phys. Rev. Lett. **58**, 2209 (1987)
- [49] G. D'Alessandro and W. J. Firth, Phys. Rev. Lett. **66**, 2597 (1991)
- [50] N. N. Rosanov, A. V. Fedorov and G. V. Khodova, Phys. Stat. Sol. B **150**, 545 (1988); N. N. Rosanov, *Spatial Hysteresis and Optical Patterns* (Springer, Berlin, 2002)
- [51] M. Tlidi, P. Mandel and R. Lefever, Phys. Rev. Lett. **73**, 640 (1994)
- [52] W. J. Firth and A. J. Scroggie, Phys. Rev. Lett. **76**, 1623 (1996)
- [53] T. Ackemann, W. J. Firth and G.-L. Oppo, Adv. Atom. Mol. Opt. Phys. **57**, 323 (2009)
- [54] P. Grelu and N. Akhmediev, Nature Photonics **6**, 84 (2012)
- [55] G.-L. Oppo, M. Brambilla and L. A. Lugiato, Phys. Rev. A **49**, 2028 (1994)
- [56] G. J. de Valcarcel, K. Staliunas, E. Roldan and V. J. Sanchez-Morcillo, Phys. Rev. A **54**, 1609 (1996)
- [57] C. Etrich, U. Peschel and F. Lederer, Phys. Rev. E **56**, 4803 (1997)
- [58] P. Lodahl and M. Saffman, Phys. Rev. A **60**, 3251 (1999)
- [59] S. Ducci, N. Treps, A. Maitre and C. Fabre, Phys. Rev. A **64**, 023803 (2001).
- [60] M. Shelton and D. P. West, Opt. Express **9**, 16 (2001).
- [61] M. Peckus, K. Staliunas, M. Saffman, G. Sleky, V. Sirutkaitis, V. Smilgevicius and R. Grigonis, Opt. Commun. **251**, 165 (2005).
- [62] M. Peckus, K. Staliunas, Z. Nizauskaite and V. Sirutkaitis, Opt. Lett. **32**, 3014 (2007)
- [63] G.-L. Oppo, M. Brambilla, D. Camesasca, A. Gatti and L. A. Lugiato, J. Mod. Opt. **41**, 1151 (1994)
- [64] G.-L. Oppo, A. J. Scroggie and W. J. Firth, Phys. Rev. E **63**, 066209 (2001)
- [65] K. Staliunas, J. Mod. Opt. **42**, 1261 (1995)
- [66] S. Longhi and A. Geraci, Phys. Rev. A **54**, 4581 (1996)

- 
- [67] V. J. Sanchez-Morcillo, E. Roldan, G. J. de Valcarcel and K. Staliunas Phys. Rev. A **56**, 3237 (1997)
- [68] M. Santagiustina, E. Hernandez-Garcia, M. San-Miguel, A. J. Scroggie and G.-L. Oppo, Phys. Rev. E **65**, 036610 (2002)
- [69] S. T. Yang, R. C. Eckardt and R. L. Byer, Opt. Lett. **18**, 971 (1993)
- [70] W. R. Bosenberg, A. Drobshoff, J. I. Alexander, L. E. Meyers and R. L. Byer, Opt. Lett. **21**, 1336 (1996)
- [71] M. E. Klein, C. K. Laue, D.-H. Lee, K.-J. Boller and R. Wallenstein, Opt. Lett. **25**, 490 (2000)
- [72] A. Henderson and R. Stafford, Opt. Express **14**, 767 (2006)
- [73] L. B. Kreuzer, in Proceedings of the Joint Conference on Lasers and Opto-Electronics (Institution of Electrical and Radio Engineers, London, 1969), page 52
- [74] W. Brunner, R. Fischer and H. Paul, Ann. Phys. (Leipzig) **30**, 299 (1973).
- [75] W. Brunner and H. Paul, Prog. Opt. **15**, 1 (1977).
- [76] E. Rosencher and C. Fabre, J. Opt. Soc. Am. B **19**, 1107 (2002)
- [77] C. R. Phillips and M. M. Fejer, J. Opt. Soc. Am. B **27**, 2687 (2010)
- [78] G.-L. Oppo, J. Math. Chem. **45**, 95 (2009)

## Squeezed States of Light and the Parametric Amplifier

To study quantum entanglement in singly resonant optical parametric oscillators, it is useful to introduce few elements of nonlinear and quantum optics. In this chapter we review first the notion of quantum squeezing and then the notion of quantum entanglement and its connection to squeezing. In particular we obtain a description of parametric amplifiers which also will be useful in chapter 3 and chapter 4.

### 2.1 Introduction to Nonlinear Optics

The regime of nonlinear optics is achieved when the response of material systems, a crystal usually, is not linear in the electric field. In particular the polarization of a medium under the influence of an applied electric field is described in terms of a power series in the field. It is convenient to express the power series as [1]:

$$\vec{P}(t) = \vec{P}^{(0)}(t) + \vec{P}^{(1)}(t) + \vec{P}^{(2)}(t) + \dots + \vec{P}^{(n)}(t) \dots \quad (2.1)$$

where  $\vec{P}^{(1)}(t)$  is linear in the field,  $\vec{P}^{(2)}(t)$  is quadratic, and so on. The term  $\vec{P}^{(0)}(t)$ , which is independent on the field, would represent, for example, the static polarization found in some crystal. Here we consider the *local* response, in which the polarization at a point in space in the nonlinear medium is determined by the electric field at that point. The general form of the various terms in series (2.1) is found by invoking a fundamental physical principle: time-invariance.

What is meant by time-invariance is that the dynamical properties of the system are assumed to be unchanged by a translation of the time origin; in this case, a time-displacement of the driving electric field merely results in a corresponding time-displacement of the induced polarization.

#### 2.1.1 Linear Response

We apply this principle first to determine the form of the linear polarization. Since  $\vec{P}^{(1)}(t)$  is linear in  $\vec{E}(t)$ , it may be expressed in the form:

$$\vec{P}^{(1)}(t) = \varepsilon_0 \int_{-\infty}^{\infty} d\tau T^{(1)}(t; \tau) \vec{E}(\tau). \quad (2.2)$$

It must be stressed that  $\vec{P}(\vec{x}, t)$  is the dipole moment per unit volume. If  $N(\vec{x})$  is the number of molecules per unit volume, we must multiply this number distribution for the response of a single

molecule eq. (2.2) and hence:

$$\vec{P}(\vec{x}, t) = N(\vec{x})\vec{P}(t), \quad (2.3)$$

and hence  $T^{(1)}(t; \tau)$  becomes also a function of  $\vec{x}$ ,  $T^{(1)}(\vec{x}, t; \tau)$ . From the principle of time invariance we must have:

$$\vec{P}^{(1)}(t) = \varepsilon_0 \int_{-\infty}^{\infty} d\tau \chi^{(1)}(t - \tau) \vec{E}(\tau). \quad (2.4)$$

Where  $\chi^{(1)}(t - \tau)$  is called the linear polarization response function (susceptibility) of the medium. Its form is subjected to two restrictions: First,  $\chi^{(1)}(t - \tau)$  must vanish for negative  $t - \tau$  to ensure that  $\vec{P}^{(1)}(t)$  depends only on the values of the field for time before  $t$ , which is the causality condition.

When the linear polarization response function does not depend on time and hence has the following form:

$$\chi^{(1)}(t - \tau) = \chi^{(1)}\delta(t - \tau), \quad (2.5)$$

then the polarization is given by the following expression:

$$\vec{P}^{(1)}(t) = \varepsilon_0 \chi^{(1)} \vec{E}(t). \quad (2.6)$$

### 2.1.2 Nonlinear Response

We may now apply essentially the same arguments to determine the form of the lowest-order nonlinear polarization, the term  $\vec{P}^{(2)}(t)$  which is quadratic in  $\vec{E}(t)$ . It may be expressed in the form:

$$\vec{P}^{(2)}(t) = \varepsilon_0 \int_{-\infty}^{\infty} d\tau_1 \int_{-\infty}^{\infty} d\tau_2 T^{(2)}(t; \tau_1, \tau_2) \vec{E}(\tau_1) \vec{E}(\tau_2), \quad (2.7)$$

where  $T^{(2)}(t; \tau_1, \tau_2)$  is a third-rank tensor which is a function of three times  $t$ ,  $\tau_1$  and  $\tau_2$ .

By applying the principle of time-invariance as we did previously for the linear response function, we find that:

$$T^{(2)}(t + t_0; \tau_1, \tau_2) = T^{(2)}(t; \tau_1 - t_0, \tau_2 - t_0), \quad (2.8)$$

for all  $t$ ,  $t_0$ ,  $\tau_1$  and  $\tau_2$ . Hence, by setting  $t = 0$  and then replacing the arbitrary time  $t_0$  by  $t$ , we find that  $T^{(2)}(t; \tau_1, \tau_2)$  depends only on the two time differences  $t - \tau_1$  and  $t - \tau_2$ . To make this fact explicit in our formulas we write:

$$T^{(2)}(t; \tau_1, \tau_2) \equiv \chi^{(2)}(t - \tau_1, t - \tau_2). \quad (2.9)$$

By substituting eq. (2.9) in eq. (2.7) we obtain the canonical form for the quadratic polarization:

$$\vec{P}^{(2)}(t) = \varepsilon_0 \int_{-\infty}^{\infty} d\tau_1 \int_{-\infty}^{\infty} d\tau_2 \chi^{(2)}(t - \tau_1, t - \tau_2) \vec{E}(\tau_1) \vec{E}(\tau_2). \quad (2.10)$$

The tensor  $\chi^{(2)}(t - \tau_1, t - \tau_2)$  may be called the quadratic polarization response function of the medium. As before the causality requirement dictates that  $\chi^{(2)}(t - \tau_1, t - \tau_2)$  is zero when either  $t - \tau_1$  or  $t - \tau_2$  is negative

Again, when the quadratic polarization response function does not depend on time and hence it has the following form:

$$\chi^{(2)}(t - \tau_1, t - \tau_2) = \chi^{(2)}\delta(t - \tau_1)\delta(t - \tau_2), \quad (2.11)$$

then the second order polarization is given by the following expression:

$$\vec{P}^{(2)}(t) = \varepsilon_0\chi^{(2)}\vec{E}^2(t). \quad (2.12)$$

The generalization of eq. (2.12) to an arbitrary order is straightforward. The optical response is described by expressing  $\vec{P}(t)$  as a power series of  $\vec{E}(t)$  as:

$$\vec{P}(t) = \varepsilon_0 \left[ \chi^{(1)}\vec{E}(t) + \chi^{(2)}\vec{E}^2(t) + \chi^{(3)}\vec{E}^3(t) + \dots \right] \quad (2.13)$$

where  $\vec{P}^{(i)}(t) = \varepsilon_0\chi^{(i)}\vec{E}^i(t)$  is the  $i^{\text{th}}$ -order polarization and the terms  $\chi^{(i)}$  are the nonlinear optical susceptibilities. The effect of the nonlinear terms in eq. (2.13) is to generate, once an electric field is injected into a nonlinear crystal, light fields not only at the frequency of the injected field but also at other frequencies, which are multiple and/or submultiple of the field.

Among the nonlinear processes which are allowed by eq. (5.11), in the rest of this thesis we will consider a particular second order  $\chi^{(2)}$  process known as *parametric down conversion* [2]. In this process an intense pump beam of amplitude  $E_p$  and frequency  $\omega_p$  and a weak beam of amplitude  $E_s$  at frequency  $\omega_s$  (seed) are injected in a nonlinear crystal. The second order nonlinear term in eq. (5.11) operates a mixing of these fields inside the crystal and generates a macroscopic field at frequency  $\omega_i = \omega_p - \omega_s$  of amplitude  $E_i$ .

From a quantum mechanical point of view the process can be depicted applying a photon energy level description. The absorption of a photon at frequency  $\omega_p$  excites a virtual atomic level which then decays emitting two photon whose generation is stimulated by the presence of the photon at frequency  $\omega_s$ . The presence of the field at frequency  $\omega_s$  is not required for the process to occur but in this case the energy of the pump beam is spread over different signal and idler frequencies and hence the intensities of the generated fields are weak. A method to obtain fields of significant intensity without using an initial seed is to place the nonlinear crystal inside a optical resonator and setting the device to be resonant with the frequencies  $\omega_s$  and/or  $\omega_i$ . Such a device is called an optical parametric oscillator (*OPO*).

## 2.2 Definition of Squeezed States of Light

*Squeezed States* of the electromagnetic field are a very general class of minimum-uncertainties state, which are quantum states for which the uncertainty principle takes the minimum value allowed by quantum mechanics. They are defined as those states which may have less noise in one quadrature than a coherent state. The noise in the conjugate quadrature must be greater than that of a coherent state if the requirement of minimum-uncertainty has to hold. Particular members of this class of states are the coherent states of the electromagnetic field for which there is equal noise in both quadratures. Our discussion takes place from the definition of this family of minimum-uncertainty states. Let us consider a single-mode electric field:

$$\hat{E}(r, t) = \left( \frac{\hbar\omega}{2V\varepsilon_0} \right)^{1/2} \left[ \hat{X}_1 \sin(k \cdot r - \omega t) - \hat{X}_2 \cos(k \cdot r - \omega t) \right], \quad (2.14)$$

where  $\hat{X}_1$  and  $\hat{X}_2$  are Hermitian operators representing the real and imaginary part of the complex amplitude. They are related to the creation and annihilation operator for a mode by:

$$\hat{X}_1 = \hat{a} + \hat{a}^\dagger, \quad (2.15)$$

$$\hat{X}_2 = -i(\hat{a} - \hat{a}^\dagger). \quad (2.16)$$

They obey the following commutation relation:

$$[\hat{X}_1, \hat{X}_2] = 2i. \quad (2.17)$$

From the commutation relation eq. (2.17) and from the general relation:

$$\Delta A \Delta B \geq \frac{1}{2} |\langle [A, B] \rangle|, \quad (2.18)$$

where  $A$  and  $B$  are two Hermitian operators, it is possible to derive a corresponding uncertainty relation, which is:

$$\Delta \hat{X}_1 \Delta \hat{X}_2 \geq 1. \quad (2.19)$$

This relation with the equal sign defines a family of minimum-uncertainty states. It is a characteristic of the coherent state, including the vacuum state, that the dispersion of the dimensionless quadrature amplitude  $\hat{X}_1$  and  $\hat{X}_2$  are equal:

$$\Delta \hat{X}_1 = \Delta \hat{X}_2 = 1, \quad (2.20)$$

so that the uncertainty relation has its minimum value. The coherent state  $|\alpha\rangle$  has the mean complex amplitude  $\alpha$  and it is a minimum uncertainty state for  $\hat{X}_1$  and  $\hat{X}_2$ , with equal uncertainties in the two quadrature operators. A coherent state may be represented by an 'error circle' in a complex amplitude plane whose axes are  $\hat{X}_1$  and  $\hat{X}_2$ . The center of the error circle lies at  $\frac{1}{2} \langle \hat{X}_1 + i\hat{X}_2 \rangle = \alpha$  and the radius  $\Delta \hat{X}_1 = \Delta \hat{X}_2 = 1$  accounts for the uncertainties in  $\hat{X}_1$  and  $\hat{X}_2$ . For a squeezed state the phase space distribution takes on an elliptic shape. There is obviously a whole family of minimum-uncertainty states defined by  $\Delta \hat{X}_1 \Delta \hat{X}_2 = 1$ . If we plot  $\Delta \hat{X}_1$  against  $\Delta \hat{X}_2$  the minimum uncertainty states lie on a hyperbole. Only points lying to the right of the hyperbole correspond to physical states. In summary we can say:

1. Coherent states:  $\Delta \hat{X}_1 \Delta \hat{X}_2 = 1$  and  $\Delta \hat{X}_1 = \Delta \hat{X}_2 = 1$ .
2. Squeezed states:  $\Delta \hat{X}_1 \Delta \hat{X}_2 \geq 1$  and  $\Delta \hat{X}_1 < 1 < \Delta \hat{X}_2$ .
3. Ideal Squeezed states:  $\Delta \hat{X}_1 \Delta \hat{X}_2 = 1$  and  $\Delta \hat{X}_1 < 1 < \Delta \hat{X}_2$ .

It is important to stress at this point that the definition of quadrature operators,  $\hat{X}_1$  or  $\hat{X}_2$ , defined by eqs. (2.15, 2.16) can be further extended to include the possibility that the major axis of the ellipse may point in a direction other than the  $\hat{X}_1$  and  $\hat{X}_2$  axes. We can then define the more general variables  $\hat{Q}$  and  $\hat{P}$  for any angle  $\beta$ , by the relations [2]:

$$\begin{cases} \hat{Q} = \hat{a}e^{-i\beta} + \hat{a}^\dagger e^{i\beta} \\ \hat{P} = \hat{a}e^{-i(\beta+\pi/2)} + \hat{a}^\dagger e^{i(\beta+\pi/2)}. \end{cases} \quad (2.21)$$

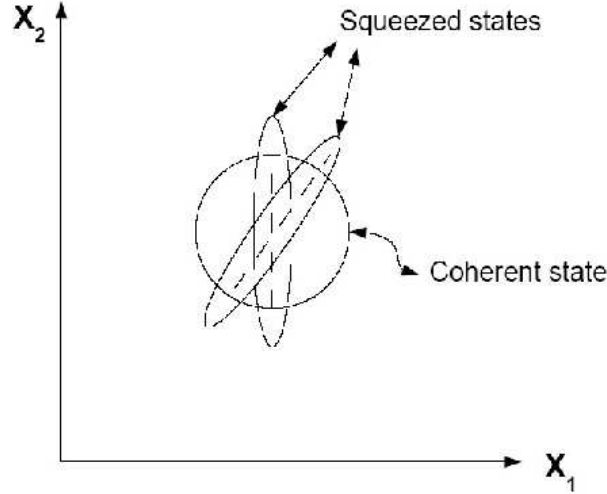


Figure 2.2.1: Representation of coherent and squeezed states of light.

These obey the same commutation and uncertainty relations as  $\hat{X}_1$  and  $\hat{X}_2$ , and their dispersions are both unity in the vacuum state. In terms of  $\hat{Q}$  and  $\hat{P}$ ,  $\hat{E}(r, t)$  is given by:

$$\hat{E}(r, t) = \left( \frac{\hbar\omega}{2V\epsilon_0} \right)^{1/2} \left[ \hat{Q} \sin(k \cdot r - \omega t + \beta) - \hat{P} \cos(k \cdot r - \omega t + \beta) \right]. \quad (2.22)$$

The only difference between  $\hat{Q}$  and  $\hat{P}$  is that the angle  $\beta$  is incremented by  $\pi/2$ .

### 2.2.1 Quantum nature of the squeezed state

It is important to analyze in detail what we really mean when we state that the squeezed states of light are non-classical states. They have a non-classical nature because the diagonal coherent-state representation of the density operator is not a classical probability density, as we can easily show.

The defining property of squeezed state is [2]:

$$\Delta\hat{Q} < 1 \quad \text{for some } \beta. \quad (2.23)$$

We can now relate, by using eqs. (2.21), the quantity  $\langle \hat{Q}^2 \rangle$  to the normally ordered expectation, where all the creation operators are to the left of all annihilation operators in the product,  $\langle : \hat{Q}^2 : \rangle$ :

$$\begin{aligned} \langle : \hat{Q}^2 : \rangle &= \langle \hat{a}^{\dagger 2} \rangle e^{2i\beta} + \langle \hat{a}^2 \rangle e^{-2i\beta} + 2 \langle \hat{a}^\dagger \hat{a} \rangle, \\ \langle \hat{Q}^2 \rangle &= \langle \hat{a}^\dagger \hat{a} \rangle e^{2i\beta} + \langle \hat{a}^2 \rangle e^{-2i\beta} + \langle \hat{a}^\dagger \hat{a} \rangle + \langle \hat{a} \hat{a}^\dagger \rangle. \end{aligned}$$

Since  $[\hat{a}, \hat{a}^\dagger] = 1$  we find immediately that:

$$\langle : \hat{Q}^2 : \rangle = \langle \hat{Q}^2 \rangle - 1,$$

so that:

$$: \Delta \hat{Q} := \Delta \hat{Q} - 1. \quad (2.24)$$

It follows from the definition eq. (2.23) that for a squeezed state:

$$\langle : \Delta \hat{Q} : \rangle < 0 \quad \text{for some } \beta. \quad (2.25)$$

The next step is to express the density operator  $\hat{\rho}$  in the diagonal coherent-state representation:

$$\hat{\rho} = \int P(\alpha) |\alpha\rangle \langle \alpha| d^2\alpha. \quad (2.26)$$

It follows that:

$$\langle : \Delta \hat{Q} : \rangle = \int P(\alpha) \Delta Q d^2\alpha. \quad (2.27)$$

Here  $\Delta Q$  is the c-number<sup>1</sup> corresponding to  $: \Delta \hat{Q} :$ , which is obtained by replacing each  $\hat{a}$  by  $\alpha$  and each  $\hat{a}^\dagger$  by  $\alpha^*$ . The condition for squeezing can now be expressed in the form:

$$\langle : \Delta \hat{Q} : \rangle = \int P(\alpha) \Delta Q d^2\alpha < 0 \quad \text{for some } \beta. \quad (2.28)$$

The reality and non-negative character of  $\Delta Q$  forbid the ‘‘probability’’ distribution,  $P(\alpha)$ , to be a classical probability density if the inequality eq. (2.28) must be satisfied. We have shown in this way that the quantity  $P(\alpha)$  cannot be interpreted as a true probability distribution for a squeezed state. This is a clear demonstration of the intrinsic quantum nature of the squeezed states of the electromagnetic field.

## 2.3 Single Mode Quadrature Squeezed States

It is possible to generate a squeezed single-mode state from a non-squeezed one by acting with the following unitary operator [2]:

$$\hat{S}(\xi) = e^{\frac{1}{2}\xi^* \hat{a}^2 - \frac{1}{2}\xi \hat{a}^{\dagger 2}}, \quad \xi = r e^{i\theta}, \quad (2.29)$$

which is known as the *squeeze operator*. It is easy to see that this operator is unitary:

$$S^\dagger(\xi) = S^{-1}(\xi) = S(-\xi). \quad (2.30)$$

With the help of the operator expansion theorem [2] which states that given two operators  $\hat{A}$  and  $\hat{B}$  that do not necessarily commute, and the function:

$$f(x) = e^{x\hat{A}} \hat{B} e^{-x\hat{A}}, \quad (2.31)$$

it follows that:

$$f(x) = \hat{B} + x [\hat{A}, \hat{B}] + \frac{x^2}{2!} [\hat{A}, [\hat{A}, \hat{B}]] + \frac{x^3}{3!} [\hat{A}, [\hat{A}, [\hat{A}, \hat{B}]]] + \dots \quad (2.32)$$

---

<sup>1</sup>The term c-number (or classical number) is an old nomenclature used by Paul Dirac which refers to real and complex numbers. It is used to distinguish from operators (q-numbers or quantum numbers) in quantum mechanics. Although c-numbers are commuting, the term anti-commuting c-number is also used to refer to a type of anti-commuting numbers that are mathematically described by Grassmann numbers.

Hence we find that for the unitary transformation of the operator  $a$ :

$$\begin{cases} \hat{S}(\xi) &= e^{\frac{1}{2}\xi^* \hat{a}^2 - \frac{1}{2}\xi \hat{a}^{\dagger 2}} = e^{-\hat{A}} \\ \hat{S}^\dagger(\xi) &= e^{\frac{1}{2}\xi \hat{a}^{\dagger 2} - \frac{1}{2}\xi^* \hat{a}^2} = e^{\hat{A}} \end{cases}$$

$$\hat{S}^\dagger \hat{a} \hat{S} = \hat{a} + [\hat{A}, \hat{a}] + \frac{1}{2!} [\hat{A}, [\hat{A}, \hat{a}]] + \frac{1}{3!} [\hat{A}, [\hat{A}, [\hat{A}, \hat{a}]]] + \dots \quad (2.33)$$

After annoying operators algebra we get:

$$\hat{S}^\dagger \hat{a} \hat{S} = \hat{a} - \xi \hat{a}^\dagger + \frac{1}{2!} |\xi|^2 \hat{a} - \frac{1}{3!} |\xi|^2 \xi \hat{a}^\dagger + \dots \quad (2.34)$$

Remembering that:

$$\sinh(\xi) = \sum_{n=0}^{\infty} \frac{\xi^{(2n+1)}}{(2n+1)!} = \xi + \frac{1}{3!} \xi^3 + \dots = r e^{i\theta} + \frac{r^3}{3!} e^{i\theta} + \dots \quad (2.35)$$

$$\cosh(\xi) = \sum_{n=0}^{\infty} \frac{|\xi|^{2n}}{(2n)!} = 1 + \frac{1}{2!} \xi^2 + \dots = 1 + \frac{r^2}{2!} + \dots \quad (2.36)$$

we can write eq. (2.33) as:

$$\begin{aligned} \hat{S}^\dagger \hat{a} \hat{S} &= \hat{a} \cosh(r) - \hat{a}^\dagger e^{i\theta} \sinh(r) \\ &= \mu \hat{a} - \nu \hat{a}^\dagger, \end{aligned} \quad (2.37)$$

where we have defined:

$$\begin{aligned} \mu &= \cosh(r) \\ \nu &= e^{i\theta} \sinh(r). \end{aligned} \quad (2.38)$$

Similarly we obtain the equation:

$$\hat{S}^\dagger \hat{a}^\dagger \hat{S} = \hat{a}^\dagger + [\hat{A}, \hat{a}^\dagger] + \frac{1}{2!} [\hat{A}, [\hat{A}, \hat{a}^\dagger]] + \frac{1}{3!} [\hat{A}, [\hat{A}, [\hat{A}, \hat{a}^\dagger]]] + \dots \quad (2.39)$$

and after some algebra:

$$\begin{aligned} S^\dagger a^\dagger S &= a^\dagger + \frac{1}{2!} |\xi|^2 a^\dagger - \xi^* a - |\xi|^2 \xi^* a \\ &= \hat{a}^\dagger \cosh(r) - \hat{a} e^{-i\theta} \sinh(r) \\ &= \mu \hat{a}^\dagger - \nu \hat{a}, \end{aligned} \quad (2.40)$$

where the quantity  $\mu$  and  $\nu$  are the same as in eqs. (2.38). The results in eq. (2.37) and in eq. (2.39) will be used in the next sections to evaluate expectation values of operators over quantum states.

### 2.3.1 Squeezing for a two-photon coherent state

A squeezed coherent state is obtained by the action of the squeezing operator on a displaced quantum state  $|\alpha\rangle$  and is often called a *two-photon coherent state* [3]:

$$\hat{S}(\xi)\hat{D}(\alpha)|0\rangle = |\xi, \alpha\rangle, \quad (2.41)$$

$$\langle 0|\hat{D}^\dagger(\alpha)\hat{S}^\dagger(\xi) = \langle \xi, \alpha|. \quad (2.42)$$

In order to prove that the state in eq. (2.41) is squeezed, it is very useful to calculate some quantities:

$$\begin{aligned} \langle \hat{a} \rangle &= \langle \xi, \alpha | \hat{a} | \xi, \alpha \rangle = \langle 0 | \hat{D}^\dagger(\alpha) \hat{S}^\dagger(\xi) \hat{a} \hat{S}(\xi) \hat{D}(\alpha) | 0 \rangle \\ &= \langle \alpha | \hat{S}^\dagger(\xi) \hat{a} \hat{S}(\xi) | \alpha \rangle = \alpha \cosh(r) - \alpha^* \exp^{-i\theta} \sinh(r), \end{aligned} \quad (2.43)$$

and:

$$\begin{aligned} \langle \hat{a}^2 \rangle &= \langle \xi, \alpha | \hat{a}^2 | \xi, \alpha \rangle = \langle 0 | \hat{D}^\dagger(\alpha) \hat{S}^\dagger(\xi) \hat{a}^2 \hat{S}(\xi) \hat{D}(\alpha) | 0 \rangle \\ &= \langle \alpha | \hat{S}^\dagger(\xi) \hat{a}^2 \hat{S}(\xi) | \alpha \rangle = \langle \alpha | \hat{S}^\dagger(\xi) \hat{a} \hat{S}(\xi) \hat{S}^\dagger(\xi) \hat{a} \hat{S}(\xi) | \alpha \rangle = \\ &= \alpha^2 \cosh^2(r) + (\alpha^*)^2 \exp^{-2i\theta} \sinh^2(r) - 2|\alpha|^2 \exp^{-i\theta} \sinh(r) \cosh(r) \\ &\quad - \exp^{-i\theta} \sinh(r) \cosh(r). \end{aligned} \quad (2.44)$$

Moreover we have that:

$$\langle (\hat{a}^\dagger)^2 \rangle = \langle \hat{a}^2 \rangle^*. \quad (2.45)$$

From the expectation values in eqs. (2.43-2.45) it is then possible to calculate the variances for the field quadratures eqs. (2.21):

$$\begin{aligned} (\Delta \hat{Q})^2 &= \langle \hat{Q}^2 \rangle - \langle \hat{Q} \rangle^2 \\ &= \cosh(2r) - \sinh(2r) \cos(\theta - 2\beta). \end{aligned} \quad (2.46)$$

The choice,  $\beta = \theta/2$  minimizes the variance of  $\hat{Q}$  in eq. (2.46) which then becomes:

$$(\Delta \hat{Q})^2 = \exp(-2r). \quad (2.47)$$

Similarly we can repeat the same calculation for the other quadrature and we obtain, by using the same choice as before for the angle  $\beta$  :

$$(\Delta \hat{P})^2 = \exp(+2r). \quad (2.48)$$

From formulas eqs. (2.47,2.48) it is clear that the fluctuations for the variable  $\hat{Q}$  are below those for the vacuum level, which are equal to one, while those for  $\hat{P}$  are bigger than the vacuum state fluctuations. On the other hand the product of uncertainties remains unity and it is then the minimum possible allowed by the Heisenberg's uncertainty principle. It is easy to see by combining eqs. (2.22,2.43) that for a vacuum squeezed-coherent state the expectation value of the electric field is zero:

$$\langle \hat{E}(r, t) \rangle = \langle \xi, 0 | \hat{E}(r, t) | \xi, 0 \rangle = 0. \quad (2.49)$$

Let us consider the mean number of photons in a *two-photon coherent state*:

$$\begin{aligned} \langle \xi, \alpha | \hat{a}^\dagger \hat{a} | \xi, \alpha \rangle &= \langle 0 | \hat{D}^\dagger(\alpha) \hat{S}^\dagger(\xi) \hat{a}^\dagger \hat{a} \hat{S}(\xi) \hat{D}(\alpha) | 0 \rangle = \langle \alpha | S^\dagger(\xi) \hat{a}^\dagger (S(\xi) S(\xi)^\dagger) \hat{a} S(\xi) | \alpha \rangle \\ &= \langle \alpha | [\hat{a}^\dagger \cosh(r) - \hat{a} \exp^{-i\theta} \sinh(r)] [\hat{a} \cosh(r) - \hat{a}^\dagger \exp^{i\theta} \sinh(r)] | \alpha \rangle \\ &= |\alpha|^2 (\cosh^2(r) + \sinh^2(r)) - (\alpha^*)^2 \sinh(r) \cosh(r) \exp^{i\theta} \\ &\quad - \alpha^2 \sinh(r) \cosh(r) \exp^{-i\theta} + \sinh^2(r), \end{aligned} \quad (2.50)$$

where we have used eqs. (2.40,2.37). For a squeezed vacuum state ( $|\alpha| = 0$ ):

$$\langle \xi, 0 | \hat{a}^\dagger \hat{a} | \xi, 0 \rangle = \sinh^2(r), \quad (2.51)$$

from which it is clear that a squeezed coherent vacuum state is not vacuum in the sense of a zero average photons number but only in the sense that the average value of the electric field is zero in such a state as it is shown in eq. (2.49).

### 2.3.2 Ideal squeezed states or displaced squeezed states

We have just seen that a *two-photon coherent state* can be obtained by acting with the squeezing operator  $\hat{S}(\xi)$  on a displaced quantum state  $|\alpha\rangle$ . Another way to produce a squeezed state of the electromagnetic field consists in acting on the vacuum state with the same operator but in the reverse order. The state that we obtain with such operation is:

$$\hat{D}(\alpha) \hat{S}(\xi) | 0 \rangle = |\alpha, \xi\rangle, \quad (2.52)$$

and is usually called an *ideal squeezed state* or a *displaced squeezed state*.

The states  $|\xi, \alpha\rangle$  and  $|\alpha, \xi\rangle$  are different from each other because the operators  $\hat{D}(\alpha)$  and  $\hat{S}(\xi)$  do not commute, but they can be related by the following relation [2]:

$$\begin{aligned} |\alpha, \xi\rangle &= |\xi, \alpha_+\rangle, \\ |\xi, \alpha\rangle &= |\alpha_-, \xi\rangle, \end{aligned} \quad (2.53)$$

where:

$$\alpha_\pm = \mu\alpha \pm \nu\alpha^*, \quad (2.54)$$

where  $\mu$  and  $\nu$  are given by eqs. (2.38). From eqs. (2.53) follows that since the *two-photon coherent state*  $|\xi, \alpha\rangle$  is squeezed, also the *ideal squeezed state*  $|\alpha, \xi\rangle$  is squeezed. The name *ideal* for the state  $|\alpha, \xi\rangle$  is made clear once that we calculate the expectation value of the annihilation operator  $\hat{a}$  on this state:

$$\langle \hat{a} \rangle = \langle \alpha, \xi | \hat{a} | \alpha, \xi \rangle = \alpha. \quad (2.55)$$

On the other hand we have already calculated the same value for the *two-photon coherent state* in eq. (2.43):

$$\langle \hat{a} \rangle = \langle \xi, \alpha | \hat{a} | \xi, \alpha \rangle = \alpha_- , \quad (2.56)$$

where we have used eq. (2.54). Since the quantity  $\langle \hat{a} \rangle$  gives an indication of the center of the phase space distribution for the state, we see from eqs. (2.55,2.56) the substantial difference between the *ideal* and the *two-photon coherent state*. For the  $|\alpha, \xi\rangle$  state, the action of the squeezing operator  $\hat{S}(\xi)$  makes the circle around the origin in the  $(Q, P)$  plane into an ellipse, which is then shifted of a quantity  $\alpha$  by the displacement operator  $\hat{D}(\alpha)$ . On the other hand for the  $|\xi, \alpha\rangle$  state, the action of the displacement operator  $\hat{D}(\alpha)$  shifts the circle in the origin of a quantity  $\alpha$  while the action of the squeezing operator  $\hat{S}(\xi)$  not just turns the circle in an ellipse but also has the effect to translate the center of the ellipse to the point  $\alpha_-$ . It is exactly the absence of this additional translation in the phase space that accounts for the name *ideal* used for the state  $|\alpha, \xi\rangle$ . These considerations have a pictorial representation in fig.(2.3.1) where the dimensions of circles and ellipses the noises in the  $Q$  and  $P$  quadratures.

Similarly to what we have done for the *two-photon coherent state* in section (2.3.1) we can show that the *ideal state*  $|\alpha, \xi\rangle$  in eq. (2.52) is indeed squeezed. Let us first introduce the following relations:

$$\begin{aligned} \hat{D}^\dagger(\alpha) \hat{a} \hat{D}(\alpha) &= \hat{a} + \alpha , \\ \hat{D}^\dagger(\alpha) \hat{a}^\dagger \hat{D}(\alpha) &= \hat{a}^\dagger + \alpha^* . \end{aligned} \quad (2.57)$$

From the relations in eqs. (2.57) we can easily calculate some quantity of interest. We have already calculated in eq. (2.55) the expectation value for the annihilation operator  $\hat{a}$  and we now move to evaluate the expectation value for the number operator  $\hat{n} = \hat{a}^\dagger \hat{a}$  :

$$\begin{aligned} \langle \alpha, \xi | \hat{n} | \alpha, \xi \rangle &= \langle 0 | \hat{S}^\dagger(\xi) \hat{D}^\dagger(\alpha) \hat{a}^\dagger \hat{a} \hat{D}(\alpha) \hat{S}(\xi) | 0 \rangle \\ &= \langle 0 | \hat{S}^\dagger(\xi) \hat{D}^\dagger(\alpha) \hat{a}^\dagger \hat{D}^\dagger(\alpha) \hat{D}(\alpha) \hat{a} \hat{D}(\alpha) \hat{S}(\xi) | 0 \rangle \\ &= |\alpha|^2 + \sinh^2(r) , \end{aligned} \quad (2.58)$$

where we have used the unitarity property of the displacement operator  $\hat{D}(\alpha)$  , namely:

$$\hat{D}^\dagger(\alpha) \hat{D}(\alpha) = \hat{D}(\alpha) \hat{D}^\dagger(\alpha) = 1 . \quad (2.59)$$

We can also calculate the variance  $(\Delta \hat{n})^2$  in the number of photons, which after some operator algebra can be cast in the following formula:

$$\langle \alpha, \xi | (\Delta \hat{n})^2 | \alpha, \xi \rangle = |\alpha \cosh(r) - \alpha^* \exp^{-i\theta} \sinh(r)|^2 + 2 \cosh^2(r) \sinh^2(r) . \quad (2.60)$$

It is than an easy task, but quite a boring one, to calculate the variances for the quadrature operators in eqs. (2.21). We only report the results:

$$(\Delta \hat{Q})^2 = \exp(-2r) , \quad (2.61)$$

$$(\Delta \hat{P})^2 = \exp(+2r) , \quad (2.62)$$

where we have made again the choice  $\beta = \theta/2$  . We conclude by saying that both states, the *two-photon coherent states*  $|\xi, \alpha\rangle$  and the *ideal squeezed states*  $|\alpha, \xi\rangle$ , are indeed squeezed as their names suggest.

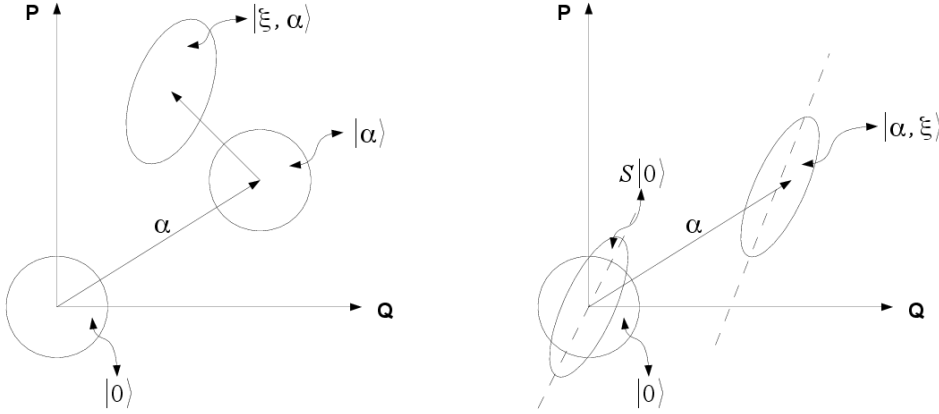


Figure 2.3.1: Generation starting from the vacuum state  $|0\rangle$  of (a) the *ideal squeezed state*  $|\alpha, \xi\rangle$  and (b) *two-photon coherent state*  $|\xi, \alpha\rangle$ .

## 2.4 Two-Mode Quadrature Squeezed States

It is possible to generate a two mode quadrature squeezed state [4]:

$$|\alpha_1, \alpha_2, \xi\rangle = \hat{D}(\alpha_1)\hat{D}(\alpha_2)\hat{S}(\xi)|0\rangle, \quad (2.63)$$

where:

$$\hat{S}(\xi) = e^{\xi^* \hat{a}_1 \hat{a}_2 - \xi \hat{a}_1^\dagger \hat{a}_2^\dagger}, \quad (2.64)$$

and  $\hat{D}(\alpha_i)$  are displacement operators and  $\xi = r e^{i\theta}$ . The transformation of the creation and destruction operators under the action of the operator  $\hat{S}(\xi)$  is the following:

$$S^\dagger a_1 S = a_1 + [A, a_1] + \frac{1}{2!} [A, [A, a_1]] + \frac{1}{3!} [A, [A, [A, a_1]]] + \dots$$

$$\begin{aligned} S^\dagger a_1 S &= a_1 + (\chi t) a_2^\dagger + \frac{1}{2!} (\chi t)^2 a_1 + \frac{1}{3!} (\chi t)^3 a_2^\dagger = \\ &= a_1 \cosh(\chi t) + a_2^\dagger \sinh(\chi t), \end{aligned} \quad (2.65)$$

and similarly for the others. We can summarize the results in the following way:

$$\begin{cases} S^\dagger a_1 S &= a_1 \cosh(r) + a_2^\dagger e^{i\theta} \sinh(r) \\ S^\dagger a_2 S &= a_2 \cosh(r) + a_1^\dagger e^{i\theta} \sinh(r) \\ S^\dagger a_1^\dagger S &= a_1^\dagger \cosh(r) + a_2 e^{-i\theta} \sinh(r) \\ S^\dagger a_2^\dagger S &= a_2^\dagger \cosh(r) + a_1 e^{-i\theta} \sinh(r). \end{cases} \quad (2.66)$$

The results summarized above are very important for the evaluation of expectation values of operators over quantum states. The generalized quadrature operators are defined as:

$$\begin{aligned} Q_\pm &= \frac{1}{\sqrt{2}} \left[ (a_1 e^{i\beta} \pm a_2^\dagger e^{-i\beta}) + c.c \right] = Q_1 \pm Q_2 \\ P_\pm &= \frac{i}{\sqrt{2}} \left[ (a_1 e^{i\beta} \mp a_2^\dagger e^{-i\beta}) + c.c \right] = P_1 \mp P_2. \end{aligned} \quad (2.67)$$

It is worth noting that since  $[Q_i, P_j] = i\delta_{ij}$  then:

$$[Q_\pm, P_\mp] = 0. \quad (2.68)$$

Hence the uncertainty relation imposes that the total variance for the linear combination of quadratures in eq. (2.68) is:

$$\langle (\Delta Q_\pm)^2 \rangle_\rho + \langle (\Delta P_\mp)^2 \rangle_\rho \geq 0. \quad (2.69)$$

From operator transformations eqs. (2.66) it can be found that, if the system starts in the vacuum state ( $\alpha_1 = \alpha_2 = 0$ ) the variances of the quadrature operators of eq. (2.67) are (in the simplified case  $\beta = 0$ ):

$$\begin{aligned} (\Delta Q_\pm)^2 &= e^{\pm 2r} \cos^2\left(\frac{\theta}{2}\right) + e^{\mp 2r} \sin^2\left(\frac{\theta}{2}\right) \\ (\Delta P_\pm)^2 &= e^{\pm 2r} \sin^2\left(\frac{\theta}{2}\right) + e^{\mp 2r} \cos^2\left(\frac{\theta}{2}\right), \end{aligned} \quad (2.70)$$

which show that, one we operate a choice for the phase of the pump field  $\theta$ , while the individual quadrature  $Q_i$  and  $P_i$  become very noisy for large squeezing parameter  $r$ , the relative position and the total momentum  $Q_\pm$  and  $P_\pm$  become quiet.

## 2.5 Quantum Entanglement

It is possible to associate to the state of a quantum system a projector operator such that:

$$|\psi\rangle \rightarrow \rho = |\psi\rangle\langle\psi|, \quad (2.71)$$

where  $\rho$  is called density operator relative to the pure state  $|\psi\rangle$ . The description of the system by  $|\psi\rangle$  or  $\rho$  is, in this case, equivalent, but the second tool is more general. Given an observable  $A$  and its eigenstates  $\{|a_j\rangle\}$ , it is possible to introduce the projectors on these states:

$$M_j = |a_j\rangle\langle a_j|, \quad (2.72)$$

hence the probability to find the system in a state  $|a_j\rangle$  after a measure of the observable  $A$  is given by:

$$p_j = Tr[M_j\rho], \quad (2.73)$$

and the expectation value of the observable  $A$  is given by:

$$\langle A \rangle = Tr[A\rho]. \quad (2.74)$$

Generally the physical state of a quantum system is not known with certainty, this is why it is useful to introduce a statistical approach. The system is no longer described by a pure state but by an ensemble of states (not necessarily orthogonal to each other), to which is associated a given probability:

$$\left\{ \begin{array}{l} |\psi_1\rangle \rightarrow p_1 \\ |\psi_2\rangle \rightarrow p_2 \\ \vdots \quad \quad \vdots \\ |\psi_n\rangle \rightarrow p_n \end{array} \right., \quad \sum_j p_j = 1 \quad (2.75)$$

In this case the expectation value for the operator  $A$  is given by a quantum and ensemble mean:

$$\langle A \rangle = \sum_j p_j \langle \psi_j | A | \psi_j \rangle. \quad (2.76)$$

Once we introduce the following definition of the density operator in the general case, as:

$$\rho = \sum_j p_j |\psi_j\rangle \langle \psi_j|, \quad (2.77)$$

it is possible to define the expectation value of  $A$  as:

$$\langle A \rangle = Tr[A\rho], \quad (2.78)$$

and the probability to measure the system in the state  $|\psi_j\rangle$  as:

$$p(a_j) = Tr[\rho M_j]. \quad (2.79)$$

The density operator  $\rho$  satisfies the following properties:

- (i)  $\rho$  is Hermitian
- (ii)  $\rho$  is non negative:

$$\langle \chi | \rho | \chi \rangle \geq 0 \quad \forall |\chi\rangle. \quad (2.80)$$

- (iii)  $\rho$  has unit trace:

$$Tr(\rho) = 1. \quad (2.81)$$

- (iv) The quantity  $P = Tr[\rho^2]$ , which is called purity, is such

$$0 \leq P \leq 1, \quad (2.82)$$

where  $P = 1$  only for pure states. It is possible to show that  $P$  is minimum when all the eigenvalues of  $\rho$  have the same value  $\lambda_j = 1/N$  (where  $N$  is the dimension of the system Hilbert space), in

this case we have  $P = 1/N$ . This case is the maximally mixed state, the one in which the lack of information is maximum. Hence we can set more precise extreme values for  $P$ :

$$\frac{1}{N} \leq P \leq 1. \quad (2.83)$$

Hence the purity  $P$  gives an indication about the degree of purity of a quantum state. The closer  $\rho$  to the unity, the closer the state to a pure quantum state.

Systems composed by different parts  $A, B, \dots, N$  are also represented by density operators, but now acting on a vectorial space  $H$  with a tensorial structure:

$$H = H_A \otimes H_B \otimes \dots \otimes H_N, \quad (2.84)$$

where  $H_A, H_B$  and  $H_N$  are the Hilbert spaces for each part.

It is in this tensor product spaces that the notion of entanglement arises but for the moment let us consider the case of bipartite systems, which are quantum systems composed of two subsystems that we call  $A$  and  $B$ . The Hilbert space is in this case:

$$H = H_A \otimes H_B. \quad (2.85)$$

If we call  $\rho_{AB}$  the density matrix of the composite system we can define a new density matrix, called *reduced density matrix*, for only one of the two subsystem. The reduced density matrix for the subsystem  $A$  is:

$$\rho_A = Tr_B[\rho_{AB}], \quad (2.86)$$

where  $Tr_B$  means the trace operation on system  $B$  degrees of freedom. In a completely symmetric way we can define the reduced density matrix for the system  $B$  as :

$$\rho_B = Tr_A[\rho_{AB}]. \quad (2.87)$$

Starting from the reduced density operator it is possible to introduce the notion of separable and entangled states.

### 2.5.1 Bipartite separability

Bipartite separable states are those which can be written as a convex combination of tensor products of density matrices, i.e. :  $\rho \in H_A \otimes H_B$  is separable if:

$$\rho = \sum_i p_i \rho_i^A \otimes \rho_i^B, \quad (2.88)$$

where  $p_i$  is a probability distribution. Alternatively, states that cannot be written in this form are called entangled. Let us consider, for example, the following pure state:

$$|\psi_{AB}\rangle = \frac{1}{\sqrt{2}}[|0_A 0_B\rangle + |1_A 1_B\rangle]. \quad (2.89)$$

The state in eq. (2.89) is an example of a bipartite entangled state. The density matrix of the system is:

$$\rho_{AB} = |\psi_{AB}\rangle\langle\psi_{AB}|, \quad (2.90)$$

while the reduced density matrices are:

$$\begin{aligned}\rho_A &= \frac{1}{2}[|0_A\rangle\langle 0_A| + |1_A\rangle\langle 1_A|] \\ \rho_B &= \frac{1}{2}[|0_B\rangle\langle 0_B| + |1_B\rangle\langle 1_B|].\end{aligned}\quad (2.91)$$

Hence while the state of the whole system is pure, the states for the individual subsystem are in a statistical mixture, which in this particular case is also a maximal mixture. As a matter of fact, while we have the maximum of information about the whole system, the information on the subsystems is minimal. This fact is clear if we consider the von Neumann entropy for the composite system which is:

$$S_{AB} = -tr\{\rho_{AB} \log_2 \rho_{AB}\} = 0, \quad (2.92)$$

while for the two subsystems:

$$S_A = S_B = -tr\{\rho_A \log_2 \rho_A\} = 1. \quad (2.93)$$

There exist a useful separability criterion for bipartite pure state [5, 6, 7] which makes use of the notion of Schmidt decomposition. Let us consider a bipartite system with dimensions  $d_A < d_B$ . A general state for the system can be written as:

$$|\psi\rangle = \sum_{n=1}^{d_A} \sum_{k=1}^{d_B} c_{n,k} |\alpha_n\rangle |\beta_k\rangle = \sum_{n=1}^{d_A} |\alpha_n\rangle |\bar{\phi}_n\rangle, \quad (2.94)$$

where  $|\alpha_n\rangle$  and  $|\beta_k\rangle$  are basis in  $A$  and  $B$  and the states  $|\bar{\phi}_n\rangle$  are defined as:

$$|\bar{\phi}_n\rangle = \sum_k c_{n,k} |\beta_k\rangle, \quad (2.95)$$

and they are not necessarily orthonormal. Let us consider the reduced density matrix relative to the state of smaller dimension:

$$\rho_A = Tr_B\{|\psi\rangle\langle\psi|\}, \quad (2.96)$$

and let us suppose we have chosen the base  $|\alpha_n\rangle$  such that  $\rho_A$  is diagonal in this base:

$$\rho_A = \sum_n p_n |\alpha_n\rangle\langle\alpha_n| = \sum_{n,m} \langle\bar{\phi}_m|\bar{\phi}_n\rangle |\alpha_n\rangle\langle\alpha_m|. \quad (2.97)$$

This hypothesis implies that  $\langle\bar{\phi}_m|\bar{\phi}_n\rangle = p_n \delta_{n,m}$  and hence:

$$|\phi_n\rangle = \frac{|\bar{\phi}_n\rangle}{\sqrt{p_n}}, \quad (2.98)$$

are orthonormal. In this way we can decompose the initial state in terms of the product of orthonormal vectors belonging to the two distinct subspaces:

$$|\psi\rangle = \sum_n \lambda_n |\phi_n\rangle_B |\alpha_n\rangle_A. \quad (2.99)$$

Using eq. (2.99) one can obtain the reduced density matrix for the subsystems:

$$\begin{aligned}\rho_A &= \sum_n \lambda_n^2 |\alpha_n\rangle\langle\alpha_n| \\ \rho_B &= \sum_n \lambda_n^2 |\phi_n\rangle\langle\phi_n|,\end{aligned}\tag{2.100}$$

that is,  $\rho_A$  and  $\rho_B$  have the same eigenvalues. It is possible to introduce a quantity called Schmidt number which indicate the number of non zero  $\lambda_n$ . The Schmidt number is related to the entanglement between the two subsystems. In particular:

- For separable states:  $m = 1$ .
- For entangled states:  $m > 1$ .
- For maximally entangled states:  $m = d_A$  with  $\lambda_n = \frac{1}{d_A}$ .

Although the Schmidt decomposition is a very useful criterion for measuring entanglement, it can be applied only to pure states. The first entanglement criterion for mixed states was proposed by A. Peres and uses the notion of partial transposition [8].

### 2.5.2 Separability criterion for mixed states

If we write a bipartite state  $\rho_{AB}$  in a product basis  $\{|ij\rangle\}$ :

$$\rho_{AB} = \sum_{ij,kl} \lambda_{ij,kl} |ij\rangle\langle kl|,\tag{2.101}$$

where  $\lambda_{ij,kl}$  are the matrix elements of  $\rho_{AB}$  in this basis, then the partial trasposition of  $\rho_{AB}$  is defined as:

$$\rho_{AB}^{T_B} = \sum_{ij,kl} \lambda_{ij,kl} |il\rangle\langle kj|.\tag{2.102}$$

Peres has shown that if  $\rho_{AB}$  is separable then  $\rho_{AB}^{T_B}$  is a positive operator, hence his criterion can be stated as follow: if  $\rho_{AB}^{T_B}$  has a negative eigenvalue,  $\rho_{AB}$  is entangled.

The Peres criterion is able to detect bipartite entangled states only for system of dimension smaller than 6. For higher dimension there exist entangled states with positive partial trasposition [9].

### 2.5.3 Separability criterion for continuous variables.

An inseparability criterion for two-mode continuous-variable systems was derived by R. Simon [10] and independently by Duan *et al* [11]. They found that for any separable continuous variable states the total variance of a pair of Einstein-Podolsky-Rosen (EPR) type operators is bounded from below by a certain value resulting from the uncertainty relation, while for entangled states this bound can be violated. Hence a violation of this bound provides a sufficient condition for inseparability of the state. In particular, if we consider a pair of EPR-like operators:

$$u = |a|x_1 + \frac{1}{a}x_2 \quad (2.103)$$

$$v = |a|p_1 - \frac{1}{a}p_2, \quad (2.104)$$

where  $a$  is a non-zero real number and  $x_i$  and  $p_j$  are such that  $[x_j, p_k] = i\delta_{jk}$  ( $j, k = 1, 2$ ), then for any **separable quantum state**  $\rho$  the following relation holds:

$$\langle(\Delta u)^2\rangle_\rho + \langle(\Delta v)^2\rangle_\rho \geq a^2 + \frac{1}{a^2}. \quad (2.105)$$

In particular for **inseparable states**, the total variance of eq. (2.105) is required by the uncertainty relation to be larger than or equal to  $|a^2 - \frac{1}{a^2}|$  which reduces to zero for  $a = 1$ .

The generalized quadratures of eqs. (2.67) are a realization of the EPR operators of eqs. (2.103-2.104) with the particular choice of  $a = 1$ . Hence the separability criterion for  $Q$  and  $P$  operators becomes:

$$\langle(\Delta Q)^2\rangle_\rho + \langle(\Delta P)^2\rangle_\rho \geq 2. \quad (2.106)$$

Since for a coherent or vacuum state  $\Delta Q = \Delta P = 1$ , we are sure that these orthogonal quadratures of the harmonic oscillator are correlated above the classical allowed limit.

On the other hand, if the state of the oscillator is a squeezed state starting from an initial vacuum state we know from eqs. (2.67) (with the choice  $\theta = 0$ ) that:

$$(\Delta Q_\pm)^2 = e^{\pm 2r} \quad (2.107)$$

$$(\Delta P_\pm)^2 = e^{\mp 2r}. \quad (2.108)$$

Hence applying the separability criterion to the quadratures  $Q_- = Q_1 - Q_2$  and  $P_+ = P_1 + P_2$  one obtains:

$$\langle(\Delta Q_-)^2\rangle + \langle(\Delta P_+)^2\rangle = 2e^{-2r} \leq 2. \quad (2.109)$$

In particular the minimum value allowed by quantum mechanics (which corresponds to the maximum correlation) is attained for  $r \rightarrow \infty$ . In general we get imperfect correlation between orthogonal quadratures of the oscillators, these correlations being always below what is permitted classically.

## 2.6 Introduction to Parametric Amplifiers

In the absence of an optical resonator no oscillations take place and the only phenomena are single pass interactions inside the nonlinear crystal. This is the simplest situation we can analyze. In this case the system is defined to be a *parametric amplifier* and the net result is the amplification of the field at frequency  $\omega_s$  (*signal* field) by pumping the crystal with a coherent beam at frequency  $\omega_p$  (pump beam). As specified in paragraph 2.1.2 an input seed at frequency  $\omega_i$  (*idler* field) can be injected inside the crystal to stimulate the parametric amplification process. To describe the *parametric amplifier* we make use of the *parametric down conversion process* in which a pump photon of frequency  $\omega_p$  is annihilated and two photons at frequencies  $\omega_s$  and  $\omega_i$  are generated.

Conservation of energy and momentum require the frequencies and momentum of the photons to satisfy the following relations:

$$\begin{aligned}\omega_p &= \omega_s + \omega_i \\ \vec{k}_p &= \vec{k}_i + \vec{k}_s,\end{aligned}\tag{2.110}$$

where  $k_\xi$  is the wave vector for the  $\xi$ -field.

The nonlinear Hamiltonian which describes the evolution of the the three fields is [4]:

$$H_{NL} = \sum_{\xi} \hbar\omega_{\xi} a_{\xi}^{\dagger} a_{\xi} + i\hbar\chi^{(2)}(a_p^{\dagger} a_s a_i - a_p a_s^{\dagger} a_i^{\dagger}),\tag{2.111}$$

where  $a_{\xi}$  is the annihilation operator for the electromagnetic field  $\xi$ -mode oscillating at frequency  $\omega_{\xi}$ . The commutation relations for the bosonic operators of the fields are:

$$\begin{aligned}[a_{\xi}, a_l] &= 0 \\ [a_{\xi}, a_l^{\dagger}] &= \delta_{\xi,l}.\end{aligned}\tag{2.112}$$

The first term in the Hamiltonian eq. (2.111) describes the free evolution of three independent harmonic oscillators which are modes of interest of the electromagnetic field. The second part of the same Hamiltonian represents the nonlinear interaction of the three modes which is responsible for the *parametric down conversion process*.

When the pump field is provided by a laser source, as usually happens in the vast majority of experiments, and the non-linear interaction is weak (which is a very usual condition since the nonlinear susceptibility  $\chi^{(2)}$  is very low), the pump amplitude is not significantly depleted during the short time of interaction in the crystal and we are allowed to replace the bosonic operator  $a_p$  with a classical amplitude  $A_p$ . The validity of this approximation is restricted to the following limit [12]:

$$\begin{aligned}\chi^{(2)}\tau &\rightarrow 0 \\ A_p &\rightarrow \infty\end{aligned}\tag{2.113}$$

which imposes a large amplitude for the pump field in such a way that it is minimally affected by traversing the crystal and at the same time a small conversion efficiency, which is obtained by requiring that  $\chi^{(2)}\tau$  is small. The two conditions in eq. 2.113 can be summarized in the following way:

$$\chi^{(2)}\tau A_p = \text{constant},\tag{2.114}$$

where  $\tau$  is the interaction time inside the crystal.

### 2.6.1 Degenerate Parametric Amplifier

When the *idler* and *signal* fields have the same frequency  $\omega$  and polarization the the system operates in the so called *degenerate* configuration. In this case the two modes are no longer

distinguishable and we can describe them with a single boson annihilation operator  $a$ . The Hamiltonian for this system is:

$$H = \hbar\omega a^\dagger a + i\hbar\frac{\chi}{2}(a^\dagger{}^2 e^{-2i\omega t} - a^2 e^{2i\omega t}), \quad (2.115)$$

where we have considered a classical pump beam of frequency  $2\omega$  and we have collected in the parameter  $\chi$ , the pump amplitude  $A_p$  and the nonlinear susceptibility  $\chi^{(2)}$ :

$$\chi = \chi^{(2)} A_p. \quad (2.116)$$

In the interaction picture we have the time independent Hamiltonian:

$$H = i\hbar\frac{\chi}{2}(a^\dagger{}^2 - a^2), \quad (2.117)$$

and hence in this representation the unitary operator for the time evolution of the degenerate parametric amplifier is:

$$U(t) = e^{\left[\frac{\chi t}{2}(a^\dagger{}^2 - a^2)\right]}. \quad (2.118)$$

Comparison with eq. (2.29) shows that  $U(t)$  is the unitary squeezing operator  $S(\xi)$  with  $\xi = -\chi t$ . Since the nonlinear Hamiltonian in eq. (2.115) is responsible for the squeezing of the mode  $a$  we are now able to give a physical interpretation of the *two-photon coherent state* described by eq. (2.41). This state, which is obtained by first displacing the vacuum and then squeezing it, can be achieved by pumping a non-linear crystal with a coherent laser field of amplitude  $A_p$  and simultaneously injecting a coherent field at the frequency of the mode we want to squeeze.

An obvious physical interpretation can be given also for a squeezed coherent vacuum. Such a state can be generated by injecting a pump laser field in a non-linear crystal governed by a degenerate parametric amplifier interaction Hamiltonian (2.115) but this time there is no need for the injection of another coherent field at the frequency of the mode we want to squeeze.

On the other hand the realization of a *displaced squeezed state* described in eq. (2.52) can be achieved by either combining a squeezed vacuum (obtained as previously described) with a coherent field (local oscillator) at a beam splitter matching the frequency of the squeezed vacuum, or by injecting the squeezed vacuum in a laser amplifier for the squeezed mode.

From the discussion in 2.3.1 and 2.3.2 we can obtain the squeezing amount in the quadrature fields for a state initially in the vacuum or in a coherent state for which  $(\Delta\hat{Q})^2 = (\Delta\hat{P})^2 = 1$ :

$$\begin{aligned} (\Delta\hat{Q})^2 &= \exp(-2\chi t) \\ (\Delta\hat{P})^2 &= \exp(2\chi t). \end{aligned} \quad (2.119)$$

Hence the parametric amplifier affects the amount of noise of the system. In particular it reduces the noise in the  $Q$  quadrature and increases the noise in the  $P$  quadrature. Equations (2.119) show that the de-amplified quadrature has less quantum noise than the vacuum level and that the amount of noise reduction is proportional to the strength of the nonlinearity, the amplitude of the pump and the interaction time. In particular, once we have chosen the nonlinear crystal and hence the  $\chi^{(2)}$  coefficient it is possible to increase the noise reduction by increasing  $A_p$  and the interaction time  $t$ . The interaction time can be increased, for example, by placing the nonlinear crystal in a resonant cavity.

The quantum evolution of quadratures themselves is affected. The Heisenberg equations of motion for the operators  $a$  and  $a^\dagger$  in the interaction picture are:

$$\begin{aligned}\frac{da}{dt} &= \frac{1}{i\hbar} [a, H] = \chi a^\dagger \\ \frac{da^\dagger}{dt} &= \frac{1}{i\hbar} [a^\dagger, H] = \chi a.\end{aligned}\tag{2.120}$$

The solution to this equation is:

$$a(t) = a(0) \cosh(\chi t) + a^\dagger(0) \sinh(\chi t).\tag{2.121}$$

In terms of the field quadratures defined by eqs. (2.21), the Heisenberg equations of motions (2.120) diagonalize:

$$\begin{aligned}\frac{dQ}{dt} &= \chi Q \\ \frac{dP}{dt} &= -\chi P.\end{aligned}\tag{2.122}$$

The equations for the quadratures demonstrate that the parametric amplifier is phase sensitive because it amplifies one quadrature and attenuates the other:

Again, by using the results of 2.3.1 and 2.3.2 it is possible to analyze the photon statistics produced by the parametric amplifier. In particular we have for a *displaced squeezed state* eq. (2.52) a mean number of photons given by:

$$\langle \alpha, \xi | \hat{n} | \alpha, \xi \rangle = |\alpha|^2 + \sinh^2(\chi t),\tag{2.123}$$

and a variance in the photon number given by:

$$\langle \alpha, \xi | (\Delta \hat{n})^2 | \alpha, \xi \rangle = |\alpha \cosh(\chi t) - \alpha^* \exp^{-i\theta} \sinh(\chi t)|^2 + 2 \cosh^2(\chi t) \sinh^2(\chi t).\tag{2.124}$$

From eqs. (2.123, 2.124) we argue that if the mode  $a$  is initially in a coherent vacuum state ( $\alpha = 0$ ), there is an amplification of the photon number and at the same time of the vacuum fluctuations. After a time  $t$   $\sinh^2(\chi t)$  photons are generated. An interesting result concern the photon number distribution for an initial coherent vacuum state ( $\alpha = 0$ ) [13]:

$$\begin{aligned}p_{2n+1} &= 0 \quad n = 0, 1, 2, \dots \\ p_{2n} &= \binom{2n}{n} \frac{1}{2^{2n} \cosh \chi t} (\tanh \chi t)^{2n}.\end{aligned}\tag{2.125}$$

The absence of an odd photon number distribution in eq. (2.125) is a manifestation of the fact that the squeezed vacuum, by its nature, originates from a two photon process and hence can only contain pairs of photons.

### 2.6.2 Non Degenerate Parametric Amplifier

The condition of non degeneracy is achieved when the fields generated by the nonlinear interaction are distinguishable. This condition can be realized either if the *signal* and *idler* fields have different frequencies or equal frequencies but different polarization. The Hamiltonian for the process of non degenerate parametric amplification is the following:

$$H = \hbar\omega_s \hat{a}_s^\dagger \hat{a}_s + \hbar\omega_i \hat{a}_i^\dagger \hat{a}_i + i\hbar\chi \left( \hat{a}_s^\dagger \hat{a}_i^\dagger e^{-2i\omega t} - \hat{a}_s \hat{a}_i e^{2i\omega t} \right), \quad (2.126)$$

where again we have considered a classical pump beam of frequency  $2\omega$ . The Hamiltonian of eq. (2.126) is a particular case of eq. (2.111) where only the signal and idler fields are considered as quantum fields while the pump is treated as a classical field. Hence, in the interaction picture the unitary operator for time evolution of the non degenerate parametric amplifier is:

$$U(t) = e^{[\chi t(\hat{a}_s^\dagger \hat{a}_i^\dagger - \hat{a}_s \hat{a}_i)]}. \quad (2.127)$$

Again comparison with eq. (2.63) shows that  $U(t)$  is the unitary squeezing operator  $S(\xi)$  with  $\xi = -\chi t$ . Hence the Hamiltonian of eq. (2.126) is responsible for the quadrature squeezing that we have analyzed in paragraph 2.4. In particular from the previous analysis it is clear that the squeezing is due to quantum correlations in the signal and idler modes. Moreover it is possible to show that the individual modes are not squeezed.

In the end we can argue from eqs. (2.70) that the squeezed fields are not the  $a_s$  and  $a_i$  separately but their combinations:

$$\begin{aligned} X_+ &= \frac{1}{\sqrt{2}}(a_s + a_i) \\ X_- &= \frac{i}{\sqrt{2}}(a_s - a_i). \end{aligned} \quad (2.128)$$

At this point one can make clear the connection between squeezing and entanglement. Assume that we induce an evolution of the entangled oscillator  $A$  and  $B$  by the action of a unitary operator:

$$R = \exp\left[\frac{\pi}{4}(ab^\dagger - a^\dagger b)\right]. \quad (2.129)$$

This means, in the Heisenberg picture that the boson operators are transformed as:

$$\begin{aligned} a_1 &= R^\dagger a R = (b + a)/\sqrt{2} \\ a_2 &= R^\dagger b R = (b - a)/\sqrt{2}. \end{aligned} \quad (2.130)$$

In terms of the new independent operators  $a_1$  and  $a_2$ , the two-mode squeezing operator is written as:

$$S_{AB}(z) = \exp\left(\frac{z^*}{2}a_1^2 - \frac{z}{2}a_1^{\dagger 2} - \frac{z^*}{2}a_2^2 + \frac{z}{2}a_2^{\dagger 2}\right) = S_1(z)S_2(-z), \quad (2.131)$$

that is, as two individual squeezing operators for each of the new modes. These relations shows that one can entangle two oscillators by squeezing them along two orthogonal direction in phase space, and then make them interact according to the unitary operator in eq. (2.129) which correspond to a 50/50 beam splitter. Hence one can generate two entangled optical beams by mixing in a beam splitter two beams that have been previously squeezed.

## 2.7 Conclusions

In this chapter I have introduced very important concepts in quantum optics, such as squeezing and entanglement and the connection between them. I have also shown how squeezed states of the electromagnetic field can be obtained via a three fields interaction in a non-linear crystal. The last part of the chapter has been devoted to the standard study of optical parametric amplifiers (OPA) and their squeezing properties, in both the degenerate and non-degenerate case. All the results included in the present chapter are standard in quantum optics text-books but usually the derivation of the final results is left to the reader.

## Bibliography

- [1] P. N. Butcher and D. Cotter, *The Elements of Nonlinear Optics*, Cambridge University Press (1990).
- [2] L. Mandel and E. Wolf, *Optical Coherence and Quantum Optics*, Cambridge University Press (1995).
- [3] H. P. Yuhen, Phys. Rev. A **13**, 2226 (1976).
- [4] D. F. Walls and Gerard J. Milburn, *Quantum Optics*, (Springer, Berlin, 2008).
- [5] E. Schmidt, Math. Ann. **63**, 433 (1907).
- [6] A. Ekert and P. Knight, Am. J. Physics, **63**.
- [7] M. A. Nielsen and I. L. Chuang, *Quantum Computation and Quantum Information* (Cambridge Univ. Press, 2000).
- [8] A. Peres, Phys. Rev. Lett. **77**, 1413 (1996).
- [9] P. Horodecki, Phys. Rev. A **54**, 1838 (1996).
- [10] R. Simon, Phys. Rev. Lett. **84**, 2726 (2000).
- [11] L. M. Duan, G. Giedke, J. I. Cirac and P. Zoller, Phys. Rev. Lett. **84**, 2722 (2000).
- [12] M. O. Scully and M. S. Zubairy, *Quantum Optics*, Cambridge University Press (2008).
- [13] U. Leonhard, *Measuring the Quantum State of Light*, Cambridge Univ. Press (1997).

## Measuring Squeezing in Optical Parametric Oscillators

This chapter is dedicated to the problem of the detection of squeezed light through the ordinary and balanced homodyne detection schemes. The input-output formulation of optical cavities will be explained and both the Heisenberg-Langevin and master equation approaches to the optical cavities problem will be analyzed. Then the last part of the chapter will deal with application of these theoretical approaches to the case of a triply resonant OPO (TROPO) in the below threshold degenerate and non-degenerate cases. All the notions introduced in this chapter will be crucial to the understanding of Chapter 4.

### 3.1 Introduction to Optical Parametric Oscillators

In Chapter 1 we illustrated the process of parametric down conversion in which a pump photon of frequency  $\omega_p$  splits in two photons at different frequencies  $\omega_s$  (signal) and  $\omega_i$  (idler) such that  $\omega_p = \omega_s + \omega_i$  by interacting with a second order nonlinear crystal. The spontaneous emission which is intrinsic in this process is driven by the vacuum fluctuations of the electromagnetic field and produces two photons which have a strong correlation in energy and momentum. The power of the signal and idler fields can be enhanced by using a classical beam of frequency  $\omega_s$  thus stimulating the emission of photons at the frequency of the idler beam. If the active medium is put in an optical cavity the parametric interaction can overcome the effect of losses thus producing oscillation. This device is called an Optical Parametric Oscillator (OPO). OPOs were initially used as laser sources due to their wide tunability properties, particularly useful for application in spectroscopy [1]. Nowadays there are available OPOs for the downconversion of pulsed laser beams, used as light sources in the range between 330 and 2000 nm. These devices are used as coherent light sources in regions of the spectra where no effective laser medium is available, converting light of Nd:YAG lasers into the mid infrared region [2]. On the other hand quantum properties of the light emitted from these sources have been investigated and make OPOs among the most used devices for the production of non classical state of light in quantum technologies.

The simplest configuration of an OPO is obtained by using a singly resonant cavity (SROPO), in which the cavity resonates only the signal field while the pump and idler beams make a single pass interaction in the nonlinear crystal and exit the cavity without any feedback. The doubly resonant configuration (DROPO), in which both signal and idler beams are resonated in the cavity, can be used in order to reduce the oscillation threshold. While the SROPO allows a broad continuous variation of the signal and idler wavelength in the phase matching range, the threshold power is much higher when compared with DROPO. On the other hand the double resonant condition and

the energy conservation condition have the effect to limit the output modes to a discrete set of values.

The threshold power can be reduced further by using a cavity which is also resonant to the pump beam, thus obtaining a triply resonant OPO (TROPO). This type of configuration reduced the threshold power to 1 *mW* for CW operation in KTP [3], while the use of new materials reduced the power to 300  $\mu$ W with quasi phase matched crystal (QPM) [4].

## 3.2 Photo-Electric Detection of Squeezed Light

In this Chapter we will review some results for the non-classical aspects of the light produced with OPOs devices with particular attention to quadrature squeezing effect in the case of TROPOs systems, but we need first to show how quantum squeezing measurement can be achieved for a general quantum field. This is why in the present section we review the principles of the photo-electric detection of squeezed light.

The principal object is the spectral density of photocurrent fluctuations defined by [5]:

$$\Phi(\omega) = \int_{-\infty}^{+\infty} \langle \Delta i(t) \Delta i(t + \tau) \rangle e^{-i\Omega\tau} d\tau, \quad (3.1)$$

where the autocorrelation function for the current fluctuations is given by:

$$\langle \Delta i(t) \Delta i(t + \tau) \rangle = \langle i(t) i(t + \tau) \rangle - \langle i \rangle^2. \quad (3.2)$$

We consider the situation in which a field  $A(t)$  is responsible for a sequence of photo-electric emissions. The time axis is broken into a series of small intervals  $\Delta t$  (only zero or one event is possible within the interval  $\Delta t$ ), with  $p_k$  as the coordinate of the  $k$ th time interval. In particular  $p_k$  is a random variable, with  $p_k = 0$  for no photo-ionization occurring at time  $t_k$  within  $\Delta t$ , and  $p_k = 1$  for the occurrence of an event at  $t_k$  within  $\Delta t$ . The photo-current  $i(t)$  can be written as:

$$i(t) = \sum_k Q(t - t_k) p_k, \quad (3.3)$$

with  $Q(t)$  indicating the shape of the current pulse that results from the emission at time  $t = 0$ . The autocorrelation of the current becomes:

$$\begin{aligned} \langle i(t) i(t + \tau) \rangle &= \left\langle \sum_{k=-\infty}^{k=\infty} Q(t - t_k) p_k \sum_{j=-\infty}^{j=\infty} Q(t + \tau - t_j) p_j \right\rangle \\ &= \sum_k Q(t - t_k) Q(t + \tau - t_k) \langle p_k \rangle \\ &+ \sum_{k \neq j} Q(t - t_k) Q(t + \tau - t_j) \langle p_k p_j \rangle, \end{aligned} \quad (3.4)$$

where we have used the fact that  $p_i^2 = p_i$ . The expectation values in eq. (3.4) can be related to the properties of the input field by noting that:

$$\langle p_1 p_2 \dots p_k \rangle = W_k(t_1, t_2, \dots, t_k) \Delta t_1 \Delta t_2 \dots \Delta t_k, \quad (3.5)$$

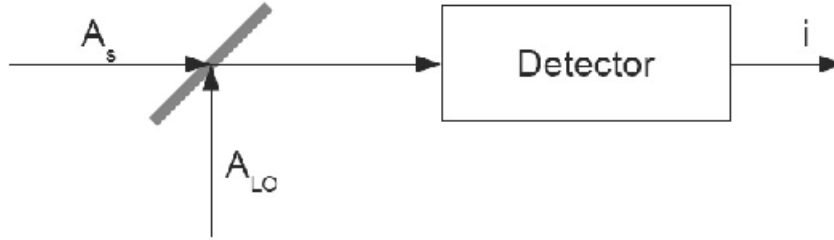


Figure 3.2.1: Schematic diagram for ordinary homodyne detection. The transmittivity  $T$  of the beam splitter is such that  $T \gg R$ .

where  $W_k(t_1, t_2, \dots, t_k)$  is the joint probability per unit time for photoemission in  $t_1$  to  $t_1 + \Delta t_1$  and  $t_2$  to  $t_2 + \Delta t_2$  and  $\dots$   $t_k$  to  $t_k + \Delta t_k$  and is related to the statistical properties of the incident field by [2]:

$$W_k(t_1, t_2, \dots, t_k) = \alpha^k \langle : I(t_1) I(t_2) \dots I(t_k) : \rangle, \quad (3.6)$$

where  $I$  is the field operator  $A^\dagger A$ , the colons indicate normal and time ordering and  $\alpha$  is the detection quantum efficiency. Hence passing to the continuous limit and assuming that:

$$Q(t - t') = Q_0 \delta(t - t'), \quad (3.7)$$

we find the following result for the autocorrelation function of  $i(t)$ :

$$\langle i(t) i(t + \tau) \rangle = Q_0^2 \alpha \langle : I(\tau) : \rangle \delta(\tau) + Q_0^2 \alpha^2 \langle : I(t) I(t + \tau) : \rangle. \quad (3.8)$$

Thus:

$$\langle \Delta i(t) \Delta i(t + \tau) \rangle = Q_0^2 \alpha \langle : I(\tau) : \rangle \delta(\tau) + Q_0^2 \alpha^2 C(\tau), \quad (3.9)$$

where:

$$C(\tau) = \langle : I(t) I(t + \tau) : \rangle - \langle : I(t) : \rangle^2. \quad (3.10)$$

In eq. (3.9) there are two contributions to the autocorrelation of the photo-current. The first term arises from the self-correlation of individual random photo-emissions and express the obvious result that the product of the current with an identical copy of itself ( $\tau = 0$ ) will yield a non-zero correlation independently from the distribution of the pulses. The second term addresses the question of the manner by which the intensity correlations of incident field modify this basic overlap near  $\tau = 0$  due to the correlated photo-electric emissions and specify the range in  $\tau$  over which correlations persists.

### 3.2.1 Ordinary Homodyne Detection

Equation (3.9) is the basic result which we will now apply to the detection of squeezing. In this detection scheme two fields  $A_{LO}$  (local oscillator) and  $A_s$  (signal field) are combined at a beam

splitter of high transmission  $t$  for the signal field  $A_s$ . A small fraction  $r$  of the local oscillator field is reflected and combined with  $A_s$  to give an output field  $A$  from the beam splitter for subsequent photo-detection (see fig.(3.2.1)), with:

$$A = rA_{LO} + tA_s. \quad (3.11)$$

We assume a coherent state for  $A_{LO}$ , with  $\langle A_{LO} \rangle = A_0 e^{-i(\omega_{LO}t + \theta)}$  and take  $rA_0$  to be large compared to either the mean value of the signal field or of its fluctuations (strong local oscillator limit). Keeping only the leading terms in  $A_0$ , and choosing the frequency of the local oscillator field  $A_{LO}$  equal to the frequency of the signal field  $A_s$  ( $\omega_{LO} = \omega_s$ ) we are able to find the following result:

$$\begin{aligned} C(\tau) &= RTA_0^2 [e^{-2i\theta} \langle A_s(t + \tau), A_s(t) \rangle + e^{2i\theta} \langle A_s^\dagger(t), A_s^\dagger(t + \tau) \rangle \\ &\quad + \langle A_s^\dagger(t), A_s(t + \tau) \rangle + \langle A_s^\dagger(t + \tau), A_s(t) \rangle], \end{aligned} \quad (3.12)$$

where  $R = r^2$  and  $T = t^2$ . After the introduction of the quadrature phase amplitude of the signal field:

$$X_\theta(t) = A_s(t)e^{-i\theta} + A_s^\dagger(t)e^{i\theta}, \quad (3.13)$$

the correlation function of eq. (3.12) can be written in the following compact form:

$$C(\tau) = RTA_0^2 \langle : X_\theta(t), X_\theta(t + \tau) : \rangle. \quad (3.14)$$

Equation (3.14) once it is inserted in eq. (3.9) gives:

$$\langle \Delta i(t) \Delta i(t + \tau) \rangle = Q_0 i_0 [\delta(\tau) + \alpha T \langle : X_\theta(t), X_\theta(t + \tau) : \rangle], \quad (3.15)$$

where  $i_0 = Q_0 \alpha R A_0^2$  is the mean photocurrent. The Fourier transform of eq. (3.15) then gives the spectral density  $\Phi(\Omega, \theta)$  for photocurrent fluctuations at the Fourier component  $\Omega$  for a specified local oscillator phase relative to the signal  $A_s$  input:

$$\Phi(\Omega, \theta) = Q_0 i_0 [1 + \alpha T S_s(\Omega, \theta)], \quad (3.16)$$

where the spectrum of squeezing  $S_s(\Omega, \theta)$  is defined by:

$$S_s(\Omega, \theta) = \int \langle : X_\theta(t), X_\theta(t + \tau) : \rangle e^{-i\Omega\tau} d\tau. \quad (3.17)$$

Remembering that the theoretical signature of nonclassical squeezed light is that  $S_s(\Omega, \theta) < 0$  for some phase  $\theta$ , we can say that the experimental signature of squeezed light is the finding  $\Phi(\Omega, \theta) < 1$  for some  $\theta$ .

It is important to note that a non-perfect transmission of the beam splitter ( $T \neq 1$ ) and a non-perfect efficiency of the detector ( $\alpha \neq 1$ ) will reduce the squeezing amount respect to the optimal value  $S_s(\Omega, \theta) = -1$ . In particular the ratio  $R(\Omega, \theta)$  of  $\Phi(\Omega, \theta)$  in the presence of squeezing to  $\Phi(\Omega, \theta)$  with a vacuum-state input for the signal field ( $|A_s\rangle = |0\rangle$ ) is simply:

$$R(\Omega, \theta) = 1 + \alpha T S_s(\Omega, \theta). \quad (3.18)$$

At this point we can show how squeezing manifests itself in sub-Poissonian statistics in homodyne detection. First of all let recall that a field  $i(t)$  shows a sub-Poissonian statistics whenever:

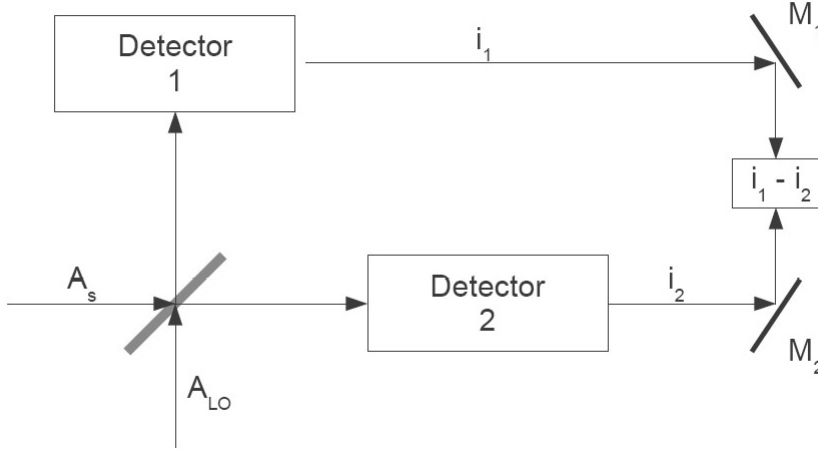


Figure 3.2.2: Schematic diagram for balanced homodyne detection.  $M_1$  and  $M_2$  are two perfectly reflecting mirrors, and the beam splitter is a 50% reflecting and 50% transmitting.

$$\overline{(i^2(t))} - \left(\overline{i(t)}\right)^2 < \overline{i(t)}. \quad (3.19)$$

Now eq. (3.15) can be written as:

$$\langle i(t)i(t+\tau) \rangle - \langle i \rangle^2 = Q_0 i_0 [\delta(\tau) - \alpha T + \alpha T \langle X_\theta(t), X_\theta(t+\tau) \rangle], \quad (3.20)$$

where we have used the fact that:

$$\langle : X_\theta(t), X_\theta(t+\tau) : \rangle = \langle X_\theta(t), X_\theta(t+\tau) \rangle - 1. \quad (3.21)$$

Remembering that for squeezed light  $\langle X_\theta(t), X_\theta(t) \rangle < 1$  we can see that for  $\tau = 0$  eq. (3.20) implies a sub-Poissonian statistics. Note, however, that the intensity measurements in homodyne detection are different from those in direct detection, in fact intensity fluctuations in this case measure the fluctuations in a quadrature of the field and the signal and its variance depends upon the local oscillator phase angle, which is an external parameter.

### 3.2.2 Balanced Homodyne Detection

The second case that we will consider in this section is the balanced homodyne detection scheme. In this case the beam splitter is 50% transmitting and 50% reflecting and gives two fields ( $A_1$  and  $A_2$ ), which are both detected to produce photo-currents ( $i_1$  and  $i_2$ ), which are then combined to give  $i_\pm = i_1 \pm i_2$  (see fig.(3.2.2)). Now the objects of interest are the spectral densities  $\Phi_\pm(\Omega, \theta)$ , defined as:

$$\Phi_\pm(\Omega, \theta) = \int \langle \Delta i_\pm(t) \Delta i_\pm(t+\tau) \rangle e^{-i\Omega\tau} d\tau. \quad (3.22)$$

Specializing the result for  $i_-$  we find:

$$\begin{aligned}
 \langle \Delta i_{\pm}(t) \Delta i_{\pm}(t + \tau) \rangle &= \alpha_1 Q_1^2 \langle : I_1(t) : \rangle \delta(\tau) + \alpha_2 Q_2^2 \langle : I_2(t) : \rangle \delta(\tau) \\
 &+ \alpha_1^2 Q_1^2 C_{11}(\tau) + \alpha_2^2 Q_2^2 C_{22}(\tau) \\
 &- \alpha_1 \alpha_2 Q_1 Q_2 [C_{12}(\tau) + C_{21}(\tau)] ,
 \end{aligned} \tag{3.23}$$

where  $Q_1$  and  $Q_2$  are the total charges for the two detectors  $D_1$  and  $D_2$  and their quantum efficiencies are  $\alpha_1$  and  $\alpha_2$ , respectively. The functions  $C_{ij}(\tau)$  are generalizations of the previously defined function  $C(\tau)$  and are given by:

$$C_{ij}(\tau) = \langle : A_i^\dagger(t) A_j^\dagger(t + \tau) A_j(t + \tau) A_i(t) : \rangle , \tag{3.24}$$

with  $i, j = 1, 2$  referring to the total fields  $(A_1, A_2)$  which are incident upon detectors  $(D_1, D_2)$ . In the limit of a strong local oscillator in a coherent state with  $\langle A_{LO} \rangle = A_0 e^{-i(\omega_{LO} t + \theta)}$ , we find after evaluating each of the functions  $C_{ij}$  and after taking the Fourier transform, the result:

$$\Phi_-(\Omega, \theta) = Q_0 i_0 [1 + \alpha \eta^2 S_s(\Omega, \theta)] , \tag{3.25}$$

with  $S_s(\Omega, \theta)$  refers to the spectrum of squeezing for the signal field at the input of the balanced detectors. We have also assumed an ideal detectors arrangement in the sense that  $\alpha_1 = \alpha_2 = \alpha$  and  $Q_1 = Q_2 = Q_0$ . The factor  $\eta^2$  takes into account the spatial overlap of the signal and local oscillator fields across the face of the photo-detector, and is given by:

$$\eta = \left| \int \int d^2 r u^*(r) \cdot v(r) \right| , \tag{3.26}$$

where  $u(r)$  and  $v(r)$  are the normalized mode functions for the signal and local oscillator fields ( $\int \int d^2 r |u(r)|^2 = 1$ ).

Once again one can introduce the ratio  $R(\Omega, \theta)$  of  $\Phi_-(\Omega, \theta)$  in the presence of squeezing to  $\Phi_-(\Omega, \theta)$  with a vacuum-state input for the signal field ( $|A_s\rangle = |0\rangle$ ):

$$R(\Omega, \theta) = 1 + \alpha \eta^2 S_s(\Omega, \theta) , \tag{3.27}$$

where the term “1” gives the shot noise term which is determined by blocking the input field  $A_s$ .

The advantage of balanced homodyne detection over ordinary homodyne detection is due to the fact that this scheme eliminates the large local oscillator term of the fluctuations in the ordinary case by taking the photocurrent difference between the two exit ports.

### 3.3 Input-Output Formulation of Optical Cavities

In order to describe the effect of an OPO cavity the system must be imagined as merged into an heat bath made up of infinite harmonic oscillators. This ensemble of oscillators describes the damping of a field mode inside a cavity with lossy mirrors and consists of a large number of phonon-like modes in the mirrors [6].

The quantum mechanical Hamiltonian for the system in the rotating-wave approximation is:

$$H = H_{sys} + H_{bath} + H_{int} , \tag{3.28}$$

where  $H_{sys}$  is the Hamiltonian for the system under consideration and that we will leave undefined for the moment;  $H_{bath}$  is the free energy of bosonic heat bath modes  $c(\omega)$  providing a description

of the field external to the cavity and coupled to the signal because of non-perfect reflection of the mirrors [7];  $H_{int}$  in the Hamiltonian (3.28) represents the interaction of the mode with this heat bath, describing the damping of the mode caused by the non-zero transmittivity of the cavity. In the rotating wave approximation, these terms have explicit forms given by:

$$H_{bath} = \hbar \int_{-\infty}^{\infty} d\omega \omega c^\dagger(\omega) c(\omega), \quad (3.29)$$

$$H_{int} = i\hbar \int_{-\infty}^{\infty} d\omega \kappa(\omega) [c^\dagger(\omega)a - c(\omega)a^\dagger]. \quad (3.30)$$

Two main idealizations have been made in the form of the Hamiltonian eqs. (3.29,3.30), the rotating wave approximation and the fact that the range of integration over frequencies extends from  $(-\infty, +\infty)$  rather than from  $(0, \infty)$ . These approximations are closely connected as follows [8].

- Without the rotating wave approximation the form of  $H_{int}$  would be:

$$H_{int} = i\hbar \int_{-\infty}^{\infty} d\omega \kappa(\omega) [c^\dagger(\omega) + c(\omega)] [a - a^\dagger]. \quad (3.31)$$

The smallness of  $H_{int}$  is such that the motion of the operators  $a$  and  $a^\dagger$  is governed by the free Hamiltonian and hence the time dependence of  $a^\dagger$  is of the form  $e^{i\Omega t}$ . Then terms like  $a^\dagger c^\dagger(\omega)$  have a time dependence of the form  $e^{i(\omega+\Omega)t}$  which is rapidly oscillating while  $a c^\dagger(\omega)$  has a time dependence of the form  $e^{i(\omega-\Omega)t}$  which is almost constant near resonance  $\omega = \Omega$ .

- Only terms which are almost resonant are important and this allows one to extend the lower limit to  $-\infty$ . Note that this extension is possible only in the rotating wave approximation.
- These simplifications generate a very simple formalism which is a formulation of white noise.

We also consider the following commutation relations for the mode  $a$  and  $c$ :

$$\begin{aligned} [a, a^\dagger] &= 1, \\ [c(\omega), c^\dagger(\omega')] &= \delta(\omega - \omega'), \end{aligned} \quad (3.32)$$

while all the other commutators are identically zero. The Heisenberg equation of motion for the bath operator  $c(\omega)$  is:

$$\frac{dc(\omega)}{dt} = -\frac{i}{\hbar} [c(\omega), H] = -i\omega c(\omega) + \kappa(\omega)a. \quad (3.33)$$

The solution to eq. (3.33) may be written in two ways depending on whether we choose to solve in terms of initial conditions at time  $t_0 < t$  (input) or in terms of the final conditions at time  $t_1 > t$  (output). The two solutions are, respectively:

$$c(\omega) = c_0(\omega)e^{-i\omega(t-t_0)} + \kappa(\omega) \int_{t_0}^t dt' e^{-i\omega(t-t')} a(t'), \quad (3.34)$$

$$c(\omega) = c_1(\omega)e^{-i\omega(t-t_1)} - \kappa(\omega) \int_{t_0}^t dt' e^{-i\omega(t-t')} a(t'), \quad (3.35)$$

where  $b_0(\omega)$  is the value of  $b(\omega)$  at  $t = t_0$  and  $b_1(\omega)$  is the value of  $b(\omega)$  at  $t = t_1$ .

The Heisenberg equation for the mode  $a$  is:

$$\begin{aligned}
 \frac{da}{dt} &= -\frac{i}{\hbar} [a_s, H] \\
 &= -\frac{i}{\hbar} \{[a, H_{sys}] + [a, H_{bath}] + [a, H_{int}]\} \\
 &= -\frac{i}{\hbar} [a, H_{sys}] - \int_{-\infty}^{+\infty} d\omega \kappa(\omega) e^{-i\omega(t-t_0)} c_o(\omega) \\
 &\quad - \int_{-\infty}^{+\infty} d\omega \kappa^2(\omega) \int_{t_0}^t dt' e^{-i\omega(t-t')} a(t').
 \end{aligned} \tag{3.36}$$

At this point it is usual to choose  $\kappa(\omega)$  independent of frequency. This introduces the first approximation necessary to obtain the Markov process. Thus we set:

$$\kappa^2(\omega) = \frac{\gamma}{\pi}. \tag{3.37}$$

We also define an input field operator:

$$a_{in}(t) = -\frac{1}{\sqrt{2\pi}} \int_{-\infty}^{+\infty} d\omega e^{-i\omega(t-t_0)} c_0(\omega), \tag{3.38}$$

which satisfies the following commutation relation:

$$[a_{in}(t), a_{in}^\dagger(t')] = \delta(t - t'). \tag{3.39}$$

At this point it is an easy task to find the Heisenberg equation for the mode  $a$  starting from eq. (3.36):

$$\frac{da}{dt} = -\frac{i}{\hbar} [a, H_{sys}] - \gamma a(t) + \sqrt{2\gamma} a_{in}(t). \tag{3.40}$$

To derive the eq. (3.40) we have used the following properties of the Dirac Delta:

1.  $\int_{-\infty}^{+\infty} d\omega e^{-i\omega(t-t')} = 2\pi\delta(t - t')$
2.  $\int_{t_0}^t dt' f(t')\delta(t - t') = \int_t^{t_1} dt' f(t')\delta(t - t') = \frac{1}{2}f(t) \quad (t_0 < t < t_1)$

The eq. (3.40) is a Langevin equation for a damped amplitude  $a(t)$  in which the noise term appears explicitly as the input field. In a similar manner we may express the solution in terms of the final condition and we get the time-reversed Langevin equation:

$$\frac{da}{dt} = -\frac{i}{\hbar} [a, H_{sys}] + \gamma a(t) - \sqrt{2\gamma} a_{out}(t). \tag{3.41}$$

At this point it is possible to derive a relation between the external and intracavity fields, known as input-output relation, by subtraction of eq. (3.40-3.41) [7, 9]:

$$a_{out}(t) + a_{in}(t) = \sqrt{2\gamma} a(t). \tag{3.42}$$

It is interesting to note that the presence of the noise operator  $a_{in}(t)$  in eq. (3.40) is necessary to preserve the commutation relation for the mode operator  $a(t)$  at all times:

$$[a(t), a^\dagger(t)] = 1. \quad (3.43)$$

Moreover the presence of the noise term along with the damping term in eq. (3.40) is also a manifestation of the fluctuation-dissipation theorem of statistical mechanics. Dissipation phenomena are always accompanied by fluctuations.

From the statistical properties of the heath bath, described by the operator  $c(\omega)$ , it is now possible to derive the statistical properties of the input field  $a_{in}(t)$ . Let us suppose, for example, that the heat bath is in thermal equilibrium at temperature  $T$ , then we have [6]:

$$\begin{aligned} \langle c(0, \omega) \rangle_R &= \langle c^\dagger(0, \omega) \rangle_R = 0 \\ \langle c^\dagger(0, \omega) c(0, \omega') \rangle_R &= \delta(\omega - \omega') \bar{n}(\omega) \\ \langle c(0, \omega) c^\dagger(0, \omega') \rangle_R &= (\bar{n}(\omega) + 1) \delta(\omega - \omega') \\ \langle c(0, \omega) c(0, \omega') \rangle_R &= \langle c^\dagger(0, \omega) c^\dagger(0, \omega') \rangle_R = 0, \end{aligned} \quad (3.44)$$

where the term  $\bar{n}(\omega)$  is the mean number of heath bath quanta at frequency  $\omega$  and is described by the Planck distribution:

$$\bar{n}(\omega) = \frac{1}{e^{h\omega/kT} - 1}. \quad (3.45)$$

From now on we will consider the case in which the heat bath is at zero temperature so that:

$$\bar{n}(\omega) = 0. \quad (3.46)$$

From eqs. (3.43, 3.46) and the definition of the input noise in eq. (3.38) we obtain:

$$\begin{aligned} \langle a_{in}(t) \rangle_R &= \langle a_{in}^\dagger(t) \rangle_R = 0 \\ \langle a_{in}^\dagger(t) a_{in}(t') \rangle_R &= 0 \\ \langle a_{in}(t) a_{in}^\dagger(t') \rangle_R &= \delta(t - t') \\ \langle a_{in}(t) a_{in}(t') \rangle_R &= \langle a_{in}^\dagger(t) a_{in}^\dagger(t') \rangle_R = 0. \end{aligned} \quad (3.47)$$

The first and second order correlations in eqs. (3.47) are a formalization of a particular noise, which in literature is called *white noise*.

Very useful relations can be obtained for the two-time normally ordered correlation functions of the output field  $a_{out}$  in terms of the input noise field  $a_{in}$  and the intracavity field  $a$  in the case of coherent or vacuum input [9]:

$$\begin{aligned} \langle a_{out}^\dagger(t), a_{out}(t') \rangle &= 2\gamma \langle a^\dagger(t), a(t') \rangle \\ \langle a_{out}(t), a_{out}(t') \rangle &= 2\gamma \langle : a(t), a(t') : \rangle \\ \langle a_{out}^\dagger(t), a_{out}^\dagger(t') \rangle &= 2\gamma \langle : a^\dagger(t), a^\dagger(t') : \rangle, \end{aligned} \quad (3.48)$$

where the symbol  $(: :)$  means time ordering and must be intended in the sense that annihilation operators are ordered with earlier times to the right, while creation operators are ordered with earlier times to the left [10]. In eqs. (3.48) the following notation has been used:

$$\langle U, V \rangle = \langle UV \rangle - \langle U \rangle \langle V \rangle. \quad (3.49)$$

A natural extension of eq. (3.40) and of the input-output relations of eq. (3.42) requires the introduction, for each loss mechanism, of a damping term of the form  $\gamma a(t)$  and a noise term of the form  $\sqrt{2\gamma}a_{in}(t)$ .

### 3.4 Heisenberg-Langevin Treatment for a TROPO

The method of section 3.3 can be applied to the case of the nonlinear Hamiltonian of eq. (2.115). This is what we are going to do in the present and next sections in order to show how one can apply all the physical concepts and mathematics previously illustrated to a concrete case. The derivation of the main results is not original but nevertheless very pedagogical and will be useful for a better understanding of some of the results in the next chapters. The Heisenberg-Langevin equations for the intracavity modes are:

$$\begin{aligned} \frac{da_s}{dt} &= -\gamma a_s + \chi^{(2)} a_p a_i^\dagger + \sqrt{2\gamma} A_s(t) \\ \frac{da_i}{dt} &= -\gamma a_i + \chi^{(2)} a_p a_s^\dagger + \sqrt{2\gamma} A_i(t) \\ \frac{da_p}{dt} &= -\gamma a_p - \chi^{(2)} a_i a_s + A_p + \sqrt{2\gamma_p} a_p^{in}(t), \end{aligned} \quad (3.50)$$

where  $A_p$  represent the external coherent pump field and we have considered an equal loss rate  $\gamma$  for the signal and idler fields. In eqs. (3.50) we have considered the case in which two coherent beams (seeds) are injected inside the cavity as input for the signal and the idler modes. The input signal and idler fields entering the mirror are:

$$A_\xi(t) = A + a_\xi^{in}(t), \quad \xi = s, i, \quad (3.51)$$

$A$  representing the non-zero mean amplitude of the seed and  $a_\xi^{in}(t)$  the vacuum fluctuations contribution. These equations are nonlinear in the bosonic operators and are usually solved by linearization of operator  $a$  around the stationary values using the following representation [11]:

$$a \rightarrow \alpha + \delta a. \quad (3.52)$$

The steady state amplitude  $\alpha$  is obtained by eqs. (3.50) when considering  $da/dt = 0 = a^{in}(t)$ . Letting  $\alpha = \alpha_s = \alpha_i$ , we obtain the following equation:

$$\alpha^3 - \frac{\chi^{(2)} A_p - \gamma \gamma_p}{(\chi^{(2)})^2} \alpha = 0. \quad (3.53)$$

From eq. (3.53) we argue that the solution for the steady state depends on the value of  $A_p$ .

In particular, for  $A_p \leq A_{th} = \gamma \gamma_p / \chi^{(2)}$  there is only one stable solution,  $\alpha = 0$ . In this case the system is said to be below threshold and the pump stationary value is  $\alpha_p = A_p / \gamma_p$ .

If  $A_p \geq A_{th} = \gamma \gamma_p / \chi^{(2)}$  the steady state values for  $\alpha_s$  and  $\alpha_i$  exhibit a pitchfork bifurcation and eq. (3.53) admits non null stable solution:

$$\alpha = \pm \sqrt{2 \left( \frac{A_p}{\chi^{(2)}} - \frac{\gamma_p \gamma}{(\chi^{(2)})^2} \right)} = \pm \left[ \frac{2}{\chi^{(2)}} (A_p - A_{th}) \right]^{1/2}, \quad (3.54)$$

and the pump stationary value is  $\alpha_p = \gamma/\chi^{(2)}$ . The existence of a threshold condition expresses the fact that in presence of losses, the pump has to be strong enough so that the losses effect can be compensated by the parametric amplification in the nonlinear crystal.

### 3.4.1 The Below-Threshold Degenerate Case

The linearization of eqs. (3.50) around the below-threshold steady state ( $\alpha_\xi = 0$ ,  $\alpha_p = A_p/\gamma_p$ ) is obtained by considering the pump as an undepleted beam of amplitude  $\alpha_p = A_p/\gamma_p$  and neglecting the quantum equation for the mode  $a_p$ . Moreover in the following we will consider the case of unseeded OPO for which  $A = 0$ . Since  $\alpha_\xi = 0$ , the equation for the operators  $a_\xi$  and those for their fluctuations coincide:

$$\frac{da_\xi}{dt} = -\gamma a_\xi + \Sigma a_\xi^\dagger + \sqrt{2\gamma} a_\xi^{in}(t), \quad \xi = s, i, \quad (3.55)$$

with  $\Sigma = \chi^{(2)} A_p / \gamma_p$ .

In the case of degenerate OPO (DOPO) that we are considering in this section, the equations for  $a_s$  and  $a_i$  become indistinguishable. Up to now we have considered the case in which the only loss mechanism is due to the only coupling mirror of the optical cavity (single ended cavity). More general results can be obtained if we consider a double ended cavity or if we take into account other loss mechanisms, such as crystal absorption and diffraction. In the following  $\gamma_1$  will indicate the damping associated to the cavity input mirror and  $\gamma_2$  the damping associated to the other loss mechanisms. Hence Langevin eq. (3.55) generalizes into:

$$\frac{da}{dt} = \Sigma a^\dagger - (\Gamma + \nu\psi) a + \sqrt{2\gamma_1} a^{in}(t) + \sqrt{2\gamma_2} b^{in}(t), \quad (3.56)$$

where  $\Gamma = \gamma_1 + \gamma_2$ ,  $\psi$  is the detuning of mode  $a$  with respect to cavity resonance and  $a^{in}$  and  $b^{in}$  are the input field due to  $\gamma_1$  and  $\gamma_2$ . The field outside the cavity, which is the one of interest, can be obtained by using the input-output relation of eq. (3.42) with  $\gamma = \gamma_1$  and by going to the Fourier space. In this case the Langevin equation for the operators  $a$  and  $a^\dagger$  become an algebraic equation which can be easily solved. The result for the output field  $a^{out}(\omega)$  is [7]:

$$\begin{aligned} a^{out}(\omega) &= \frac{[(\gamma_1 - \nu\psi)^2 - (\gamma_2 - \nu\psi)^2 + \Sigma^2] a^{in}(\omega) + 2\Sigma\gamma_1 a^{in\dagger}(-\omega)}{(\Gamma - i\omega) + \psi^2 - \Sigma^2} \\ &+ 2\sqrt{\gamma_1\gamma_2} \frac{(\Gamma - i\omega - \nu\psi) b^{in}(\omega) + \Sigma b^{in\dagger}(-\omega)}{(\Gamma - i\omega) + \psi^2 - \Sigma^2}. \end{aligned} \quad (3.57)$$

At this point it is possible to calculate the squeezing spectra which is obtained by the following expression:

$$\langle \Delta X_\theta \rangle^2 = (1 + 4\langle : \Delta X_\theta^2 : \rangle). \quad (3.58)$$

For zero detuning ( $\psi = 0$ ) it has been shown that [7]:

$$\begin{aligned} S_+(\omega) &= \langle \Delta X^{out}(\omega) \rangle^2 = \left( 1 + 4 \frac{\gamma_1 \Sigma}{(\Gamma - \Sigma)^2 + \omega^2} \right) \\ S_-(\omega) &= \langle \Delta Y^{out}(\omega) \rangle^2 = \left( 1 - 4 \frac{\gamma_1 \Sigma}{(\Gamma + \Sigma)^2 + \omega^2} \right), \end{aligned} \quad (3.59)$$

while the quadrature variance product is:

$$\langle \Delta X^{out}(\omega) \rangle^2 \langle \Delta Y^{out}(\omega) \rangle^2 = \left( 1 + \frac{16\gamma_1\gamma_2\Sigma^2}{((\Gamma - \Sigma)^2 + \omega^2)((\Gamma + \Sigma)^2 + \omega^2)} \right), \quad (3.60)$$

The eqs. (3.57) show that the output fields exhibit a noise enhancement for the amplitude quadrature  $X^{out}$  and noise reduction on the phase quadrature  $Y^{out}$ . The optimal noise reduction correspond to the case  $\omega = 0$  (cavity resonance) and for a pump amplitude equal to the threshold value, say for  $\Sigma = \Gamma$ :

$$\langle \Delta Y^{out}(0) \rangle^2 = \left( 1 - \frac{\gamma_1}{\Gamma} \right). \quad (3.61)$$

For the ideal case in which the only loss mechanism is due to the coupling mirror ( $\gamma_2 = 0$ ), the OPO output has a complete noise suppression:

$$\langle \Delta Y^{out}(0) \rangle^2 = 0. \quad (3.62)$$

For double ended cavity the squeezing level is optimized by the choice  $\gamma_1 = \gamma_2 \neq 0$ , known as symmetrical cavity. In this case, which is the best obtainable for a given choice of  $\gamma_1$  and  $\gamma_2$ , the noise level in the squeezed quadrature is:

$$\langle \Delta Y^{out}(0) \rangle^2 = \frac{1}{2}, \quad (3.63)$$

which is one half of the input state noise 1.

The prediction of zero noise level at threshold for a single ended cavity with no detuning is unphysical because it implies an infinite noise in the amplitude quadrature  $X^{out}$  which is impossible. The heart of the problem resides in the linearization procedure used to obtain these results and a perturbative approach shows that the nonlinear corrections become important in the region close to threshold, hence correcting the bad behaviour of the squeezing spectra in this regime [12].

### 3.4.2 The Below-Threshold Non-Degenerate Case

In this section we will consider the case of a non-degenerate OPO (NOPO) below threshold of oscillation and in frequency degenerate condition with cross polarized signal and idler fields. Moreover we will extend the results to the general case of a seeded NOPO. The steady state value for the pump and signal-idler fields are:

$$\begin{aligned} \alpha_p &= \frac{\gamma}{\chi^{(2)}} - \frac{A}{\sqrt{2\gamma}\chi^{(2)}\alpha} \\ 0 &= \alpha^3 - \frac{\chi^{(2)}A_p - \gamma\gamma_p}{(\chi^{(2)})^2}\alpha - \frac{\gamma_p A}{\sqrt{2\gamma}(\chi^{(2)})^2}. \end{aligned} \quad (3.64)$$

In the case  $A = 0$  the equations for signal and idler fields reduce to those for the unseeded NOPO while in the case  $A \neq 0$  where the threshold becomes [13]:

$$A_{th} = \frac{\gamma\gamma_p}{\chi^{(2)}} + 3 \left( \frac{A^2\gamma_p}{4\chi^{(2)}} \right)^{1/3}. \quad (3.65)$$

Below threshold of oscillation eq. (3.64) has only one stable solution which remains stable even above threshold where the system admits two other solutions, one stable and the other unstable. Equations (3.74) can be linearized around the steady state solution for the pump  $\alpha_p$  and signal-idler fields  $\alpha$  to obtain:

$$\begin{aligned} \frac{d\delta a_\xi}{dt} &= -\gamma\delta a_\xi + \chi^{(2)}\alpha_p\delta a_\xi^\dagger + \alpha\delta a_p + \sqrt{2\gamma}a_\xi^{in} \\ \frac{d\delta a_p}{dt} &= -\gamma_p\delta a_p - \chi^{(2)}[\delta a_s + \delta a_i] + \sqrt{2\gamma_p}a_p^{in}, \end{aligned} \quad (3.66)$$

where we explicitly used the fluctuations of the fields because the steady state values for signal and idler are different from zero and hence the equations for the fields and for fluctuations are different. The coupled eqs. (3.66) can be diagonalized by introducing the fields  $d_\pm = \frac{1}{\sqrt{2}}(a_s \pm a_i)$  and their quadratures  $X_\pm$  and  $Y_\pm$ .

In the case  $A = 0$  we have:

$$\begin{aligned} \frac{d\delta X_\pm}{dt} &= -(\gamma \mp \chi^{(2)}\alpha_p)\delta X_\pm + \sqrt{2\gamma}X_\pm^{in} \\ \frac{d\delta Y_\pm}{dt} &= -(\gamma \pm \chi^{(2)}\alpha_p)\delta Y_\pm + \sqrt{2\gamma}Y_\pm^{in}, \end{aligned} \quad (3.67)$$

The squeezing spectra for  $\delta X_\pm$  and  $\delta Y_\pm$  outside the cavity have been calculated and the result is [14]:

$$\begin{aligned} S_+(\omega) &= \left( 1 + 4 \frac{\chi^{(2)}\alpha_p\gamma}{(\gamma - \chi^{(2)}\alpha_p)^2 + \omega^2} \right) = \langle \Delta\delta X_+^{out}(\omega) \rangle^2 = \langle \Delta\delta Y_-^{out}(\omega) \rangle^2 \\ S_-(\omega) &= \left( 1 - 4 \frac{\chi^{(2)}\alpha_p\gamma}{(\gamma + \chi^{(2)}\alpha_p)^2 + \omega^2} \right) = \langle \Delta\delta X_-^{out}(\omega) \rangle^2 = \langle \Delta\delta Y_+^{out}(\omega) \rangle^2. \end{aligned} \quad (3.68)$$

Equations (3.68) show that the field combination  $d_+$  is antisqueezed on the amplitude quadrature while it is squeezed on the phase quadrature, where perfect noise suppression occurs at threshold,  $\chi^{(2)}\alpha_p = \gamma$ . Conversely, the field combination  $d_-$  is antisqueezed on the phase quadrature while it is squeezed on the amplitude quadrature.

On the other hand the fluctuations of the signal and idler fields are phase insensitive and satisfy the following relation:

$$S(\omega) = \frac{(\gamma^2 + (\chi^{(2)}\alpha_p)^2 + \omega^2)^2 + 4\gamma^2(\chi^{(2)}\alpha_p)^2}{(\gamma^2 - (\chi^{(2)}\alpha_p)^2 - \omega^2)^2 + 4\gamma^2\omega^2}. \quad (3.69)$$

This equation demonstrates that signal and idler fields are not individually squeezed but only the measure of the combination  $d_\pm$  shows non classical effect.

## 3.5 Master Equation Approach to Optical Cavities

An alternative method to include loss mechanisms in optical processes is described in this section. Once again the system of interest will be considered as being coupled to a heat bath or reservoir. Hence one can derive an operator master equation for the density operator in the Schrödinger or interaction picture. Equations of motion for the expectation values of the system operators may be derived from the operator master equation. Hence using the quasi-probability representation for the density operator [15, 8], the operator master equation can be converted to a c-number Fokker-Planck equation, then using method familiar in stochastic precesses the Fokker-Planck equation can be converted into an equivalent set of stochastic differential equations. In this Chapter we will analyze the case of TROPO and we will show a well known general result whereby the evolution equations of the Wigner field amplitudes are the same as the Heisenberg equations of motion of the quantum field amplitudes, whenever these are linear.

### 3.5.1 Master Equation Approach for a TROPO

The Heisenberg picture Hamiltonian that describes this open system is given by [16]:

$$\begin{aligned}
 H &= \sum_{i=0}^2 \hbar\omega_i a_i^\dagger a_i + i\hbar\chi \left( a_1^\dagger a_2^\dagger a_0 - a_1 a_2 a_0^\dagger \right) \\
 &+ i\hbar \left( E e^{-i\omega_0 t} a_0^\dagger - E^* e^{i\omega_0 t} a_0 \right) \\
 &+ \sum_{i=0}^2 a_i \Gamma_i^\dagger + a_i^\dagger \Gamma_i,
 \end{aligned} \tag{3.70}$$

where  $E$  is the external coherent driving pump field at frequency  $\omega_0$ . The operators  $a_0$ ,  $a_1$  and  $a_2$  represent the pump, signal and idler fields, respectively. They satisfy the following frequency matching condition:

$$\omega_0 = \omega_1 + \omega_2. \tag{3.71}$$

The terms  $\Gamma_i$  represent damping reservoir operators which are a useful description of the non-perfect reflection of the fields on the cavity mirrors:

$$\Gamma_i = \sum_j b_j e^{-\omega_j t}, \tag{3.72}$$

where  $b_j$  are boson annihilation operators for the thermal bath and  $\chi$  is the nonlinear coupling constant due to the second order polarizability of the nonlinear crystal.

The master equation for the reduced density operator, after tracing out the heat bath is given by [16]:

$$\begin{aligned}
 \frac{\partial \rho}{\partial t} &= -\imath \sum_{i=0}^2 \omega_i [a_i^\dagger a_i, \rho] + \chi [a_1^\dagger a_2^\dagger a_0, \rho] - \chi [a_1 a_2 a_0^\dagger, \rho] \\
 &+ E e^{-i\omega_0 t} [a_0^\dagger, \rho] - E^* e^{i\omega_0 t} [a_0, \rho] \\
 &+ \sum_{i=0}^2 \gamma_i \left( 2a_i \rho a_i^\dagger - a_i^\dagger a_i \rho - \rho a_i^\dagger a_i \right), \tag{3.73}
 \end{aligned}$$

which is valid for a heat bath at thermal equilibrium at temperature  $T = 0$ .

The density matrix can be treated in a much simpler way as a quasi-probability distribution in phase space. We can use a Wigner distribution of the field in phase space, where one has the replacement of the operators  $(a_i, a_i^\dagger)$  of the fields by complex amplitudes  $(\alpha_i, \alpha_i^*)$ . The density matrix is also replaced by a quasi-probability distribution in phase space, leading to Fokker-Planck equation [15]. An important characteristic of the Wigner representation is that the operators are replaced by classical variables that can be interpreted as an average value plus a fluctuation term. This leads to a simple interpretation of the field as a classical field with added vacuum fluctuations. The crucial properties of the Wigner representation is that the ensemble average of any polynomial of the random variables  $\alpha$  and  $\alpha^*$  weighted by the Wigner density corresponds to the Hilbert-space expectation of the corresponding symmetrized product of the annihilation and creation operators  $a$  and  $a^\dagger$ , respectively. That is:

$$\begin{aligned}
 \langle P(\alpha, \alpha^*) \rangle &= \int P(\alpha, \alpha^*) W(\alpha, \alpha^*) d^{2M} \alpha \\
 &= \text{Tr} \{ \rho S [P(a, a^\dagger)] \}, \tag{3.74}
 \end{aligned}$$

where  $M$  is the number of  $\alpha$  variables and  $S[\ ]$  means symmetrization, which consists of taking the average of all possible orderings of the operators. For instance:

$$S [a^\dagger a] = 1/2 [a^\dagger a + a a^\dagger]. \tag{3.75}$$

We can write the master equation (2.111) in the Wigner representation by using the following characteristic function:

$$\begin{aligned}
 \chi_w(z, z^*) &= \text{Tr}(\rho e^{\imath z^* a^\dagger + \imath z a}) \\
 &= \text{Tr}(\rho e^{\imath z^* a^\dagger} e^{\imath z a} e^{-|z|^2/2}), \tag{3.76}
 \end{aligned}$$

so that the Wigner distribution can be written as a Fourier transform of the characteristic function:

$$W(\alpha, \alpha^*) = \frac{1}{\pi^2} \int_{-\infty}^{+\infty} d^2 z \chi_w(z, z^*) e^{\imath z^* \alpha^\dagger} e^{\imath z \alpha}. \tag{3.77}$$

The phase space Wigner equation for the TROPO that correspond to the master equation (2.111) is:

$$\begin{aligned}
\frac{\partial W(\{\alpha_j\})}{\partial t} = & \left\{ \frac{\partial}{\partial \alpha_0} (\imath\omega_0\alpha_0 + \gamma_0\alpha_0 + \chi\alpha_1\alpha_2 - Ee^{-\imath\omega_0 t}) \right. \\
& + \frac{\partial}{\partial \alpha_0^*} (-\imath\omega_0\alpha_0^* + \gamma_0\alpha_0^* + \chi\alpha_1^*\alpha_2^* - E^*e^{\imath\omega_0 t}) \\
& + \frac{\partial}{\partial \alpha_1} (\imath\omega_1\alpha_1 + \gamma_1\alpha_1 - \chi\alpha_2^*\alpha_0) \\
& + \frac{\partial}{\partial \alpha_1^*} (-\imath\omega_1\alpha_1^* + \gamma_1\alpha_1^* - \chi\alpha_2\alpha_0^*) \\
& + \frac{\partial}{\partial \alpha_2} (\imath\omega_2\alpha_2 + \gamma_2\alpha_2 - \chi\alpha_1^*\alpha_0) \\
& + \frac{\partial}{\partial \alpha_2^*} (-\imath\omega_2\alpha_2^* + \gamma_2\alpha_2^* - \chi\alpha_1\alpha_0^*) \\
& + \gamma_0 \frac{\partial^2}{\partial \alpha_0 \partial \alpha_0^*} + \gamma_1 \frac{\partial^2}{\partial \alpha_1 \partial \alpha_1^*} + \gamma_2 \frac{\partial^2}{\partial \alpha_2 \partial \alpha_2^*} \\
& \left. + \frac{\chi}{4} \left( \frac{\partial^3}{\partial \alpha_1 \alpha_2 \alpha_0^*} + \frac{\partial^3}{\partial \alpha_1^* \alpha_2^* \alpha_0} \right) \right\} W(\{\alpha_j\}), \tag{3.78}
\end{aligned}$$

where the vector  $\{\alpha_j\}$  has six terms for the fields and their complex conjugates  $(\alpha_1, \alpha_1, \alpha_3, \alpha_1^*, \alpha_2^*, \alpha_3^*)$ . This is not a Fokker-Planck equation due to the third order derivative term, but in the case  $\chi$  is small enough this term can be dropped. The truncated equation obtained in such a way is a genuine Fokker-Planck equation with positive definite diffusion term and eq. (3.78) can be written in the following way:

$$\begin{aligned}
\frac{\partial W(\{\alpha_j\})}{\partial t} = & - \sum_{j=1}^3 \frac{\partial}{\partial \alpha_j} A_j W(\{\alpha_j\}) \\
& + \frac{1}{2} \sum_{j,k} \frac{\partial}{\partial \alpha_j} \frac{\partial}{\partial \alpha_k} [BB^T]_{jk} W(\{\alpha_j\}), \tag{3.79}
\end{aligned}$$

where the vector  $A$  is called the drift vector, and the matrix product  $BB^T$  is the diffusion matrix.

The Fokker-Planck equation (3.79) is equivalent to a set of Stochastic Differential Equation (SDE), also known as Langevin equations:

$$\frac{d\alpha_j}{dt} = A_j + [B\xi(t)]_j, \tag{3.80}$$

where  $\xi(t)$  is a vector of fluctuating variables  $\xi_i(t)$  with zero mean value  $\langle \xi_i(t) \rangle = 0$  and the property that:

$$\langle \xi_i(t) \xi_j(t') \rangle = \delta_{ij} \delta(t - t'), \tag{3.81}$$

In the rotating frame ( $\tilde{\alpha}_j = \alpha_j e^{\imath\omega_j t}$  with  $j = 0, 1, 2$ ) the system of SDE corresponding to the Fokker-Planck equation (3.79) is:

$$\begin{aligned}
\frac{d\tilde{\alpha}_1}{dt} &= -\gamma_0\tilde{\alpha}_0 + E - \chi\tilde{\alpha}_1\tilde{\alpha}_2 + \sqrt{\gamma_0}\xi_0(t) \\
\frac{d\tilde{\alpha}_2}{dt} &= -\gamma_1\tilde{\alpha}_1 + \chi\tilde{\alpha}_0\tilde{\alpha}_2^* + \sqrt{\gamma_1}\xi_1(t) \\
\frac{d\tilde{\alpha}_3}{dt} &= -\gamma_2\tilde{\alpha}_2 + \chi\tilde{\alpha}_0\tilde{\alpha}_1^* + \sqrt{\gamma_2}\xi_2(t).
\end{aligned} \tag{3.82}$$

By comparison between eqs. (3.82) and eqs. (3.50) it is clear that the quantum Heisenberg equation for amplitude operators are the same as the c-fields amplitude equation of motion in the Wigner representation. This important result will be used in the next chapter in which we will consider the squeezing properties of a singly resonant optical parametric oscillator.

## 3.6 Conclusions

Chapter 3 has been devoted to the problem of the detection of squeezed light through the ordinary and balanced homodyne detection schemes. The input-output formulation of optical cavities has been explained and both the Heisenberg-Langevin and master equation approaches to the optical cavities problem have been analyzed. Then in the last part of the chapter, I have shown an application of these theoretical approaches to the case of a triply resonant OPO (TROPO) in the below threshold degenerate and non-degenerate cases.

## Bibliography

- [1] J. A. Giordmaine and R. C. Miller, *Phys. Rev. Lett.* **14**, 973 (1965).
- [2] Special edition on “*Optical Parametric Oscillation and Amplification*” of *J. Opt. Soc. Am. B* **10**, n.9 and 11, Robert L. Byer and Algis Piskarskas eds. (1993).
- [3] K. Kasay, G. Jiangrui and C. Fabre, *Europhys. Lett.* **40**, 25 (1997).
- [4] M. Martinelli, K. S. Zhang, T. Coudreau, A. Maitre, C. Fabre, *J. Opt, A: Pure Appl. Opt.* **3**, 300 (2001).
- [5] H.J. Kimble, *Quantum fluctuations in quantum optics*, in Les Houches 1990.
- [6] M. O. Scully and M. S. Zubairy, *Quantum Optics*, (Cambridge University Press, Cambridge, 2008).
- [7] M. J. Collett and C. W. Gardiner, *Phys. Rev. A* **30**, 1386 (1984).
- [8] C. Gardiner and P. Zoller, *A Handbook of Markovian and Non-Markovian Quantum Stochastic Methods with Applications to Quantum Optics*, Springer Verlag (2004).
- [9] C. W. Gardiner, *Handbook of Stochastic Processes*, (Springer, 1985).
- [10] L. Mandel and E. Wolf, *Optical Coherence and Quantum Optics*, (Cambridge University Press, 1995).
- [11] R. Graham and H. Haken, *Zeitschrift fur Physik*, **210**, 276 (1968).
- [12] S. Chaturvedi, K. Dechoum and P. D. Drummond, *Phys. Rev. A*, **65**, 00385 (2002).
- [13] F. E. Herrison, D. F. Walls, *Opt. Comm.*, **123**, 331 (1996).
- [14] Z. Y. Ou, S. F. Pereira, H. J. Kimble, *Appl. Phys. B*, **55**, 265 (1992).
- [15] D. Walls, G. J. Milburn, *Quantum Optics*, (Springer-Verlag, Berlin, 1995).
- [16] H. J. Carmichael, *Statistical Methods in Quantum Optics 1*, (Springer, Berlin, 1999).

## Squeezing and Quantum Entanglement in a SROPO Below Threshold

### 4.1 Introduction

Squeezed states of light, where the noise in one quadrature of the fields is reduced below the vacuum level, are important elements in several applications such as sub-shot-noise phase measurements [1, 2], interferometric detection of gravitational radiation [3, 4] and quantum information with continuous variables [5]. In the latter case, squeezed states are used to generate continuous variable entanglement and achieve high fidelity in quantum teleportation protocols [5]. To squeeze quantum fluctuations of the electromagnetic field one needs nonlinear optical effects such as parametric down conversion or four-wave mixing [6]. In parametric down conversion a pump photon at frequency  $\omega_p$  splits into a photon at frequency  $\omega_s$ , the signal, and another at  $\omega_i$ , the idler, by interacting with a nonlinear crystal with a second order nonlinear susceptibility  $\chi^{(2)}$  [6]. Strong nonlinearities required to achieve large noise reductions are however uncommon in many crystals. To overcome this limitation optical cavities are used to form an optical parametric oscillator (OPO). In this case, by setting the device into resonance at the desired frequencies, the oscillation build-up inside the cavity increases noise reduction by considerably extending the interaction time. Theoretical and experimental efforts in non-degenerate cases have mainly concerned the doubly (or even triply) resonant configurations where both the signal and idler fields are resonated [7, 8, 9]. The singly-resonant cavity is in principle a simpler configuration to realize experimentally but, to the best of our knowledge, theoretical investigations of squeezing and entanglement of the light from a singly-resonant OPO (SROPO) are missing. One of the reasons is that SROPOs operate with strongly non-degenerate frequencies while much of the literature on squeezing focuses on the degenerate or close to degeneracy cases [10, 11]. Recent interest in non-classical correlations of the strongly non-degenerate regime of parametric down-conversion [12] makes the study of entanglement in SROPO important for the optimization of coherent sources with fluctuations below the shot-noise level. There are clear technical advantages for SROPO configurations: only resonance of the signal field has to be maintained, continuous temperature tuning and suppression of mode-hopping. It is the aim of this chapter to investigate the squeezing and entanglement properties of SROPOs when signal and idler fields have large frequency separations (two-colour case). Our approach is similar to what has been used in the case of second harmonic generation [13, 14], namely a two-photon loss model in which a cavity mode is coupled quadratically to a continuum of output modes rather than linearly as usual in the input-output formulation of optical cavities.

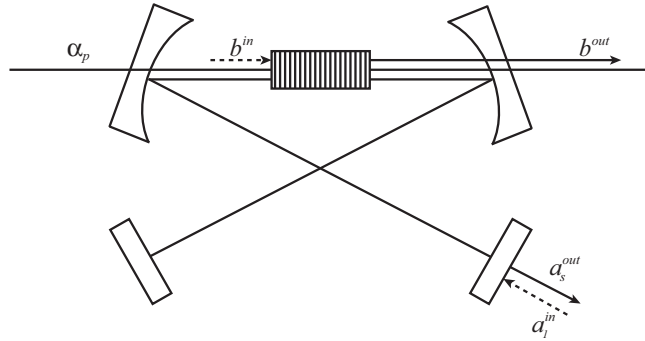


Figure 4.2.1: The singly-resonant OPO cavity scheme.  $\alpha_p$  is the input pump amplitude,  $a_1^{in}$  and  $b^{in}$  are the input signal and idler fields,  $a_s^{out}$  and  $b^{out}$  are the output signal and idler fields.

## 4.2 The Langevin Equation

We consider parametric down conversion in a monolithic cavity, resonant to the signal field only and pumped with a monochromatic classical beam at frequency  $\omega_p$  (see Fig. 4.2.1).

By assuming perfect collinear phase matching and considering energy conservation, one has [6]:

$$\vec{k}_p = \vec{k}_s + \vec{k}_i, \quad (4.1)$$

$$\omega_p = \omega_s + \omega_i, \quad (4.2)$$

where  $\vec{k}_p$ ,  $\vec{k}_s$  and  $\vec{k}_i$  are the wave vectors of the pump, the signal and the idler fields respectively. In the case of perfect phase matching the frequencies of the signal and idler fields depend only on the frequency of the pump and the orientation of the crystal with respect to the direction of the pump beam. The quantum mechanical Hamiltonian for the system in the rotating-wave approximation is:

$$H = H_{sys} + H_{bath,1} + H_{bath,2} + H_{int,1} + H_{int,2} + H_{int,3}. \quad (4.3)$$

where  $H_{sys}$  is the sum of the free energies for the single signal mode  $a_s$  and the continuum of idler modes  $b(\omega)$  treated here within the approach of [15];  $H_{bath,1}$  is the free energy of bosonic heat bath modes  $c_1(\omega)$  providing a description of the field external to the cavity and coupled to the signal because of non-perfect reflection of the mirrors [16];  $H_{int,1}$  in the Hamiltonian (4.3) represents the interaction of the signal mode with this heat bath, describing the damping of the signal mode caused by the non-zero transmittivity of the cavity;  $H_{bath,2}$  is the free energy of different bosonic heat bath modes  $c_2(\omega)$  while the term  $H_{int,2}$  is the interaction between the signal field and these modes, describing the damping of the signal mode associated with other loss mechanisms like other mirror transmissions or crystal absorptions and diffraction; the term  $H_{int,3}$  is the interaction between signal and idler modes and the pump field  $\alpha_p$  describing the process of parametric down conversion inside the nonlinear crystal [6]. In the rotating wave approximation, all these terms

have explicit forms given by:

$$H_{sys} = \hbar\omega_s a_s^\dagger a_s + \hbar \int_{-\infty}^{\infty} d\omega \omega b^\dagger(\omega) b(\omega), \quad (4.4)$$

$$H_{bath,1} = \hbar \int_{-\infty}^{\infty} d\omega \omega c_1^\dagger(\omega) c_1(\omega), \quad (4.5)$$

$$H_{bath,2} = \hbar \int_{-\infty}^{\infty} d\omega \omega c_2^\dagger(\omega) c_2(\omega), \quad (4.6)$$

$$H_{int,1} = i\hbar \int_{-\infty}^{\infty} d\omega \kappa_1 [c_1(\omega) a_s^\dagger - c_1^\dagger(\omega) a_s], \quad (4.7)$$

$$H_{int,2} = i\hbar \int_{-\infty}^{\infty} d\omega \kappa_2 [c_2(\omega) a_s^\dagger - c_2^\dagger(\omega) a_s], \quad (4.8)$$

$$H_{int,3} = i\hbar \int_{-\infty}^{\infty} d\omega \kappa_3 [b^\dagger(\omega) a_s^\dagger \alpha_p - b(\omega) a_s \alpha_p^*]. \quad (4.9)$$

The coupling constants  $\kappa_1$ ,  $\kappa_2$ , and  $\kappa_3$  are considered to be independent of the frequency  $\omega$  according to the Markov approximation. We also consider the following commutation relations for the modes:

$$[a_s, a_s^\dagger] = 1, \quad (4.10)$$

$$[c_i(\omega), c_i^\dagger(\omega')] = \delta(\omega - \omega'), \quad (4.11)$$

$$[b(\omega), b^\dagger(\omega')] = \delta(\omega - \omega'), \quad (4.12)$$

where  $i = 1, 2$  while all the other commutators are identically zero. For the non resonant idler field we use the theory of Collett and Levien [13] who showed that systems described by a continuum of mode operators  $\bar{b}(\omega)$  and possessing an isolated mode of particular interest, can be redescribed in terms of an orthonormal set formed by this one mode and a new continuum  $b(\omega)$ . The Heisenberg equation of motion for the bath operator  $b(\omega)$ , which describe the idler field, is:

$$\begin{aligned} \frac{db(\omega)}{dt} &= -\frac{i}{\hbar} [b(\omega), H] = -\frac{i}{\hbar} \{ [b(\omega), H_{bath,2}] + [b(\omega), H_{int,2}] \} \\ &= -i \left[ b(\omega), \int_{-\infty}^{+\infty} d\omega' b^\dagger(\omega') b(\omega') \omega' \right] + \\ &+ \left[ b(\omega), \int_{-\infty}^{+\infty} d\omega' \kappa_2(\omega') [b^\dagger(\omega') a_s^\dagger \alpha_p - \alpha_p^* a_s b(\omega')] \right] \end{aligned} \quad (4.13)$$

We obtain:

$$\frac{db(\omega)}{dt} = -i\omega b(\omega) + \kappa_2(\omega) a_s^\dagger \alpha_p \quad (4.14)$$

The solution to eq. (4.14) may be written in two ways depending on whether we choose to solve in terms of initial conditions at time  $t_0 < t$  (input) or in terms of the final conditions at time  $t_1 > t$  (output). The two solution are, respectively:

$$b(\omega) = b_0(\omega) e^{-i\omega(t-t_0)} + \kappa_2(\omega) \int_{t_0}^t dt' e^{-i\omega(t-t')} a_s^\dagger(t') \alpha_p(t') \quad (4.15)$$

$$b(\omega) = b_1(\omega) e^{-i\omega(t-t_1)} - \kappa_2(\omega) \int_{t_0}^t dt' e^{-i\omega(t-t')} a_s^\dagger(t') \alpha_p(t') \quad (4.16)$$

where  $b_0(\omega)$  is the value of  $b(\omega)$  at  $t = t_0$  and  $b_1(\omega)$  is the value of  $b(\omega)$  at  $t = t_1$ .

We can derive similar equations for the  $c_i(\omega)$  fields. The Heisenberg equation for the signal mode  $a_s$  is:

$$\begin{aligned} \frac{da_s}{dt} &= -\frac{i}{\hbar} [a_s, H] = -\frac{i}{\hbar} \{[a_s, H_{int,1}] + [a_s, H_{int,2}] + [a_s, H_{int,3}]\} \\ &= \mu a_s |\alpha_0|^2 - \sqrt{2\mu} b^{\dagger in} \alpha_0 - (\gamma_1 + \gamma_2) a_s + \sqrt{2\gamma_1} a_1^{in} + \sqrt{2\gamma_2} a_2^{in} \end{aligned} \quad (4.17)$$

where  $b_{in}$  is the idler field noise,  $\gamma_1 = \kappa_1^2 \pi$  is the signal cavity damping rate and  $a_1^{in}$  the input vacuum modes entering the cavity from the environment. The term  $\gamma_2 = \kappa_2^2 \pi$  is the intracavity loss rate, mainly due to absorption by the crystal, and  $a_2^{in}$  the quantum noise associated with this loss and defined in the usual way [15]. We also consider  $\gamma = \gamma_1 + \gamma_2$  as the total damping rate and we define,  $\mu = \kappa_3^2 \pi$ .

To derive the eq. (4.17) we have used the following properties of the Dirac Delta:

1.  $\int_{-\infty}^{+\infty} d\omega e^{-i\omega(t-t')} = 2\pi \delta(t-t')$
2.  $\int_{t_0}^t dt' f(t') \delta(t-t') = \int_{t_0}^{t_1} dt' f(t') \delta(t-t') = \frac{1}{2} f(t) \quad (t_0 < t < t_1)$

and we have defined the input field operators:

$$b^{in}(t) = -\frac{1}{\sqrt{2\pi}} \int_{-\infty}^{+\infty} d\omega e^{-i\omega(t-t_0)} b_0(\omega) \quad (4.18)$$

$$a_i^{in}(t) = -\frac{1}{\sqrt{2\pi}} \int_{-\infty}^{+\infty} d\omega e^{-i\omega(t-t_0)} c_{0,i}(\omega) \quad (4.19)$$

From equation (4.17) we can find the pump threshold value for oscillation, which is obtained by putting at zero the left-hand side and the noise terms. The result is:

$$\alpha_p^{tr} = \sqrt{\frac{\gamma}{\mu}} \quad (4.20)$$

At this point we can rewrite eq. (4.17) parametrized respect to the pump threshold value,  $\alpha_p = \varepsilon \alpha_{th}$  by introducing a pump parameter  $\varepsilon$ , whose range is:  $0 < \varepsilon < 1$ .

$$\frac{da_s}{dt} = a_s \varepsilon^2 \gamma - \sqrt{2\gamma \varepsilon} b^{\dagger in} - \gamma a_s + \sqrt{2\gamma_1} a_1^{in} + \sqrt{2\gamma_2} a_2^{in} \quad (4.21)$$

which can be reordered in the following way:

$$\frac{da_s}{dt} = a_s \gamma (\varepsilon^2 - 1) - \sqrt{2\gamma \varepsilon} b^{\dagger in} + \sqrt{2\gamma_1} a_1^{in} + \sqrt{2\gamma_2} a_2^{in} \quad (4.22)$$

In a similar way we may substitute the solution in terms of the final conditions eq. (2.6) to obtain the time reversed Langevin equation:

$$\frac{da_s}{dt} = a_s \gamma (\varepsilon^2 - 1) + \sqrt{2\gamma \varepsilon} b^{\dagger out} - \sqrt{2\gamma_1} a_1^{out} - \sqrt{2\gamma_2} a_2^{out} \quad (4.23)$$

By equating eq. (4.22) and eq. (4.23) we can obtain a set of input-output relations:

$$\begin{cases} a_1^{out} = -a_1^{in} + \sqrt{2\gamma_1}a_s \\ b^{out} = -b^{in} + \sqrt{2\gamma}\varepsilon a_s^\dagger \end{cases} \quad (4.24)$$

Note that the input-output relation of the signal field is written at the cavity mirror of the SROPO while that of the idler field makes explicit the propagation of the idler fluctuations through the crystal (see Fig. 4.2.1). The formal solution of eq. (4.22) is:

$$\begin{aligned} a_s(t) = & a_s(0)e^{\gamma(\varepsilon^2-1)t} + \sqrt{2\gamma_1} \int_0^t dt' a_1^{in}(t') e^{\gamma(\varepsilon^2-1)(t-t')} \\ & + \sqrt{2\gamma_2} \int_0^t dt' a_2^{in}(t') e^{\gamma(\varepsilon^2-1)(t-t')} \\ & - \sqrt{2\gamma}\varepsilon \int_0^t dt' b^{\dagger in}(t') e^{\gamma(\varepsilon^2-1)(t-t')} \end{aligned} \quad (4.25)$$

### 4.3 Two-Time Correlation Functions

Integrating eq. (4.15) over  $\omega$  provides:

$$\begin{aligned} \int_{-\infty}^{+\infty} d\omega b(\omega) &= \int_{-\infty}^{+\infty} d\omega b_0(\omega) e^{-i\omega(t-t_0)} + \int_{-\infty}^{+\infty} d\omega \kappa_2(\omega) \int_{t_0}^t dt' e^{-i\omega(t-t')} a_s^\dagger(t') \alpha_p(t') \\ &= -\sqrt{2\pi} b^{in}(t) + \varepsilon \sqrt{\gamma\pi} a_s^\dagger(t) \end{aligned} \quad (4.26)$$

which can be rewritten in the form:

$$b^{in}(t) = \varepsilon \sqrt{\frac{\gamma}{2}} a_s^\dagger(t) - \frac{1}{\sqrt{2\pi}} \int_{-\infty}^{+\infty} d\omega b(\omega) \quad (4.27)$$

From eq. (4.27) we can derive the following commutators:

1.  $[a_s(t), b^{in}(t)] = \varepsilon \sqrt{\frac{\gamma}{2}} [a_s(t), a_s^\dagger(t)] \quad (t' = t)$
2.  $[a_s(t), b^{in}(t')] = 0 \quad (t' > t)$
3.  $[a_s(t), b^{out}(t')] = 0 \quad (t' < t)$

The value at equal times easily comes by inserting eq. (4.27) in the commutator, while the second and third ones reflect the fact that  $a_s(t)$  can be a function of  $b^{in}(t')$  only for earlier times  $t' < t$  and of  $b^{out}$  only for later times  $t' > t$ . From the last commutator and from eq. (4.24) we have:

$$[a_s(t), b^{in}(t')] = \varepsilon \sqrt{2\gamma} [a_s(t), a_s^\dagger(t')] \quad (t' < t) \quad (4.28)$$

Putting together these expressions we get:

$$[a_s(t), b^{in}(t')] = \varepsilon \sqrt{2\gamma} \theta(t-t') [a_s(t), a_s^\dagger(t')] \quad (4.29)$$

where we have defined the theta function in the following way:

$$\theta(t-t') = \begin{cases} 1 & (t > t') \\ 0 & (t < t') \\ \frac{1}{2} & (t = t') \end{cases} \quad (4.30)$$

The commutator of  $a_s$  and  $a_1^{in}$  is the usual one:

$$\left[ a_s(t), a_1^{\dagger in}(t') \right] = \sqrt{2\gamma_1} \theta(t-t') \left[ a_s(t), a_s^\dagger(t') \right] \quad (4.31)$$

Now we can evaluate some output correlation functions which will be all useful for the calculation of the spectra in the following sections:

$$\begin{aligned} \langle a^{\dagger out}(t), a^{out}(t') \rangle &= \langle -a_1^{\dagger in}(t) + \sqrt{2\gamma_1} a_s^\dagger(t), -a_1^{in}(t') + \sqrt{2\gamma_1} a_s(t') \rangle \\ &= \langle a_1^{\dagger in}(t), a_1^{in}(t') \rangle + 2\gamma_1 \langle a_s^\dagger(t), a_s(t') \rangle \\ &\quad - \sqrt{2\gamma_1} \langle a_1^{\dagger in}(t), a_s(t') \rangle - \sqrt{2\gamma_1} \langle a_s^\dagger(t), a_1^{in}(t') \rangle \\ &= 2\gamma_1 \langle a_s^\dagger(t), a_s(t') \rangle \end{aligned}$$

$$\begin{aligned} \langle b^{\dagger out}(t), b^{out}(t') \rangle &= \langle -b^{\dagger in}(t) + \sqrt{2\gamma} \varepsilon a_s(t), -b^{in}(t') + \sqrt{2\gamma} \varepsilon a_s^\dagger(t') \rangle \\ &= \langle b^{\dagger in}(t), b^{in}(t') \rangle + 2\gamma \varepsilon^2 \langle a_s(t), a_s^\dagger(t') \rangle \\ &\quad - \sqrt{2\gamma} \varepsilon \langle b^{\dagger in}(t), a_s^\dagger(t') \rangle - \sqrt{2\gamma} \varepsilon \langle a_s(t), b^{in}(t') \rangle \\ &= 2\gamma \varepsilon^2 \langle a_s(t), a_s^\dagger(t') \rangle \end{aligned}$$

$$\begin{aligned} \langle b^{\dagger out}(t), a^{\dagger out}(t') \rangle &= \langle -b^{\dagger in}(t) + \sqrt{2\gamma} \varepsilon a_s(t), -a_1^{\dagger in}(t') + \sqrt{2\gamma_1} a_s^\dagger(t') \rangle \\ &= \langle b^{\dagger in}(t), a_1^{\dagger in}(t') \rangle + 2\sqrt{\gamma_1} \gamma \varepsilon \langle a_s(t), a_s^\dagger(t') \rangle \\ &\quad - \sqrt{2\gamma_1} \langle b^{\dagger in}(t), a_s^\dagger(t') \rangle - \sqrt{2\gamma} \varepsilon \langle a_s(t), a_1^{\dagger in}(t') \rangle \\ &= 2\sqrt{\gamma_1} \gamma \varepsilon \langle a_s(t), a_s^\dagger(t') \rangle - \sqrt{2\gamma} \varepsilon \langle a_s(t), a_1^{\dagger in}(t') \rangle \\ &= 2\sqrt{\gamma_1} \gamma \varepsilon \langle a_s(t), a_s^\dagger(t') \rangle - \sqrt{2\gamma} \varepsilon \langle [a_s(t), a_1^{\dagger in}(t')] \rangle \\ &= 2\sqrt{\gamma_1} \gamma \varepsilon \langle a_s(t), a_s^\dagger(t') \rangle - 2\sqrt{\gamma_1} \gamma \varepsilon \langle [a_s(t), a_s^\dagger(t')] \rangle \theta(t-t') \end{aligned}$$

It follows that:

$$\langle b^{\dagger out}(t), a^{\dagger out}(t') \rangle = \begin{cases} 2\sqrt{\gamma_1} \gamma \varepsilon \langle a_s^\dagger(t'), a_s(t) \rangle & (t > t') \\ 2\sqrt{\gamma_1} \gamma \varepsilon \langle a_s(t), a_s^\dagger(t') \rangle & (t < t') \end{cases}$$

$$\begin{aligned}
\langle b^{\text{out}}(t), a^{\text{out}}(t') \rangle &= \langle -b^{\text{in}}(t) + \sqrt{2\gamma}\varepsilon a_s^\dagger(t), -a_1^{\text{in}}(t') + \sqrt{2\gamma_1}a_s(t') \rangle \\
&= \langle b^{\text{in}}(t), a_1^{\text{in}}(t') \rangle + 2\sqrt{\gamma_1\gamma}\varepsilon \langle a_s^\dagger(t), a_s(t') \rangle \\
&\quad - \sqrt{2\gamma_1} \langle b^{\text{in}}(t), a_s(t') \rangle - \sqrt{2\gamma}\varepsilon \langle a_s^\dagger(t), a_1^{\text{in}}(t') \rangle \\
&= 2\sqrt{\gamma_1\gamma}\varepsilon \langle a_s^\dagger(t), a_s(t') \rangle - \sqrt{2\gamma_1} \langle b^{\text{in}}(t), a_s(t') \rangle \\
&= 2\sqrt{\gamma_1\gamma}\varepsilon \langle a_s^\dagger(t), a_s(t') \rangle - \sqrt{2\gamma_1} \langle [b^{\text{in}}(t), a_s(t')] \rangle \\
&= 2\sqrt{\gamma_1\gamma}\varepsilon \langle a_s^\dagger(t), a_s(t') \rangle + 2\sqrt{\gamma_1\gamma}\varepsilon \langle [a_s(t'), a_s^\dagger(t)] \rangle \theta(t' - t)
\end{aligned}$$

It follows that:

$$\langle b^{\text{out}}(t), a^{\text{out}}(t') \rangle = \begin{cases} 2\sqrt{\gamma_1\gamma}\varepsilon \langle a_s^\dagger(t), a_s(t') \rangle & (t > t') \\ 2\sqrt{\gamma_1\gamma}\varepsilon \langle a_s(t'), a_s^\dagger(t) \rangle & (t < t') \end{cases}$$

$$\begin{aligned}
\langle a^{\dagger\text{out}}(t), b^{\dagger\text{out}}(t') \rangle &= \langle -a_1^{\dagger\text{in}}(t) + \sqrt{2\gamma_1}a_s^\dagger(t), -b^{\dagger\text{in}}(t') + \sqrt{2\gamma}\varepsilon a_s(t') \rangle \\
&= \langle a_1^{\dagger\text{in}}(t), b^{\dagger\text{in}}(t') \rangle + 2\sqrt{\gamma_1\gamma}\varepsilon \langle a_s^\dagger(t), a_s(t') \rangle \\
&\quad - \sqrt{2\gamma_1} \langle a_s^\dagger(t), b^{\dagger\text{in}}(t') \rangle - \sqrt{2\gamma}\varepsilon \langle a_1^{\dagger\text{in}}(t), a_s(t') \rangle \\
&= 2\sqrt{\gamma_1\gamma}\varepsilon \langle a_s^\dagger(t), a_s(t') \rangle - \sqrt{2\gamma}\varepsilon \langle a_s^\dagger(t), b^{\dagger\text{in}}(t') \rangle \\
&= 2\sqrt{\gamma_1\gamma}\varepsilon \langle a_s^\dagger(t), a_s(t') \rangle - \sqrt{2\gamma}\varepsilon \langle [a_s^\dagger(t), b^{\dagger\text{in}}(t')] \rangle \\
&= 2\sqrt{\gamma_1\gamma}\varepsilon \langle a_s^\dagger(t), a_s(t') \rangle - 2\sqrt{\gamma_1\gamma}\varepsilon \langle [a_s^\dagger(t), a_s(t')] \rangle \theta(t - t')
\end{aligned}$$

It follows that:

$$\langle a^{\dagger\text{out}}(t), b^{\dagger\text{out}}(t') \rangle = \begin{cases} 2\sqrt{\gamma_1\gamma}\varepsilon \langle a_s(t'), a_s^\dagger(t) \rangle & (t > t') \\ 2\sqrt{\gamma_1\gamma}\varepsilon \langle a_s^\dagger(t), a_s(t') \rangle & (t < t') \end{cases}$$

$$\begin{aligned}
\langle a^{\text{out}}(t), b^{\text{out}}(t') \rangle &= \langle -a_1^{\text{in}}(t) + \sqrt{2\gamma_1}a_s(t), -b^{\text{in}}(t') + \sqrt{2\gamma}\varepsilon a_s^\dagger(t') \rangle \\
&= \langle a_1^{\text{in}}(t), b^{\text{in}}(t') \rangle + 2\sqrt{\gamma_1\gamma}\varepsilon \langle a_s(t), a_s^\dagger(t') \rangle \\
&\quad - \sqrt{2\gamma_1} \langle a_s(t), b^{\text{in}}(t') \rangle - \sqrt{2\gamma}\varepsilon \langle a_1^{\text{in}}(t), a_s^\dagger(t') \rangle \\
&= 2\sqrt{\gamma_1\gamma}\varepsilon \langle a_s(t), a_s^\dagger(t') \rangle - \sqrt{2\gamma}\varepsilon \langle a_1^{\text{in}}(t), a_s^\dagger(t') \rangle \\
&= 2\sqrt{\gamma_1\gamma}\varepsilon \langle a_s(t), a_s^\dagger(t') \rangle - 2\sqrt{\gamma_1\gamma}\varepsilon \langle [a_1^{\text{in}}(t), a_s^\dagger(t')] \rangle \\
&= 2\sqrt{\gamma_1\gamma}\varepsilon \langle a_s(t), a_s^\dagger(t') \rangle + 2\sqrt{\gamma_1\gamma}\varepsilon \langle [a_s^\dagger(t'), a_s(t)] \rangle \theta(t' - t)
\end{aligned}$$

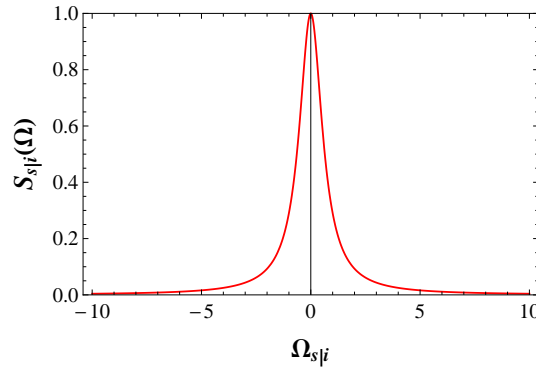


Figure 4.4.1: Signal or idler spectrum of eq. (4.33) for  $\varepsilon = 0.8$ .

It follows that:

$$\langle a^{out}(t), b^{out}(t') \rangle = \begin{cases} 2\sqrt{\gamma_1\gamma}\varepsilon \langle a_s(t), a_s^\dagger(t') \rangle & (t > t') \\ 2\sqrt{\gamma_1\gamma}\varepsilon \langle a_s^\dagger(t'), a_s(t) \rangle & (t < t') \end{cases}$$

The results of this section will be crucial for the evaluation of quantities of physical interest, such as spectra of squeezing and of intensity difference.

## 4.4 Intensity Difference Correlation

Quantities that can be readily calculated are the signal and idler output spectra. For the signal field, the spectrum is defined as:

$$S_s(\omega) = \int_{-\infty}^{+\infty} d\tau \langle : a_s^{\dagger out}(0) a_s^{out}(\tau) : \rangle e^{i\omega\tau}, \quad (4.32)$$

where the symbols  $\langle : \cdot : \rangle$  denote time averaging and normal ordering, respectively, and with an analogous expression valid for the idler field. By using formal solutions of the Langevin eq. (4.22), it is possible to evaluate the signal and idler spectra as a function of the normalized pump amplitude  $\varepsilon$ :

$$S_{s|i}(\Omega) = \frac{(1 - \varepsilon^2)^2}{(1 - \varepsilon^2)^2 + \Omega_{s|i}^2}, \quad (4.33)$$

where we have defined  $\Omega_{s|i} = (\omega - \omega_{s|i})/\gamma$  and normalized to the value of the spectrum at resonance. The spectrum of eq. (4.33) is shown in Fig. 4.4.1; the spectra for signal and idler fields are two Lorentzians centred at the signal and idler frequencies, respectively. Although the idler is not resonated, this field still experiences the presence of the cavity because of the frequency entanglement which is peculiar to the process of parametric down conversion in the crystal.

Direct detection of intensity fluctuations of signal and idler fields is the simplest type of measurement one can perform in a two-colour OPO. A reduction in the intensity difference fluctuations below the shot noise level in doubly resonant OPOs above the threshold of oscillation was calculated by Reynaud et al. [17] and Lane, Reid and Walls [18] and demonstrated by Heidmann et al. [19] for a Type II non-degenerate OPO. Here we extend those approaches to include the study of signal-idler intensity fluctuations in singly resonant OPO below the threshold of oscillation. In this

type of measurement the signal and idler fields hit two different photodetectors and then the resulting difference intensity fluctuations are analyzed with a power spectrum analyzer. Specializing the analysis of section 3.2 to the case of intensity difference correlations we obtain from eq. (3.9, 3.10) that the measurable output is related to the Fourier transform of the intensity difference correlation function:

$$\frac{\langle \Delta I_D^{out}(0), \Delta I_D^{out}(\tau) \rangle}{\langle I_s^{out} \rangle + \langle I_I^{out} \rangle} = \delta(\tau) + \frac{\langle : I_D^{out}(0), I_D^{out}(\tau) : \rangle}{\langle I_s^{out} \rangle + \langle I_I^{out} \rangle} \quad (4.34)$$

which is:

$$\frac{S_D[\omega]}{S_0} = 1 + \frac{1}{S_0} \int_{-\infty}^{+\infty} d\tau \langle : I_D^{out}(0), I_D^{out}(\tau) : \rangle e^{i\omega\tau}, \quad (4.35)$$

In eq. (4.35) we have introduced the quantity,  $I_D^{out}(t) = I_s^{out}(t) - I_I^{out}(t)$ , where  $I_s^{out}(t) = a_s^{\dagger out}(t)a_s^{out}(t)$  and  $I_I^{out}(t) = b^{\dagger out}(t)b^{out}(t)$  are the output intensity operators for signal and idler fields,  $S_0$  is the shot noise level, which in this case is given by the sum of the intensities of signal and idler beams,  $S_0 = I_s^{out} + I_I^{out}$ . Furthermore, for any operators  $A$  and  $B$ :

$$\langle A, B \rangle = \langle AB \rangle - \langle A \rangle \langle B \rangle. \quad (4.36)$$

We define:

$$G_{si}^{(2)}(\tau) = \langle : (I_s^{out}(t) - I_I^{out}(t)) (I_s^{out}(t + \tau) - I_I^{out}(t + \tau)) : \rangle$$

$G_{si}^{(2)}(\tau)$  can be rewritten in the following way:

$$\begin{aligned} G_{si}^{(2)}(\tau) &= \langle : I_s^{out}(t) I_s^{out}(t + \tau) : \rangle + \langle : I_I^{out}(t) I_I^{out}(t + \tau) : \rangle \\ &\quad - \langle : I_s^{out}(t) I_I^{out}(t + \tau) : \rangle - \langle : I_I^{out}(t) I_s^{out}(t + \tau) : \rangle \end{aligned} \quad (4.37)$$

Let us calculate the first one of the terms that appear in eq. (4.37):

$$\begin{aligned} \langle : I_s^{out}(t) I_s^{out}(t + \tau) : \rangle &= \langle : \hat{a}_s^{\dagger out}(t) \hat{a}_s^{out}(t) \hat{a}_s^{\dagger out}(t + \tau) \hat{a}_s^{out}(t + \tau) : \rangle \\ &= \langle \hat{a}_s^{\dagger out}(t) \hat{a}_s^{\dagger out}(t + \tau) \hat{a}_s^{out}(t) \hat{a}_s^{out}(t + \tau) \rangle \end{aligned} \quad (4.38)$$

For coherent or vacuum input eq. (4.38) can be factorized in the following way:

$$\begin{aligned} \langle : I_s^{out}(t) I_s^{out}(t + \tau) : \rangle &= \langle \hat{a}_s^{\dagger out}(t) \hat{a}_s^{\dagger out}(t + \tau) \rangle \langle \hat{a}_s^{out}(t) \hat{a}_s^{out}(t + \tau) \rangle \\ &\quad + \langle \hat{a}_s^{\dagger out}(t) \hat{a}_s^{out}(t) \rangle \langle \hat{a}_s^{\dagger out}(t + \tau) \hat{a}_s^{out}(t + \tau) \rangle \\ &\quad + \langle \hat{a}_s^{\dagger out}(t) \hat{a}_s^{out}(t + \tau) \rangle \langle \hat{a}_s^{\dagger out}(t + \tau) \hat{a}_s^{out}(t) \rangle \\ &= 4\gamma_1^2 \langle \hat{a}_s^{\dagger}(t) \hat{a}_s(t) \rangle \langle \hat{a}_s^{\dagger}(t + \tau) \hat{a}_s(t + \tau) \rangle \\ &\quad + 4\gamma_1^2 \langle \hat{a}_s^{\dagger}(t) \hat{a}_s(t + \tau) \rangle \langle \hat{a}_s^{\dagger}(t + \tau) \hat{a}_s(t) \rangle \\ &= 4\gamma_1^2 AB + 4\gamma_1^2 C^2 \end{aligned} \quad (4.39)$$

$$= 4\gamma_1^2 AB + 4\gamma_1^2 C^2 \quad (4.40)$$

A similar expression can be derived for the second term in (4.37):

$$\begin{aligned} \langle : I_i^{out}(t) I_i^{out}(t + \tau) : \rangle &= 4\gamma\varepsilon^2 T \langle \hat{a}_s(t) \hat{a}_s^\dagger(t) \rangle \langle \hat{a}_s(t + \tau) \hat{a}_s^\dagger(t + \tau) \rangle \\ &+ 4\gamma\varepsilon^2 T \langle \hat{a}_s(t) \hat{a}_s^\dagger(t + \tau) \rangle \langle \hat{a}_s(t + \tau) \hat{a}_s^\dagger(t) \rangle \end{aligned} \quad (4.41)$$

$$= 4\gamma^2 AB + 4\gamma^2 C^2 \quad (4.42)$$

Let us now calculate the third term in (4.37):

$$\begin{aligned} \langle : I_s^{out}(t) I_i^{out}(t + \tau) : \rangle |_{\tau < 0} &= \langle \hat{a}^{\dagger out}(t) \hat{a}^{out}(t) \hat{b}^{\dagger out}(t + \tau) \hat{b}^{out}(t + \tau) \rangle \\ &= \langle \hat{a}^{\dagger out}(t) \hat{a}^{out}(t) \rangle \langle \hat{b}^{\dagger out}(t + \tau) \hat{b}^{out}(t + \tau) \rangle \\ &+ \langle \hat{a}^{\dagger out}(t) \hat{b}^{\dagger out}(t + \tau) \rangle \langle \hat{a}^{out}(t) \hat{b}^{out}(t + \tau) \rangle \\ &+ \langle \hat{a}^{\dagger out}(t) \hat{b}^{out}(t + \tau) \rangle \langle \hat{a}^{out}(t) \hat{b}^{\dagger out}(t + \tau) \rangle \\ &= 4\gamma\gamma_1\varepsilon^2 \langle \hat{a}^\dagger(t) \hat{a}(t) \rangle \langle \hat{a}(t + \tau) \hat{a}^\dagger(t + \tau) \rangle \\ &+ 4\gamma\gamma_1\varepsilon^2 \langle \hat{a}(t + \tau) \hat{a}^\dagger(t) \rangle \langle \hat{a}(t) \hat{a}^\dagger(t + \tau) \rangle \end{aligned} \quad (4.43)$$

$$= 4\gamma\gamma_1 AB + 4 \frac{\gamma\gamma_1}{\varepsilon^2} C^2 \quad (4.44)$$

$$\langle : I_s^{out}(t) I_i^{out}(t + \tau) : \rangle |_{\tau > 0} = 4\gamma\gamma_1 AB + 4\gamma\gamma_1\varepsilon^2 C^2 \quad (4.45)$$

$$\begin{aligned} \langle : I_i^{out}(t) I_s^{out}(t + \tau) : \rangle |_{\tau < 0} &= \langle \hat{b}^{\dagger out}(t) \hat{b}^{out}(t) \hat{a}^{\dagger out}(t + \tau) \hat{a}^{out}(t + \tau) \rangle \\ &= \langle \hat{b}^{\dagger out}(t) \hat{b}^{out}(t) \rangle \langle \hat{a}^{\dagger out}(t + \tau) \hat{a}^{out}(t + \tau) \rangle \\ &+ \langle \hat{b}^{\dagger out}(t) \hat{a}^{\dagger out}(t + \tau) \rangle \langle \hat{b}^{out}(t) \hat{a}^{out}(t + \tau) \rangle \\ &+ \langle \hat{b}^{\dagger out}(t) \hat{a}^{out}(t + \tau) \rangle \langle \hat{b}^{out}(t) \hat{a}^{\dagger out}(t + \tau) \rangle \\ &= 4\gamma\gamma_1\varepsilon^2 \langle \hat{a}(t) \hat{a}^\dagger(t) \rangle \langle \hat{a}^\dagger(t + \tau) \hat{a}(t + \tau) \rangle \\ &+ 4\gamma\gamma_1\varepsilon^2 \langle \hat{a}^\dagger(t + \tau) \hat{a}(t) \rangle \langle \hat{a}^\dagger(t) \hat{a}(t + \tau) \rangle \\ &= 4\gamma\gamma_1 AB + 4\gamma\gamma_1\varepsilon^2 C^2 \end{aligned} \quad (4.46)$$

$$\langle : I_i^{out}(t) I_s^{out}(t + \tau) : \rangle |_{\tau > 0} = 4\gamma\gamma_1 AB + 4 \frac{\gamma\gamma_1}{\varepsilon^2} C^2 \quad (4.47)$$

$$G_{si}^{(2)}(\tau) = 4\gamma_1^2 (AB + C^2) + 4\gamma^2 (AB + C^2) - \left[ 8\gamma\gamma_1 AB + 4 \frac{\gamma\gamma_1}{\varepsilon^2} C^2 + 4\gamma\gamma_1\varepsilon^2 C^2 \right] \quad (4.48)$$

We have defined:

$$\begin{aligned} A &= \langle \hat{a}^\dagger(t) \hat{a}(t) \rangle \\ B &= \langle \hat{a}^\dagger(t + \tau) \hat{a}(t + \tau) \rangle \\ C &= \langle \hat{a}^\dagger(t + \tau) \hat{a}(t) \rangle \end{aligned} \quad (4.49)$$

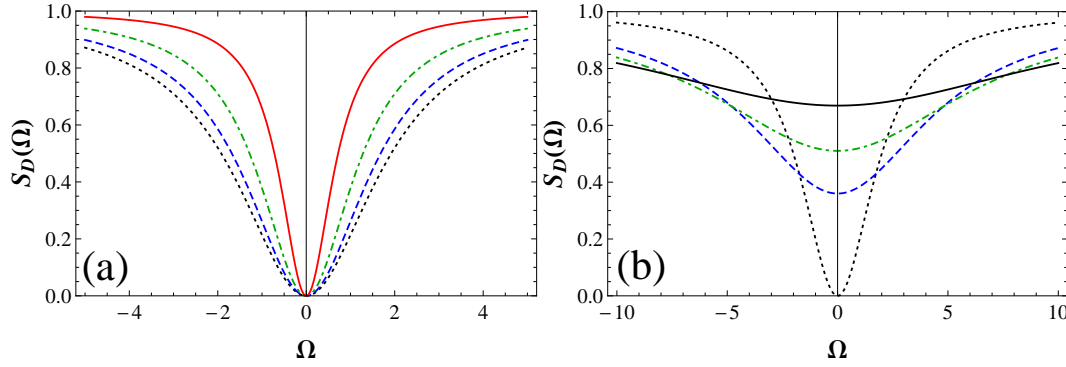


Figure 4.4.2: (a) Intensity difference correlation spectrum of (4.52) plotted for a range of input powers and  $\Gamma = 1$ . Curves correspond to  $\varepsilon = 0.2$  (black-dotted line),  $\varepsilon = 0.4$  (blue-dashed line),  $\varepsilon = 0.6$  (green-dash-dotted line),  $\varepsilon = 0.8$  (red-solid line). (b) Intensity difference correlation spectrum of (4.53) plotted for a range of  $Z = \gamma_i/\gamma_s$  values. Curves correspond to  $Z = 1$  (black-dotted line),  $Z = 4$  (blue-dashed line),  $Z = 6$  (green-dash-dotted line), and  $Z = 10$  (black-solid line).  $\Omega = 0$  is the cavity resonance condition.

The intensity difference correlation function is then:

$$\frac{\langle \Delta I_D^{out}(0), \Delta I_D^{out}(\tau) \rangle}{\langle I_s^{out} \rangle + \langle I_I^{out} \rangle} = \delta(\tau) + \frac{G_{si}^{(2)}(\tau)}{2A\gamma + 2A\gamma_1} \quad (4.50)$$

The Intensity-Difference Spectrum is then:

$$\frac{S_D[\Omega]}{S_0} = 1 + \frac{8(-\Gamma + \varepsilon^2)(1 - \Gamma\varepsilon^2)}{(1 + \Gamma)[4(-1 + \varepsilon^2)^2 + \Omega^2]}, \quad (4.51)$$

where we have defined  $\Gamma = \gamma_1/\gamma$  and we have introduced the variable:

$$\Omega = \frac{\omega}{\gamma}$$

The spectrum (4.51) is plotted in Fig. 4.4.2(a) for different values of the pump parameter  $\varepsilon$  and for  $\Gamma = 1$  (i.e.  $\gamma_2 = 0$ ). In this case (4.51) reduces to:

$$\frac{S_D[\Omega]}{S_0} = 1 - \frac{4}{4 + [\Omega/(1 - \varepsilon^2)]^2}, \quad (4.52)$$

where a narrowing of the spectrum when approaching threshold clearly confirms the plots of Fig. 4.4.2. The dependence of the spectrum (4.51,4.52) on the pump parameter which leads to the narrowing of the spectral lines when threshold is approached is peculiar to the singly-resonant case. No dependence on the pump is observed in the doubly-resonant OPO where the spectrum has the following analytical expression [7, 20].

$$\frac{S_D[\Omega]}{S_0} = 1 - \frac{4}{\frac{\Omega^2}{\gamma_s\gamma_i} + \left[ \sqrt{\frac{\gamma_s}{\gamma_i}} + \sqrt{\frac{\gamma_i}{\gamma_s}} \right]^2}. \quad (4.53)$$

One could be tempted, in order to study the behaviour of the singly-resonant configuration, to find the limit of eq. (4.53) as the signal or idler cavity damping rates,  $\gamma_s$  and  $\gamma_i$  respectively, approach

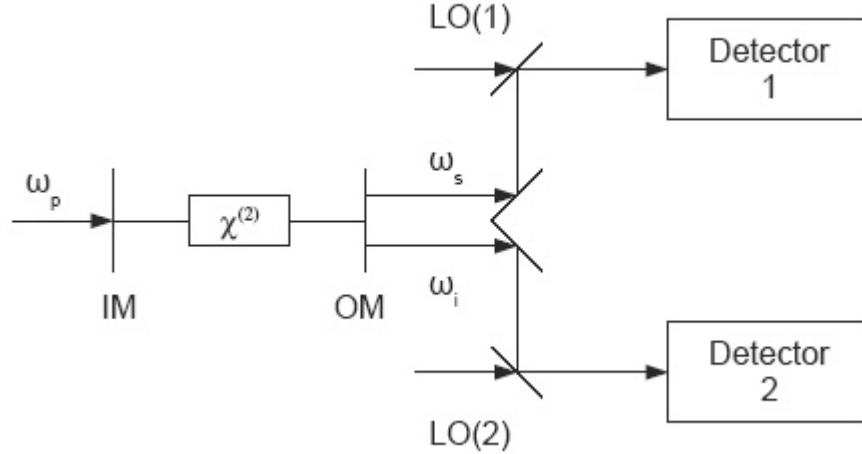


Figure 4.5.1: Typical experiment for correlation in nondegenerate parametric oscillation. The input mirror  $IM$  is highly reflective at the signal and idler frequencies. The output mirror  $OM$  is more transmissive. The two beam splitters are highly reflecting and the local oscillators  $LO(1)$  and  $LO(2)$  have the same frequencies of the signal and idler fields, respectively.

infinite. In this case the eq. (4.53) reaches the asymptotic value of 1 (see Fig. 4.4.2(b) where  $Z = \gamma_i/\gamma_s$  is increased from 1 to 10), meaning that no squeezing would be observable in such a measurement. Such a limit, however, is not well posed because in doing so we break the mean field limit approximation from which eq. (4.53) is derived. Our calculation predicts, in fact, that suppression of the shot noise is indeed possible in the singly-resonant configuration. It is worth noting that, analogous to the doubly-resonant case, perfect suppression of noise below the shot noise level at resonance ( $\Omega = 0$ ) is independent of the pump power.

## 4.5 Quadrature Correlations

The intensity correlation function calculated in section 4.4 contains no phase information since it is a measure of the fluctuations in the photon numbers. A useful approach to characterize squeezing is a phase sensitive scheme that measures the variance of a quadrature of the field as shown in [21, 22]. Such a scheme is based on homodyne detection and consists of superimposing the input field with the field from a strong local oscillator (LO). In this section we consider the case in which the signal and idler beams from the SROPO are spatially separated and then combined separately with their own local oscillator, one at the frequency of the signal and the other at the frequency of the idler field, before hitting two different photodetectors (see Fig.(4.5.1)). The fluctuations in the signal-idler intensity difference are then investigated with the use of a power spectrum analyzer. Specializing the analysis of section 3.2.1 to the case of intensity difference correlations we obtain from eq. (3.15, 3.16) that the measurable output is related to the Fourier Transform of signal-idler quadrature difference fluctuations:

$$V_D[\omega] = 1 + \int_{-\infty}^{+\infty} d\tau \langle : X_D^{out}(0) X_D^{out}(\tau) : \rangle e^{i\omega\tau}, \quad (4.54)$$

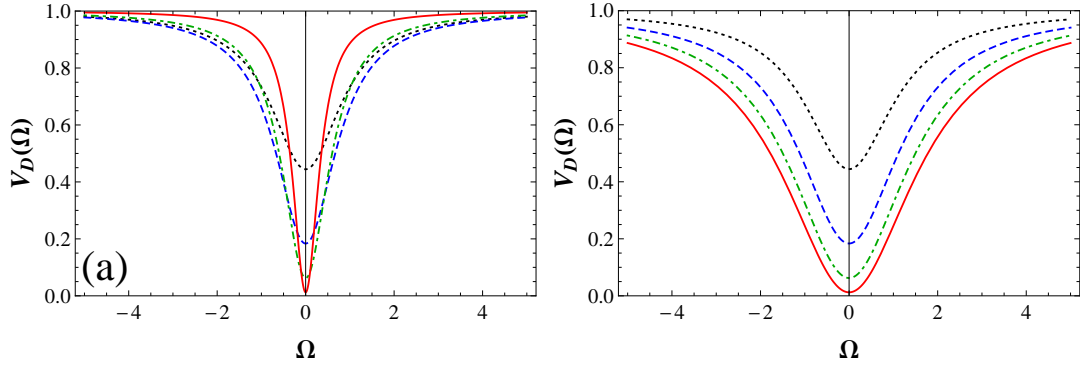


Figure 4.5.2: (a) Quadrature squeezing spectrum (4.28) for a range of input powers and  $\Gamma = 1$ . Curves correspond to  $\varepsilon = 0.2$  (black-dotted line),  $\varepsilon = 0.4$  (blue-dashed line),  $\varepsilon = 0.6$  (green-dash-dotted line),  $\varepsilon = 0.8$  (red-solid line). (b) Quadrature squeezing spectrum in the doubly-resonant case for a range of input powers and  $Z = \gamma_i/\gamma_s = 1$ . Curves correspond to  $\varepsilon = 0.2$  (black-dotted line),  $\varepsilon = 0.4$  (blue-dashed line),  $\varepsilon = 0.6$  (green-dash-dotted line),  $\varepsilon = 0.8$  (red-solid line). Only minimal fluctuations corresponding to  $\theta + \phi = 0$  are shown.  $\Omega = 0$  is the cavity resonance condition.

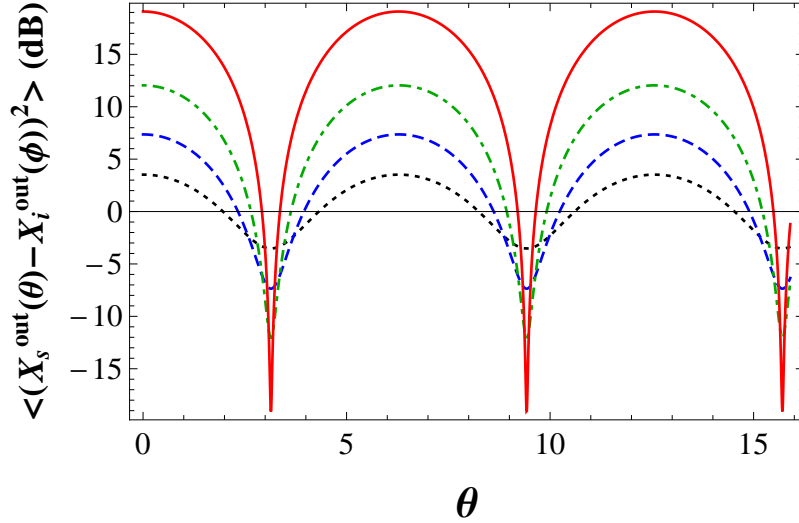


Figure 4.5.3: Quantum Fluctuations of the signal-idler quadrature difference at  $\omega = \omega_s/i$  for several values of the pump parameter  $\varepsilon$  and  $\Gamma = 1$ .  $\phi$  is kept constant while  $\theta$  is scanned linearly. Curves correspond to  $\varepsilon = 0.2$  (black-dotted line),  $\varepsilon = 0.4$  (blue-dashed line),  $\varepsilon = 0.6$  (green-dash-dotted line),  $\varepsilon = 0.8$  (red-solid line).

where  $X_D^{out}(t) = X_\theta^{s,out}(t) - X_\phi^{i,out}(t)$  and

$$\begin{aligned} X_\theta^{s,out}(t) &= \frac{1}{\sqrt{2}} [a_s^{out}(t)e^{-i(\theta+\omega_s t)} + a_s^{\dagger out}(t)e^{+i(\theta+\omega_s t)}] , \\ X_\phi^{i,out}(t) &= \frac{1}{\sqrt{2}} [b^{out}(t)e^{-i(\phi+\omega_i t)} + b^{\dagger out}(t)e^{+i(\phi+\omega_i t)}] , \end{aligned} \quad (4.55)$$

are the quadrature operators for signal and idler beams corresponding to the angles  $\theta$  and  $\phi$  respectively.

The squeezing spectrum for the output quadratures is:

$$: S^{out}(\omega, \theta, \phi) := \int_{-\infty}^{+\infty} d\tau \langle : X_\theta^{s,out}(t) X_\phi^{i,out}(t + \tau) : \rangle e^{-i\omega\tau} \quad (4.56)$$

This normally ordered spectrum  $: S^{out}(\omega, \theta) :$  is related to the squeezing spectrum of the quadrature by the following relation:

$$V_D[\omega] = 1 + : S^{out}(\omega, \theta, \phi) : \quad (4.57)$$

Let us explicitly calculate the expression 4.56:

$$\begin{aligned} : S^{out}(\omega, \theta, \phi) : &= \frac{1}{2} \int_{-\infty}^{+\infty} d\tau [\langle : X_{\theta}^{s,out}(t), X_{\theta}^{s,out}(t+\tau) : \rangle + \langle : X_{\phi}^{i,out}(t), X_{\phi}^{i,out}(t+\tau) : \rangle \\ &\quad - \langle : X_{\theta}^{s,out}(t), X_{\phi}^{i,out}(t+\tau) : \rangle + - \langle : X_{\phi}^{i,out}(t), X_{\theta}^{s,out}(t+\tau) : \rangle] \end{aligned} \quad (4.58)$$

we can rewrite eq. (4.58) as:

$$: S^{out}(\omega, \theta, \phi) := \frac{1}{2} ( : S_{ss}^{out}(\omega, \theta, \phi) : + : S_{ii}^{out}(\omega, \theta, \phi) : - : S_{si}^{out}(\omega, \theta, \phi) : - : S_{is}^{out}(\omega, \theta, \phi) : ) \quad (4.59)$$

we can express the elements in the sum of eq. (4.59) in terms of internal fields as follows:

$$\begin{aligned} : S_{ss}^{out}(\omega, \theta, \phi) : &= \int_{-\infty}^{+\infty} d\tau \langle : X_{\theta}^{s,out}(t), X_{\theta}^{s,out}(t+\tau) : \rangle \\ &= \int_{-\infty}^{+\infty} d\tau \langle a_s^{out}(t), a_s^{out}(t+\tau) \rangle \exp(-2i\theta) \\ &\quad + \int_{-\infty}^{+\infty} d\tau \langle a_s^{\dagger out}(t+\tau), a_s^{out}(t) \rangle \\ &\quad + \int_{-\infty}^{+\infty} d\tau \langle a_s^{\dagger out}(t), a_s^{out}(t+\tau) \rangle \\ &\quad + \int_{-\infty}^{+\infty} d\tau \langle a_s^{\dagger out}(t), a_s^{\dagger out}(t+\tau) \rangle \exp(2i\theta) \end{aligned} \quad (4.60)$$

The second and fifth terms in eq. (4.60) are zero, hence we are left with:

$$: S_{ss}^{out}(\omega, \theta, \phi) := 2\gamma_1 T \int_{-\infty}^{+\infty} d\tau \langle a_s^{\dagger}(t+\tau), a_s(t) \rangle + \langle a_s^{\dagger}(t), a_s(t+\tau) \rangle \quad (4.61)$$

where the symbol  $T$  means temporal ordering.

A similar calculation leads to:

$$\begin{aligned} : S_{ss}^{out}(\omega, \theta, \phi) : &= 2\gamma_1 T \int_{-\infty}^{+\infty} d\tau \langle a_s^{\dagger}(t+\tau) a_s(t) \rangle + \langle a_s^{\dagger}(t) a_s(t+\tau) \rangle \quad (4.62) \\ : S_{ii}^{out}(\omega, \theta, \phi) : &= 2\gamma \varepsilon^2 T \int_{-\infty}^{+\infty} d\tau \langle a_s(t+\tau) a_s^{\dagger}(t) \rangle + \langle a_s(t) a_s^{\dagger}(t+\tau) \rangle \\ : S_{si}^{out}(\omega, \theta, \phi) : &= T \int_{-\infty}^{+\infty} d\tau \langle a^{out}(t) b^{out}(t+\tau) \rangle \exp(-i(\theta + \phi)) + \langle a^{\dagger out}(t) b^{\dagger out}(t+\tau) \rangle \exp(i(\theta + \phi)) \\ : S_{is}^{out}(\omega, \theta, \phi) : &= T \int_{-\infty}^{+\infty} d\tau \langle b^{out}(t) a^{out}(t+\tau) \rangle \exp(-i(\theta + \phi)) + \langle b^{\dagger out}(t) a^{\dagger out}(t+\tau) \rangle \exp(i(\theta + \phi)) \end{aligned}$$

where:

$$\begin{aligned} T \langle a^{\text{out}}(t)b^{\text{out}}(t+\tau) \rangle &= 2\varepsilon\sqrt{\gamma_1\gamma} [\vartheta(\tau) \langle a_s(t)a_s^\dagger(t+\tau) \rangle + \vartheta(-\tau) \langle a_s^\dagger(t+\tau)a_s(t) \rangle] \\ T \langle a^{\dagger\text{out}}(t)b^{\dagger\text{out}}(t+\tau) \rangle &= 2\varepsilon\sqrt{\gamma_1\gamma} [\vartheta(\tau) \langle a_s(t+\tau)a_s^\dagger(t) \rangle + \vartheta(-\tau) \langle a_s^\dagger(t)a_s(t+\tau) \rangle] \\ T \langle b^{\text{out}}(t)a^{\text{out}}(t+\tau) \rangle &= 2\varepsilon\sqrt{\gamma_1\gamma} [\vartheta(\tau) \langle a_s^\dagger(t)a_s(t+\tau) \rangle + \vartheta(-\tau) \langle a_s(t+\tau)a_s^\dagger(t) \rangle] \quad (4.63) \\ T \langle b^{\dagger\text{out}}(t)a^{\dagger\text{out}}(t+\tau) \rangle &= 2\varepsilon\sqrt{\gamma_1\gamma} [\vartheta(\tau) \langle a_s^\dagger(t+\tau)a_s(t) \rangle + \vartheta(-\tau) \langle a_s(t)a_s^\dagger(t+\tau) \rangle] \quad (4.64) \end{aligned}$$

Lengthy calculations (but feasible by well prepared PhD students) provide the quadrature squeezing spectrum:

$$V_D[\Omega] = 1 + \frac{4\varepsilon \left[ (1 + \Gamma)\varepsilon - \sqrt{\Gamma}(1 + \varepsilon^2) \cos(\theta + \phi) \right]}{(-1 + \varepsilon^2)^2 + \Omega^2}. \quad (4.65)$$

The spectrum (4.65) is plotted in Fig. 4.5.2(a) for different values of the pump parameter  $\varepsilon$  and for  $\Gamma = 1$ . In this case eq. (4.65) reduces to:

$$V_D[\Omega] = 1 - \frac{4\varepsilon}{(1 + \varepsilon)^2 + [\Omega/(1 - \varepsilon)]^2}, \quad (4.66)$$

showing again a line narrowing when approaching threshold. Such result should be contrasted with the doubly-resonant OPO where one obtains the same formula (4.66) after replacing  $Z = \gamma_i/\gamma_s$  and  $\Omega/(1 - \varepsilon) = \Delta$  and where no line narrowing is observed [8, 22]. This is made clear in the plots of Fig. 4.5.2(b). Singly and doubly resonant cases, however, have coincident spectra at  $\Omega = 0$ . The squeezing spectrum is symmetric around  $\Omega = 0$ , which corresponds to the local oscillators frequencies  $\omega_{s/i}$ . One difference with the intensity case of Section 4.4.2 is that a progressive growth in the squeezing level when approaching threshold of oscillation is observed.

Another useful way to visualize squeezing is shown in Fig. 4.5.3 where we plot the quantum fluctuations of the signal-idler quadrature difference at  $\omega = \omega_{s/i}$  in a decibel scale with respect to the shot noise level obtained by blocking the SROPO pump. The plot is obtained by keeping the phase  $\phi$  of one of the two local oscillators fixed while varying the phase  $\theta$  of the other. The shot noise level or standard quantum limit (SQL) is represented by the zero black line. It is evident that a large amount of squeezing (-19 dB) can, in principle, be obtained in this situation.

Fig. 4.5.4 displays the noise spectrum as a function of the normalized pump amplitude in the case in which the signal field experiences other losses besides those due to the mirror transmittance ( $\Gamma = 0.8$  in this plot). Fig. 4.5.5 shows the signal-idler quadrature fluctuations for  $\Gamma = 0.8$  for several values of the pump parameter as a function of  $\theta$ , the phase of the signal local oscillator. It is clear from these figures that the squeezing level is severely affected by other asymmetric loss mechanisms and that squeezing degradation becomes more important as we approach threshold. The degradation of squeezing in Fig. 4.5.4 and Fig. 4.5.5 reflects the difficulty to achieve noise cancellation in the signal-idler intensity for an asymmetric cavity in the presence of growth of the single beam noise. It is, however, possible to compensate for this behaviour by introducing the optimal squeezing angle [8]. In the case in which signal and idler beams experience other asymmetric losses the symmetric combination of quadrature operators in eq. (4.54) is no longer the best choice and we have to use a more general linear combination of signal-idler quadrature operators parametrized by an angle  $\psi$ .

$$X_D(t) = \cos(\psi)X_\theta^s(t) - \sin(\psi)X_\phi^i(t). \quad (4.67)$$

In this, more general, case the calculated squeezing spectrum turns out to be:

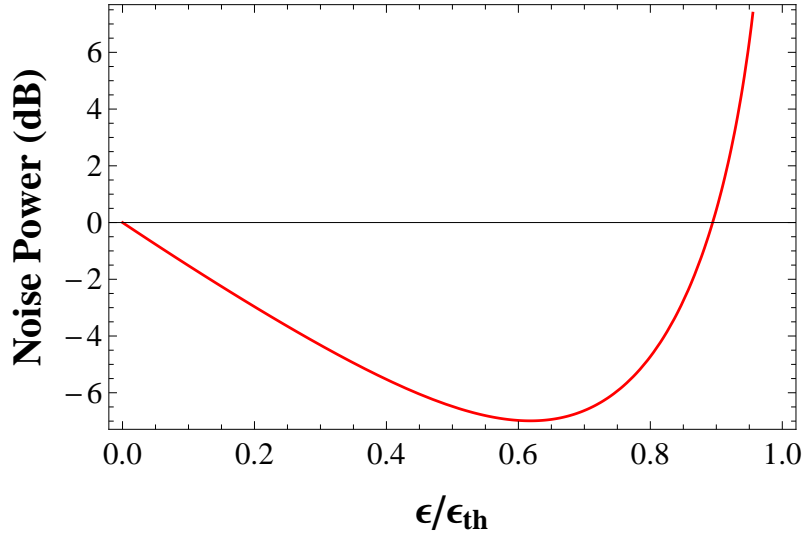


Figure 4.5.4: Noise power at resonance as a function of normalized pump amplitude. Here  $\Gamma = 0.8$ .

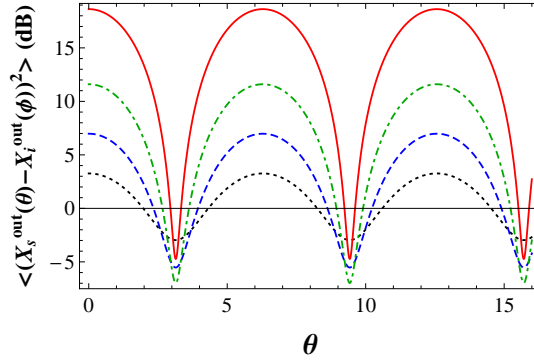


Figure 4.5.5: Quantum fluctuations of the signal-idler quadrature difference at  $\omega = \omega_{s/i}$  for several values of the pump parameter  $\varepsilon$  and  $\Gamma = 0.8$ . Curves correspond to  $\varepsilon = 0.2$  (black-dotted line),  $\varepsilon = 0.4$  (blue-dashed line),  $\varepsilon = 0.6$  (green-dash-dotted line),  $\varepsilon = 0.8$  (red-solid line).  $\phi$  is kept constant while  $\theta$  is scanned linearly in time.

$$V_D[\Omega] = 1 + \frac{4\varepsilon \left[ 2\varepsilon \cos^2[\psi] + 2\Gamma\varepsilon \sin^2[\psi] - \sqrt{\Gamma}(1 + \varepsilon^2) \sin[2\psi] \right]}{(-1 + \varepsilon^2)^2 + \Omega^2}. \quad (4.68)$$

The optimization of signal-idler correlations is achieved by minimizing eq. (4.68) with respect to  $\psi$  for a given fixed value of all the other parameters and by choosing the frequency  $\Omega$  where minimal fluctuations occur (in our case  $\Omega = 0$ ). The optimal angle  $\psi_0$  is found from:

$$\tan(2\psi_0) = \frac{\sqrt{\Gamma}(1 + \varepsilon^2)}{(1 - \Gamma)\varepsilon}. \quad (4.69)$$

The squeezing spectrum plotted in Fig. 4.5.6 for  $\Gamma = 0.8$  and  $\varepsilon = 0.8$  shows a non-optimal choice of the angle  $\psi$  (narrower curve) and an optimal one (broader curve). From this figure it is evident that by operating at the optimal choice of the angle  $\psi$  one obtains an improvement in the squeezing level.

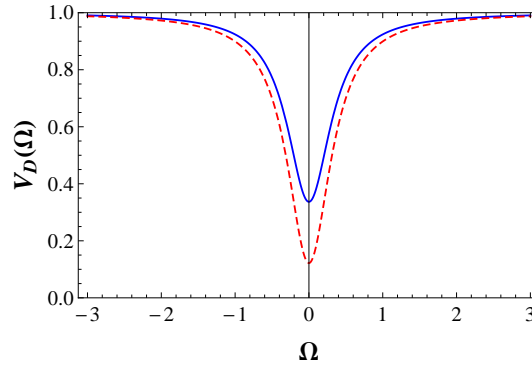


Figure 4.5.6: Optimized quadrature spectrum. In this case  $\Gamma = 0.8$ ,  $\varepsilon = 0.8$  and  $\psi = \pi/4$  (blue-solid line),  $\psi = \psi_0$  (red-dashed line).

## 4.6 Quantum Entanglement in SROPO

In order to claim state inseparability and consequently entanglement for the signal-idler state we apply the separability criterion of Simon-Duan [23, 24] introduced in eq. (2.105) of section 2.5 to quadrature operators of eq. (4.55) which satisfy the condition of the separability theorem for two mode continuous variable systems, as to say:

$$[X_{\theta}^s, X_{\theta+\pi/2}^s] = i \quad (4.70)$$

$$[X_{\phi}^i, X_{\phi+\pi/2}^i] = i \quad (4.71)$$

Hence according to the Simon-Duan criterion a sufficient condition for state inseparability is that the quantity:

$$S = \langle [X_{\theta}^s - X_{\phi}^i]^2 \rangle + \langle [X_{\theta+\pi/2}^s + X_{\phi+\pi/2}^i]^2 \rangle \quad (4.72)$$

is such that:

$$S < 2. \quad (4.73)$$

We have calculated  $S = 0.024$  for the case where  $\varepsilon = 0.8$  and  $\Gamma = 1$ ,  $S = 0.67$  for  $\varepsilon = 0.8$ ,  $\Gamma = 0.8$  and  $\psi = \pi/4$ . Finally  $S = 0.5$  for  $\Gamma = 0.8$ ,  $\varepsilon = 0.8$  and  $\psi = \psi_0$ . Hence we conclude that the signal and idler beams are in an entangled state for wide ranges of parameters values and different configurations of SROPO operation. The dependence of the amount of entanglement on the normalized pump value is shown in Fig. 4.6.1 where the dB scale is evaluated with respect to the value 2 which sets the limit of state separability in eq. (4.72).

## 4.7 Numerical Results for Intensity Difference Spectra

We can derive the relation between the intensity difference correlation function eq. (4.50) written in terms of normally ordered operators and the c-numbers  $\alpha$  in the Wigner representation using the following substitutions [21]:

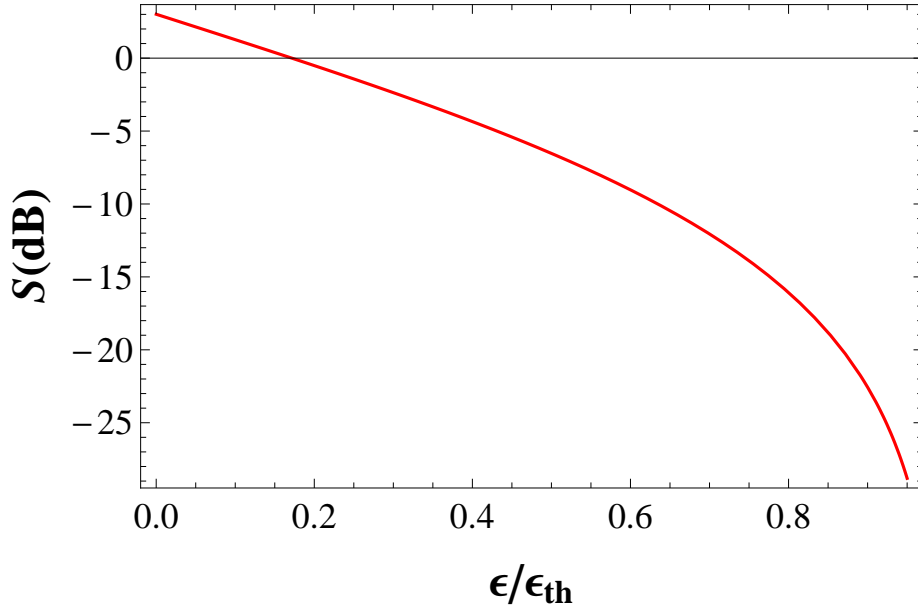


Figure 4.6.1: Amount of entanglement as a function of the normalized pump value. The dB scale is evaluated respect to the value 2 which sets the limit of state separability in eq. (4.72).  $\Gamma = 1$  in this figure.

$$\begin{aligned}
\langle \hat{a}^\dagger(t)\hat{a}(t) \rangle &= \langle \alpha^*(t)\alpha(t) \rangle_W - \frac{1}{2} \\
\langle \hat{a}^\dagger(t+\tau)\hat{a}(t+\tau) \rangle &= \langle \alpha^*(t+\tau)\alpha(t+\tau) \rangle_W - \frac{1}{2} \\
\langle \hat{a}^\dagger(t+\tau)\hat{a}(t) \rangle &= \langle \alpha^*(t)\alpha(t+\tau) \rangle_W - (\langle \alpha^*(t)\alpha(t+\tau) \rangle_W)_0
\end{aligned} \tag{4.74}$$

where:

$$\begin{aligned}
\langle \alpha^*(t)\alpha(t) \rangle_W &= \int W(\alpha^*, \alpha) |\alpha|^2 d^2\alpha \\
\langle \alpha^*(t+\tau)\alpha(t+\tau) \rangle &= \int W(\alpha^*, \alpha) |\alpha|^2 d^2\alpha \\
\langle \alpha^*(t)\alpha(t+\tau) \rangle_W - (\langle \alpha^*(t)\alpha(t+\tau) \rangle_W)_0 &= \int W(\alpha^*, \alpha) |\alpha|^2 d^2\alpha \\
&\quad - \left( \int W(\alpha^*, \alpha) |\alpha|^2 d^2\alpha \right)_0
\end{aligned} \tag{4.75}$$

where the subscript “0” means that we have to evaluate the mean value in the vacuum state, that is we have to set to zero the input pump field.

In order to solve numerically the quantum equation for SROPO in eq. (4.22) we consider that, as showed in the previous chapter, the evolution equations of the Wigner field amplitudes are the same as the Heisenberg equations of motion of the quantum field amplitudes, whenever these are linear. Having this in mind we can consider the annihilation operator  $a$  of eq. (4.22) to be a classical  $c$ -number  $\alpha$  and numerically integrate the semi-classical equation of motion for SROPO.

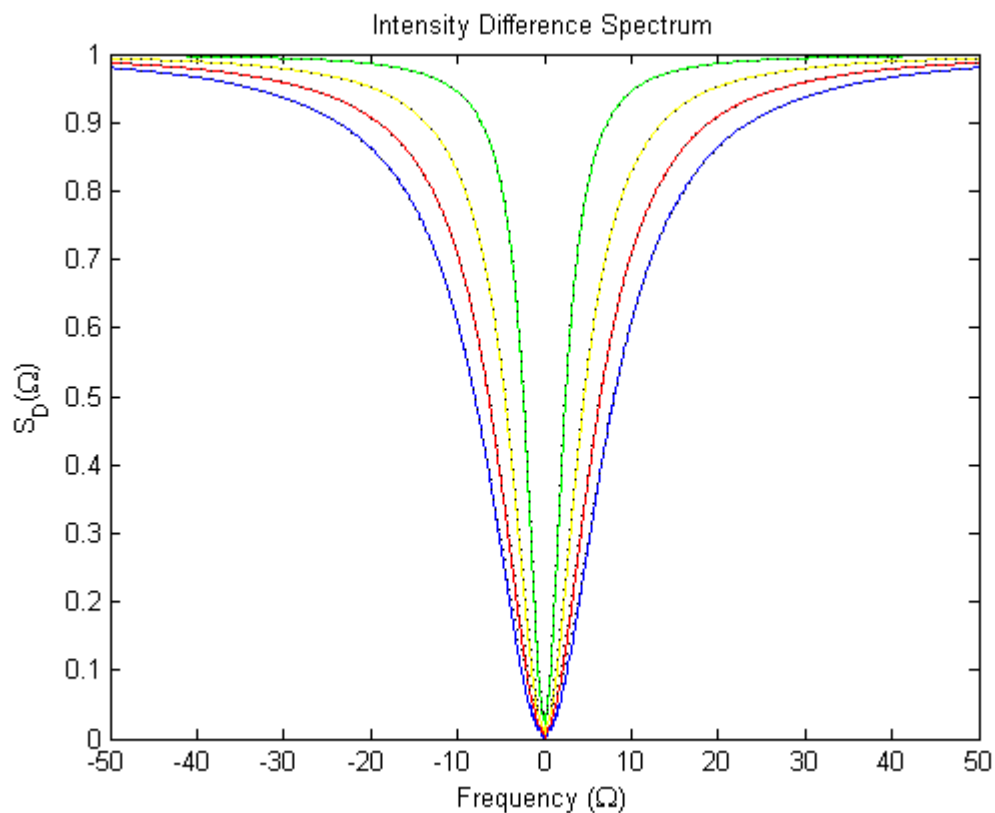


Figure 4.7.1: Numerical intensity difference correlation spectrum plotted for a range of input powers. Curves corresponds to  $\epsilon = 0.6$  (blue line),  $\epsilon = 0.7$  (red line),  $\epsilon = 0.8$  (yellow line),  $\epsilon = 0.9$  (green line). Black dotted lines corresponds to the theoretically predicted spectra.

We have solved the equation of motion using a split-step method with gaussian noise. From the numerical solution for the field  $\alpha$  it is possible to obtain, by using eqs. (4.74,4.75) and eq. (4.50), the intensity difference spectra for the SROPO system.

The results of the simulations are illustrated in Fig. 4.7.1 where intensity difference spectra are plotted for different values of pump parameter (solid lines) and also the analytical results are inserted as black dotted lines. The figure shows a very remarkable agreement between numerical and theoretically predicted spectra of eq. (4.52).

## 4.8 Conclusions

We have applied the input-output theory of [16] to study the quantum fluctuations of singly resonant optical parametric oscillators. The model has been used to calculate intensity and quadrature squeezing spectra. We have shown that below threshold of oscillation the fluctuations in the light outside the cavity at the frequencies of the signal and the idler fields are squeezed below the shot noise as much as the doubly resonant case. We have also shown that signal and idler fields are entangled over a wide range of pump parameter values in SROPO by using the Simon-Duan criterion of state separability.

One major difference of the SROPO from the doubly resonant case is that we observe an unexpected dependence of the intensity difference spectrum on the pump parameter leading to a narrowing of the spectral line as the threshold of oscillation is approached. An analogous dependence of the quadrature spectrum on the pump parameter is also found. A peculiar feature of singly-resonant configurations is that the narrowing of the spectral lines does not affect the squeezing minimum which is capable to reach values similar to those of the doubly-resonant case as threshold is approached. Since the singly resonant cavity is one of the most simple OPO configuration to realize and since there is no difference in the squeezing properties of the light coming from this device with respect to the doubly resonant cavity, we conclude that the singly resonant configuration could be an ideal candidate for the realization of two-color entangled light in quantum information processes.

## Bibliography

- [1] P. Grangier, R.E. Slusher, B. Yurke and A. La Porta, *Phys. Rev. Lett.* **59**, 2153 (1987).
- [2] M. Xiao, L. A. Wu and H. J. Kimble, *Phys. Rev. Lett.* **59**, 278 (1987).
- [3] C. M. Caves, *Phys. Rev. Lett.* **45**, 75 (1980).
- [4] A. F. Pace, M. J. Collett, D. F. Walls, *Phys. Rev. A* **47**, 3173 (1993).
- [5] S. L. Braunstein, P. Van Loock, *Reviews of Modern Physics* **77**, 513 (2005).
- [6] L. Mandel and E. Wolf, *Optical Coherence and Quantum Optics* (Cambridge University Press, Cambridge, 1995).
- [7] C. Fabre, E. Giacobino, A. Heidmann and S. Reynaud, *J. Phys. France* **50** 1209 (1989).
- [8] C. Schori, J. L. Sorensen and E. S. Polzik, *Phys. Rev. A* **66**, 033802 (2002).
- [9] J. Laurat, T. Coudreau, G. Keller, N. Treps, and C. Fabre, *Phys. Rev. A* **71**, 022313 (2005).
- [10] C. W. Gardiner and P. Zoller, *Quantum Noise*, (Springer, Berlin, 2004).
- [11] D. F. Walls and Gerard J. Milburn, *Quantum Optics*, (Springer, Berlin, 2008).
- [12] I. N. Agafonov, M. V. Chekhova and G. Leuchs, *Phys. Rev. A* **82**, 011801(R) (2010).
- [13] M. J. Collett and R. B. Levien, *Phys. Rev. A* **43**, 5068 (1991).
- [14] R. Paschotta, M. Collett, P. Kürz, K. Fiedler, H. A. Bachor and J. Mlynek, *Phys. Rev. Lett.* **72**, 3807 (1994).
- [15] K. J. Blow, R. Loudon, S. J. D. Phoenix, and T. J. Shepherd *Phys. Rev. A* **42**, 4102 (1990).
- [16] M. J. Collett and C. W. Gardiner, *Phys. Rev. A* **30**, 1386 (1984).
- [17] S. Reynaud, C. Fabre and E. Giacobino, *J. Opt. Soc. Am. B* **4**, 1520 (1988).
- [18] A. S. Lane, M. D. Reid and D. F. Walls, *Phys. Rev. A* **38**, 788 (1988).

- 
- [19] A. Heidmann, R. J. Horowicz, S. Reynaud, E. Giacobino, C. Fabre and G. Camy, Phys. Rev. Lett. **59**, 2555 (1987).
- [20] A. S. Lane, M. D. Reid and D. F. Walls, Phys. Lett. **60**, 1940 (1988).
- [21] M. O. Scully and M. S. Zubairy, *Quantum Optics*, (Cambridge University Press, Cambridge, 2008).
- [22] P. D. Drummond and M. D. Reid, Phys. Rev. A **41**, 3930 (1990).
- [23] R. Simon, Phys. Rev. Lett. **84**, 2726 (2000).
- [24] L. M. Duan, G. Giedke, J. I. Cirac and P. Zoller, Phys. Rev. Lett. **84**, 2722 (2000).

## Short pulse generation in the synchronously pumped SROPO

### 5.1 Introduction

The usual way to analyze optical propagation systems and optical resonators is the search for the eigenmodes of these systems. The motivation of this approach is the assumption that the fields in such optical systems can be expanded in a complete set of such eigenmodes, which are usually called “normal modes” of the system. The word “normal” in this context means that the eigenmodes of the system  $u_n$  are orthogonal to each other in the usual sense and can be normalized to one, as to say:

$$\int u_n^*(x)u_m(x) dx = 0 \quad (5.1)$$

$$\int u_n^*(x)u_n(x) dx = 1 \quad (5.2)$$

where the integrals are over all the coordinates of the eigenfunctions.

In optical system these modes, resonant or propagating, are eigensolutions of a linear operator which describes the electro-magnetic field inside the material under study. In most cases this linear operator is Hermitian and it is then rigorously true that the eigenmodes of this operator and hence the modes of the optical system, are orthogonal as defined in equations (5.1-5.2).

However many optical systems, such as unstable resonator and gain-guided amplifiers, are described by modes which are not orthogonal in the usual sense. These systems are described in terms of eigenmodes, referred to as Fox-Li modes [1], of a propagation operator which is non-Hermitian and hence they are not orthogonal in the usual sense, as we will see later in this chapter.

Closely related to non-normality is the notion of pseudospectra, which we will analyze later in this chapter. Let's say that spectra and eigenvalues are imperfect tools for analyzing non-normal matrices and operator because they are not efficient means to understand the behaviour of physical system described by non-Hermitian matrices.

## 5.2 Mathematical Overview of Non-Normal Operators

In general it is possible to find the eigenmodes of a system whose evolution is described by an operator  $L$  by means of an operator equation of the type:

$$Lu_n(x) = \gamma_n u_n(x) \quad (5.3)$$

where  $L$  can be a differential or integral operator which admits a set of eigenfunctions  $u_n(x)$  and eigenvalues  $\gamma_n$  which satisfy the equation for the system and at the same time the boundary conditions.

Now the crucial point is that for many real systems the operator  $L$  does not satisfy neither the Hermitianity condition:

$$L = L^\dagger = (L^*)^T \quad (5.4)$$

where  $L^\dagger$  is the Hermitian adjoint of the operator  $L$ , while  $(L^*)^T$  indicates the transposition and complex conjugation of the operator  $L$ , nor the “normality” condition:

$$[L, L^\dagger] = 0 \quad (5.5)$$

Note that normal matrices, defined by eq. (5.5), include along with Hermitian matrices all those which are skew-Hermitian, unitary, circulant as well as others.

The important consequence of the lack of “normality” is that it does not guarantee the existence of a set of eigenfunctions and even in the case this set exists it cannot be guaranteed that the eigenmodes are orthogonal to each other in the sense of equations (5.1-5.2). Hence if we consider two different eigenmodes of the system  $u_n$  and  $u_m$  [2, 3]:

$$\int u_n^*(x)u_m(x) dx \neq 0 \quad (5.6)$$

It is always possible to show that these eigenmodes can be normalized to unit such that:

$$\int u_n^*(x)u_n(x) dx = 1 \quad (5.7)$$

In the case that the operator  $L$  has a set of eigenmodes  $u_n$  then the Hermitian adjoint operator  $L^\dagger$  will have a set of eigenmodes,  $v_n$ , which satisfy the equation:

$$L^\dagger v_n(x) = \gamma_n^* v_n(x) \quad (5.8)$$

It can than been shown that the eigenmodes  $u_n$  and  $v_n$  will be bi-orthogonal to each other in the sense that:

$$\int u_n^*(x)v_m(x) dx = \delta_{nm} \quad (5.9)$$

As in the case of the eigenmodes of the operator  $L$ , also the eigenmodes  $v_n$  of the operator  $L^\dagger$  are not orthogonal to each other and it can also be shown that if the set  $u_n$  is properly normalized to unity than the set  $v_n$  is such that:

$$\int v_n^*(x)v_n(x) dx > 1 \quad (5.10)$$

In order to show the last property consider the function:

$$v_n(x) = u_n^*(x) + \Delta u_n^*(x) \quad (5.11)$$

and its complex conjugate. The function  $\Delta u_n^*(x)$  represents the difference between the eigenmode  $u_n$  and the eigenmode  $v_n^*$  having the same eigenvalue  $\gamma_n^*$ . The bi-orthogonality of the two sets of eigenmodes and the normalization to one of the set  $u_n$  leads to:

$$\int u_n(x) \Delta u_n^*(x) dx = \int u_n^*(x) \Delta u_n(x) dx = 0 \quad (5.12)$$

and so the normalization of the  $v_n$  eigenmodes becomes:

$$\int v_n(x) v_n^*(x) dx = 1 + \int \Delta u_n(x) \Delta u_n^*(x) dx \geq 1 \quad (5.13)$$

and this integral is greater than unity unless the difference  $\Delta u_n^*(x)$  is identically zero.

### 5.2.1 The Case of Optical Resonator Eigenmodes

Consider a pulse of radiation making a complete round trip around an optical cavity. After a complete round trip the pattern of the field  $E^{(1)}(s, z)$  at a definite reference plane  $z$  will be different from its starting pattern  $E^{(0)}(s, z)$  before the round trip because of diffraction, reflection and aperturing effects. Moreover after a second round trip the pattern  $E^{(2)}(s, z)$  may again be still different. We have used the notation  $s = (x, y)$  to indicate the transverse coordinates in the optical cavity and  $z$  to indicate the longitudinal coordinate.

What we ask is if it is possible to find patterns, call them  $E_{n,m}(s, z)$ , such that if a pulse is launched with an initial transverse profile matching one of these transverse mode patterns, it will return one round trip later with the same transverse pattern at any reference plane  $z$  but possibly with a reduced amplitude because of diffraction or other losses during round trip. These self-reproducing transverse patterns are what is known in the literature under the name of transverse mode.

Mathematically the propagation through one round trip in an optical resonator can be described by a propagation integral of the following form:

$$E^{(1)}(s, z + p) = e^{-ikp} \int_A ds_0 K(s, s_0, z) E^{(0)}(s, z) \quad (5.14)$$

where  $k$  is the propagation constant at the carrier frequency of the optical signal and  $p$  is the length of the round trip. The differential  $ds = dx_0 dy_0$  is integrated over the full cross section  $A$  of the resonator at the selected reference plane  $z$ . The function  $K(s, s_0, z)$  appearing in eq. (5.14) is called the propagation kernel, generally similar to Huygen's integral and its particular form will depend on the reference plane chosen, on mirror apertures and on the intracavity optics in the optical structures. In other words this integral describes the propagation of the optical pulse from the chosen reference plane  $z$  to the corresponding reference plane  $z + p$  one period  $p$  later.

Hence the self reproducing transverse pattern  $E_{n,m}(s, z)$  must be such that each of them, after one round trip, satisfy the round trip propagation expression:

$$E_{n,m}^{(1)}(s, z) = e^{-ikp} \int_A ds_0 K(s, s_0, z) E_{n,m}^{(0)}(s_0, z) = \gamma_{n,m} E_{n,m}^{(0)}(s, z) \quad (5.15)$$

If eigensolutions that satisfy eq. (5.15) exist, then these eigensolutions will provide the self reproducing transverse eigenmodes that we are looking for. Hence if we launch an optical pulse in the form of any single one of these eigenmodes in the proper direction at the selected reference plane, then after one round trip the field at the same plane will be:

$$E_{n,m}^{(1)}(s, z) = \gamma_{n,m} e^{-ikp} E_{n,m}^{(0)}(s, z) \quad (5.16)$$

As it is clear from eq. (5.16), the field after one round trip will have the same transverse pattern but will be reduced in amplitude by the eigenvalue  $\gamma_{n,m}$ . In fact if we deal with open-sided resonators with finite diameter mirrors, for example, some of the radiation will spread out past the mirror edges at each round trip, and the magnitude of the transverse eigenvalues will be less than unity (if no gain mechanisms are present in the resonator):

$$|\gamma_{n,m}| < 1 \quad (5.17)$$

Hence even with perfectly lossless mirrors the n,m-th mode of an optical resonator will always have a power loss for round trip given by:

$$P_{loss} = 1 - |\gamma_{n,m}|^2 \quad (5.18)$$

It is usual to consider that such resonant eigenmodes always exist and this is because one often deals with closed cavities with lossless walls where the wave equation describing the propagation of the fields is an Hermitian operator. In this case the existence of a complete set of normal modes can be rigorously proven and at the same time also its orthogonality. This means that any arbitrary field pattern inside the cavity can be expanded using this set of eigenmodes as the basis set:

$$E(s, z) = \sum_{n,m} c_{n,m}(z) E_{n,m}(s, z) \quad (5.19)$$

which satisfy an orthogonality property similar to the one of eq. (5.6):

$$\int_A ds E_{n,m}(s, z) E_{s,p}(s, z) = \delta_{n,p} \delta_{m,q} \quad (5.20)$$

where  $\delta_{n,p}$  is the Kronecker delta function.

On the other hand, for the case of an open resonator there is a problem related to the fact that the round trip propagation kernel  $K(s, s_0, z)$  is not in general an Hermitian operator. This means that the existence of a complete and orthogonal set of eigenfunctions of eq. (5.15) is not guaranteed in advance and must be proven mathematically in each case so that the expansion in eq. (5.19) and the property in eq. (5.20) are no more automatic.

As an example consider the fundamental equation governing the evolution of electric field  $E(s, z)$  in an empty optical resonator of longitudinal length  $L$ :

$$[\nabla^2 + k^2(x)] E(s, z) = 0 \quad (5.21)$$

and since one is concerned with the propagation in the  $z$  direction, we replace  $E$  by the variable  $u$  defined by  $E(s, z) = e^{-ikz} u(s, z)$ . The solution of this equation is the well known Huygens-Fresnel integral representing the solution at position  $z$  in terms of the solution at  $z = 0$ :

$$u(s, z) = \sqrt{\frac{ik}{2\pi z}} \int_{-\infty}^{+\infty} dt e^{-ik(s-t)^2/2z} u(t, 0) \quad (5.22)$$

This integral operator mapping  $u(s, 0)$  to  $u(s, z)$  is unitary and hence normal and energy conserving. The existence of a complete set of orthogonal eigenfunctions is guaranteed. The search for the eigenmodes and eigenvalues of the system leads, by means of the Fox and Lie method [1] to an integral equation of the type:

$$\int_A K(s, s_0, z) u_{n,m}(s_0, z) ds_0 = \gamma_{n,m} u_{n,m}(s, z) \quad (5.23)$$

where  $K$  is the Huygens integral for propagation once around the optical cavity which in this case is given by:

$$K(s, s_0, z) = \sqrt{\frac{ik}{2\pi z}} e^{-ik(s-s_0)^2/2z} \quad (5.24)$$

On the other hand if we consider the case of an open cavity of length  $L$  and transverse dimensions with endpoints  $s = (x, y) = (\pm 1, \pm 1)$  the signal field inside the resonator after one round trip will evolve according to the truncation of eq. (5.22):

$$u(s, z) = Au(s, z_0) = \sqrt{\frac{ik}{2\pi L}} \int_{-1}^{+1} dt e^{-ik(s-t)^2/2L} u(t, 0) \quad (5.25)$$

In this situation a pulse of light starts to propagate with transverse field given by  $u(s, 0)$  and as it reaches the second mirror, its portion with  $|s| \leq 1$  reflects, while its portion with  $|s| > 1$  radiates to infinity and is lost. Mathematically the operator in eq. (5.25) is a compact operator but it is not Hermitian and hence all the problems about the existence of a complete set of eigenfunctions and on their eventual orthogonality arise.

## 5.3 Overview Of the Concept Of Pseudo-Spectra

The crucial role of eigenvalues in science lies in the fact that in most cases these entities are what one observes in the first place in physical systems. For example the frequencies of oscillation of strings and drums are immediately perceived by human ears while the energy levels of atoms and molecules are identified, by quantum mechanics, to be eigenvalues of a self-adjoint Schrödinger operator. Historically the search for eigenmodes and eigenvalues started in connection with the analysis of Hermitian matrices and self-adjoint linear operators.

Eigenvalues problems are also important, as we know, because they are used to investigate the stability of fixed points of a dynamical system [4]. It is well known that fixed points are stable if all the eigenvalues of the linearized equations have negative real part implying in this case that any small perturbation of the initial conditions decays asymptotically to zero. Where the spectral analysis fails is in the lack of prediction of transient growth of the solution of the system before decaying monotonically to the steady state. This problem arises in connection with the study of systems whose evolution is described by non-normal operators. In these cases the eigenvalues and eigenvectors are imperfect tools for analyzing the behaviour of the system because they do not dominate anymore the evolution of the highly non normal systems.

Consider for example a dynamical system governed by the following differential equation:

$$\frac{d\vec{u}}{dt} = A\vec{u} \quad (5.26)$$

where  $\vec{u}$  is a vector and  $A$  is a matrix. The formal solution for eq. (5.26) is :

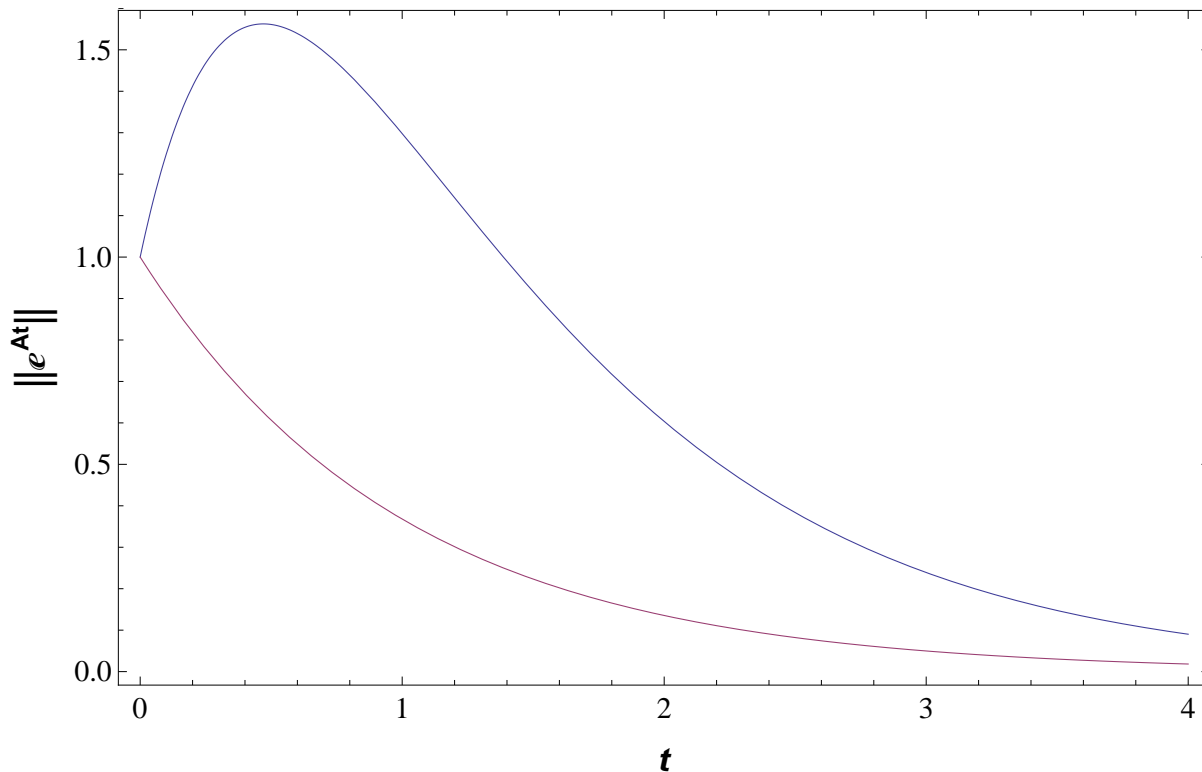


Figure 5.3.1:  $\|e^{At}\|$  versus  $t$  for the matrices  $A_1$  and  $A_2$ .

$$\vec{u}(t) = \vec{u}(0)e^{At} \quad (5.27)$$

Consider now the two matrices:

$$A_1 = \begin{pmatrix} -1 & 1 \\ 0 & -1 \end{pmatrix}, \quad A_2 = \begin{pmatrix} -1 & 5 \\ 0 & -2 \end{pmatrix} \quad (5.28)$$

The matrix  $A_1$  has a stable fixed point at  $\vec{u}(t) = (0, 0)$  with eigenvalues and eigenvectors:

$$\lambda_{1,2} = -1, \quad v_{1,2} = (1, 0) \quad (5.29)$$

while the matrix  $A_2$  has a stable fixed point at  $\vec{u}(t) = (0, 0)$  with eigenvalues and eigenvectors:

$$\lambda_1 = -2, \quad v_{1,2} = (-5, 1); \quad \lambda_2 = -1, \quad v_{1,2} = (1, 0); \quad (5.30)$$

The eigenvalue  $-1$  of  $A_1$  is defective and therefore some growth must be expected in the transient before decay. On the other hand the eigenvalues of  $A_2$  are distinct and negative and so no growth should occur. Looking at figure 5.3.1, where the 2-norm of  $e^{tA}$  versus time is shown, tells a different story. In fact while the function  $\|e^{tA_1}\|_2$  decays monotonically, the function  $\|e^{tA_2}\|_2$  grows in a transient phase before decaying to the steady state. The difference between the prediction based on the eigenvalues of  $A$  and the behaviour of  $\|e^{tA}\|_2$  is the fact that the eigenvectors are not orthogonal. A linear combination of these eigenvectors may have large coefficients but small norm because of cancellation. If the coefficients drift out of phase with increasing time the cancellation may be lost, the norm of the linear combination may increase even though each individual component is decaying monotonically (negative eigenvalues).

From eq. (5.27) it is clear that the maximum growth at any time  $t$  of the solution  $\vec{u}(t)$  is given by:

$$\mathit{Sup}_{\vec{u}(0)} \frac{\|\vec{u}(t)\|_2}{\|\vec{u}(0)\|_2} = \|e^{At}\|_2 \quad (5.31)$$

and the maximum transient growth is:

$$\mathit{Sup}_{t>0} \|e^{At}\|_2 \quad (5.32)$$

In simple cases, like the one we have presented in this section, it is possible to calculate analytically the transient growth of the system. In more complicated situations an analytical or a numerical tool is necessary to investigate the magnitude of the transient growth. In particular it is useful to know the frequency dependence of the amplification factor of a periodic forcing term.

Let's consider the response of a linear system:

$$\dot{\vec{x}} = M\vec{x} + \vec{f}(t) \quad (5.33)$$

to a modulation  $\vec{f}(t) = \vec{f}_0 e^{zt}$  with  $z \in \mathbb{C}$ . The asymptotic behaviour is given by:

$$\vec{x}_\infty = (zI - M)^{-1} \vec{f}_0 \quad (5.34)$$

provided that the eigenvalues of  $M$  have negative real part. The amplification factor is:

$$\mathit{Sup}_{\vec{f}(0)} \frac{\|\vec{x}_\infty\|_2}{\|\vec{f}_0\|_2} = \|(zI - M)^{-1}\| = \|R(z, M)\| \quad (5.35)$$

Where  $R(z, M)$  is the resolvent of the matrix  $M$ . This equation tells us that the norm of the resolvent of  $M$  is the amplification factor of an exponential perturbation with complex exponent  $z$ . Let us consider as function of  $z$ , the norm of the resolvent  $(zI - M)^{-1}$ . When  $z$  is an eigenvalue of  $M$ ,  $\|(zI - M)^{-1}\|$  is infinite, otherwise it is finite.

If the matrix  $M$  is normal then:

$$\|(zI - M)^{-1}\| = \frac{1}{\mathit{dist}(z, S(M))} \quad (5.36)$$

where  $\mathit{dist}(z, S(M))$  represents the distance of  $z$  from the spectrum of  $M$ ,  $S(M)$ :

$$\mathit{dist}(z, S(M)) = \mathit{Inf}_{\lambda \in S(M)} d(z, \lambda) \quad (5.37)$$

Hence, in the normal case the surface  $\|(zI - M)^{-1}\|$  is determined entirely by the eigenvalues. On the other hand for non normal matrices eq. (5.36) is only a lower bound and the shape of the surface cannot be inferred from the eigenvalues. For example  $\|(zI - M)^{-1}\|$  can have values as great as  $10^{10}$  or  $10^{20}$  even when  $z$  is far from the spectrum of  $M$ .

It is then natural to define the  $\varepsilon$ -pseudospectrum [6, 5], for each  $\varepsilon > 0$ , by:

$$\Lambda_\varepsilon(M) = \{z \in \mathbb{C} : \|zI - M\|^{-1} \geq \varepsilon^{-1}\} \quad (5.38)$$

The  $\varepsilon$ -pseudospectra of  $M$  are closed, strictly nested sets with  $\Lambda_0(M) = \Lambda(M)$ . If  $M$  is normal, eq. (5.36) implies that  $\Lambda_\varepsilon(M)$  is equal to the union of the closed  $\varepsilon$ -balls about the eigenvalues of  $M$ . In general it may be much larger.

The norm of  $(zI - M)^{-1}$  is its largest singular value, i.e. the inverse of the smallest singular value of  $(zI - M)$ . Therefore an equivalent definition of the pseudospectrum is:

$$\Lambda_\varepsilon(M) = \{z \in \mathbb{C} : \sigma_N(zI - M) \leq \varepsilon\} \quad (5.39)$$

This is also the usual way pseudospectra of matrices are computed numerically.

The pseudospectrum is also related to the magnitude of the transient growth,  $\mathit{Sup}_{t>0} \|e^{(tM)}\|$ . It can be shown that [6]:

$$\mathit{Sup}_{t>0} \|e^{(tM)}\| \geq K(M) \quad (5.40)$$

where the constant  $K$  is the Kreiss constant of the matrix  $M$  which is defined as:

$$K(M) = \mathit{Sup}_{\varepsilon>0} \frac{\alpha_\varepsilon(M)}{\varepsilon} = \mathit{Sup}_{\Re(z)>0} \Re(z) \|R(z, M)\| \quad (5.41)$$

where  $\alpha_\varepsilon(M)$  is the largest real part of all the elements of the set  $\Lambda_\varepsilon(M)$ .

This concepts naturally extend to the case of maps, which are relations that express the state of a system at stage  $n + 1$ ,  $x^{(n+1)}$ , in terms of its previous state as:

$$x^{(n+1)} = Mx^n \quad (5.42)$$

where  $M$  is a matrix which usually is obtained by linearizing a non linear map around one of its fixed point. The definition of pseudospectrum remains the same of eq. (5.38), while the Kreiss constant for maps is defined as [6]:

$$K = \mathit{Sup}_{\varepsilon>0} K_\varepsilon, \quad K_\varepsilon = \frac{\rho_\varepsilon(M) - 1}{\varepsilon} \quad (5.43)$$

where  $\rho_\varepsilon(M)$  is the radius of the smallest circle in the complex plane that contains  $\Lambda_\varepsilon(M)$ . Geometrically,  $K_\varepsilon$  is the maximum distance of the boundary of  $\Lambda_\varepsilon(M)$  from the unitary circle divided by  $\varepsilon$ .

## 5.4 The Synchronously Pumped Optical Parametric Model

Synchronously pumped optical parametric oscillator (SPOPO) is a concrete example in which non-normality plays a crucial role in the evolution of the system. A SPOPO is an OPO with the characteristic that the cavity-round trip time is equal to the delay between successive pulse of the pumping laser ( $T_R$ ), so that the successive intense pump pulses add coherently reducing the oscillation threshold of the device.

### 5.4.1 The SPOPO Model

All electromagnetic phenomena are governed by the Maxwell's equation for the electric and magnetic fields  $E(\vec{r}, t)$  and  $B(\vec{r}, t)$  which are [7] :

$$\begin{aligned}
\nabla \times E(\vec{r}, t) &= -\frac{\partial B(\vec{r}, t)}{\partial t} \\
\nabla \times H(\vec{r}, t) &= \frac{\partial D(\vec{r}, t)}{\partial t} + J(\vec{r}, t) \\
\nabla \cdot E(\vec{r}, t) &= \rho(\vec{r}, t) \\
\nabla \cdot B(\vec{r}, t) &= 0
\end{aligned} \tag{5.44}$$

where

$$D(\vec{r}, t) = \varepsilon_0 E(\vec{r}, t) + P(\vec{r}, t) \tag{5.45}$$

and where  $J(\vec{r}, t)$  and  $\rho(\vec{r}, t)$  are the current and charge densities, respectively. They are related by the charge conservation law:

$$\nabla \cdot J(\vec{r}, t) + \frac{\partial \rho(\vec{r}, t)}{\partial t} = 0 \tag{5.46}$$

$D(\vec{r}, t)$  is the displacement field within the medium,  $B(\vec{r}, t)$  is the magnetic flux density,  $E(\vec{r}, t)$  is the electric field strength,  $H(\vec{r}, t)$  is the magnetic field strength and  $P(\vec{r}, t)$  is now the only time-varying source term. In general,  $P(\vec{r}, t)$  is a function of  $E(\vec{r}, t)$  that describes fully the response of the medium to the field, and it is often known as the constitutive equation. If we could just write the constitutive equation and find the solution for the resulting set of Maxwell's equations with appropriate boundary conditions, then all optical phenomena would be predictable and easily understood. Unfortunately, this seldom is possible. Physically reasonable approximations must be resorted to in order to make the mathematical solution of the equations feasible.

We are primarily interested in the solution of these equations in the regions of space that contain no free charges, so that

$$\rho(\vec{r}, t) = 0 \tag{5.47}$$

We assume that the material is nonmagnetic, so that

$$B(\vec{r}, t) = \mu_0 H(\vec{r}, t). \tag{5.48}$$

It is well known that optical beams are propagating electromagnetic fields. To describe these propagating fields two Maxwell's equations can be combined to form a single decoupled wave equation that will describe the electric or magnetic field. To get an equation that describes the electric field propagating within a material, the electric and magnetic field in Maxwell's equation must be decoupled. For the electric field this can be done by taking the curl of the first of eqs. (5.44),

$$\nabla \times \nabla \times E(\vec{r}, t) = -\frac{\partial}{\partial t}(\nabla \times B(\vec{r}, t)) = -\frac{\partial}{\partial t}(\nabla \times \mu_0 H(\vec{r}, t)) \tag{5.49}$$

since the spatial and temporal derivatives can commute. Then substituting the second of eqs. (5.44) into (5.49),

$$\nabla \times \nabla \times E(\vec{r}, t) + \mu_0 \frac{\partial}{\partial t} J(\vec{r}, t) + \mu_0 \frac{\partial^2}{\partial t^2} D(\vec{r}, t) = 0. \tag{5.50}$$

We now use (5.45) to eliminate  $D(\vec{r}, t)$  from this equation, and we obtain the expression

$$\nabla \times \nabla \times E(\vec{r}, t) + \mu_0 \frac{\partial}{\partial t} J(\vec{r}, t) + \frac{1}{c^2} \frac{\partial^2}{\partial t^2} E(\vec{r}, t) = -\mu_0 \frac{\partial^2 P(\vec{r}, t)}{\partial t^2}. \quad (5.51)$$

where we have used the following relation:

$$c = \frac{1}{\sqrt{\varepsilon_0 \mu_0}} \quad (5.52)$$

It is often convenient to split  $P(\vec{r}, t)$  into its linear and nonlinear parts as

$$P(\vec{r}, t) = P^{(1)}(\vec{r}, t) + P^{(NL)}(\vec{r}, t). \quad (5.53)$$

Here  $P^{(1)}(\vec{r}, t)$  is the part of  $P(\vec{r}, t)$  that depends linearly on the electric field strength  $E(\vec{r}, t)$ . We can similarly decompose the displacement field  $D(\vec{r}, t)$  into its linear and nonlinear parts as

$$D(\vec{r}, t) = \varepsilon_0 E(\vec{r}, t) + (P^{(1)}(\vec{r}, t) + P^{(NL)}(\vec{r}, t)) = D^{(1)}(\vec{r}, t) + P^{(NL)}(\vec{r}, t). \quad (5.54)$$

In terms of this quantity, the wave equation (5.50) becomes

$$\nabla \times \nabla \times E(\vec{r}, t) + \mu_0 \frac{\partial}{\partial t} J(\vec{r}, t) + \mu_0 \frac{\partial^2}{\partial t^2} D^{(1)}(\vec{r}, t) = -\mu_0 \frac{\partial^2 P^{(NL)}(\vec{r}, t)}{\partial t^2}. \quad (5.55)$$

Using the vector identity:

$$\nabla \times \nabla \times E(\vec{r}, t) = \nabla (\nabla \cdot E(\vec{r}, t)) - \nabla^2 E(\vec{r}, t) \quad (5.56)$$

we can rewrite the eq. (5.55) as:

$$\nabla^2 E(\vec{r}, t) - \mu_0 \frac{\partial^2}{\partial t^2} D^{(1)}(\vec{r}, t) - \mu_0 \frac{\partial}{\partial t} J(\vec{r}, t) = \mu_0 \frac{\partial^2 P^{(NL)}(\vec{r}, t)}{\partial t^2} \quad (5.57)$$

In the Fourier space for the time coordinate we have:

$$\frac{\partial^2}{\partial z^2} E(z, \omega) + \mu_0 \omega^2 \varepsilon(\omega) E(z, \omega) + i\omega \mu_0 \sigma E(z, \omega) = -\omega^2 \mu_0 P^{NL}(z, \omega) \quad (5.58)$$

where we have used the relations:

$$\begin{aligned} D^{(1)}(z, \omega) &= \varepsilon^{(1)}(\omega) E(z, \omega) \\ J(z, \omega) &= \sigma E(z, \omega) \end{aligned}$$

and where  $\varepsilon^{(1)}(\omega) = \varepsilon_0 \varepsilon_r$  is the linear dielectric constant. The three fields that interact in the medium are:

$$E_1(z, t) = \frac{1}{2} [A_1(z, t) e^{i(k_1 z - \omega_1 t)} + c.c.] \quad (5.59)$$

$$E_2(z, t) = \frac{1}{2} [A_2(z, t) e^{i(k_2 z - \omega_2 t)} + c.c.] \quad (5.60)$$

$$E_3(z, t) = \frac{1}{2} [A_3(z, t) e^{i(k_3 z - \omega_3 t)} + c.c.] \quad (5.61)$$

all measured in  $V \cdot m^{-1}$ . The symbols  $k_i$  and  $\omega_i$  represent the wave number and the frequency, respectively, of the three fields. The constant  $\mu_i$  are such that the slowly varying envelopes  $A_i$  are adimensional. They are defined as:

$$\mu_i = \frac{c}{d_{eff}L} \sqrt{\left(\frac{n_{i+1}n_{i+2}}{\omega_{i+1}\omega_{i+2}}\right)}$$

where  $c$  is the speed of light in vacuum,  $d_{eff}$  is the effective nonlinear coefficient for the three-wave interaction,  $n_i$  is the refractive index of the field  $i$ , and the subscripts permute cyclically.

If we scale time to the time taken by the pump field to cross the crystal and the coordinate  $z$  to the crystal length, so that the crystal extend from  $z = 0$  to  $z = 1$ :

$$\begin{aligned} z &= \bar{z}/L \\ t &= \bar{t}/T \end{aligned}$$

where  $T = L/v_1$ , where  $v_1 = [dk(\omega_i)/d\omega]^{-1}$  is the group velocity of the field  $A_i$ . Note that in these units  $v_1 = 1$ . By introducing the following quantities:

$$\beta_i = -\frac{1}{2L}v_1^2 \frac{\partial^2 k(\omega)}{\partial \omega^2} \Big|_{\omega=\omega_i} \quad (5.62)$$

$$\rho_i = \frac{\sigma\omega_i c \mu_0}{2n_i} L \quad (5.63)$$

we obtain the following equations:

$$\frac{\partial A_1}{\partial z} = -v_1^{-1} \frac{\partial A_1}{\partial t} + i\beta_1 \frac{\partial^2 A_1}{\partial t^2} - \rho_1 A_1 - A_2 A_3 e^{-i(\Delta k)z} \quad (5.64)$$

$$\frac{\partial A_2}{\partial z} = -v_2^{-1} \frac{\partial A_2}{\partial t} + i\beta_2 \frac{\partial^2 A_2}{\partial t^2} - \rho_2 A_2 + A_1 \bar{A}_3 e^{+i(\Delta k)z} \quad (5.65)$$

$$\frac{\partial A_3}{\partial z} = -v_3^{-1} \frac{\partial A_3}{\partial t} + i\beta_3 \frac{\partial^2 A_3}{\partial t^2} - \rho_3 A_3 + A_1 \bar{A}_2 e^{+i(\Delta k)z} \quad (5.66)$$

where  $\Delta k = k_3 - k_2 - k_1$  is the phase mismatch between the three waves. If we finally define the fields as follows:

$$\begin{aligned} E_1 &= A_1 e^{+i(\Delta k)z} \\ E_2 &= A_2 \\ E_3 &= A_3 \end{aligned}$$

we obtain:

$$\begin{aligned} \frac{\partial E_1}{\partial z} &= -v_1^{-1} \frac{\partial E_1}{\partial t} - (\rho_1 - i\Delta k) E_1 + i\beta_1 \frac{\partial^2 E_1}{\partial t^2} - E_2 E_3 \\ \frac{\partial E_2}{\partial z} &= -v_2^{-1} \frac{\partial E_2}{\partial t} - \rho_2 E_2 + i\beta_2 \frac{\partial^2 E_2}{\partial t^2} + E_1 \bar{E}_3 \\ \frac{\partial E_3}{\partial z} &= -v_3^{-1} \frac{\partial E_3}{\partial t} - \rho_3 E_3 + i\beta_3 \frac{\partial^2 E_3}{\partial t^2} + E_1 \bar{E}_2 \end{aligned} \quad (5.67)$$

In the end we write the SPOPO eqs. (5.67) in the reference frame of the pump pulse. We indicate with  $(z', t')$  the coordinates in the laboratory frame and with  $z = z'$  and  $t = t' + v_1^{-1}z'$  the coordinates in the pump pulse reference frame. The SPOPO equations in this coordinates become:

$$\begin{aligned}\frac{\partial E_1}{\partial z} &= -(\rho_1 - i\Delta k) E_1 + i\beta_1 \frac{\partial^2 E_1}{\partial t^2} + -E_2 E_3 + A_1 \xi_1 \\ \frac{\partial E_2}{\partial z} &= -\gamma_2 \frac{\partial}{\partial t} E_2 - \rho_2 E_2 + i\beta_2 \frac{\partial^2 E_2}{\partial t^2} + E_1 \bar{E}_3 + A_2 \xi_2 \\ \frac{\partial E_3}{\partial z} &= -\gamma_3 \frac{\partial}{\partial t} E_3 - \rho_3 E_3 + i\beta_3 \frac{\partial^2 E_3}{\partial t^2} + E_1 \bar{E}_2 + A_3 \xi_3\end{aligned}\quad (5.68)$$

where the quantity  $\gamma_i = v_i^{-1} - v_1^{-1}$  was introduced and we have also added complex functions  $\xi_j = \xi_j(z, t)$  which represent stochastic noise terms whose real and imaginary parts are Gaussian distributed around zero with standard deviation equal to one. These noise terms are delta correlated in both space and time and they represents noise sources inside the crystal:

$$\langle \xi_i^*(z, t) \xi_j(z', t') \rangle = \delta_{ij} \delta(z - z') \delta(t - t') \quad (5.69)$$

The real parameters  $A_j$  are a measure of the strength of these noise terms.

## 5.5 Giant Noise Amplification in SPOPO

Equations (5.68) are the starting point of the work of [8, 9] in which giant noise amplification in SPOPO has been investigated in relation to the condition of non-normality of the linearized dynamic matrix of the system. Although the singly resonant OPO case was considered there, the cavity losses were large and only classical noise was included in the treatment. We will first extend the results of the singly resonant case to larger cavity finesses and then introduce a treatment of the quantum fluctuations to see if these can be capable to drive the SPOPO in the regime of giant pulses due to quantum noise amplification (see section 5.6)

### 5.5.1 The Singly Resonant Case

In the case we deal with in this section the only resonated field in the cavity is the signal field, with cavity round trip time  $T_c$ , while the mirrors are transparent to the pump and idler fields.

The effect of the cavity, which is resonant only for the signal field, is considered by means of the boundary conditions:

$$\begin{aligned}E_1(0, t) &= P(t) + \psi_1(t) \\ E_2(0, t) &= \exp(-i\theta) \sqrt{R} E_2(1, t + 1 + \gamma_2 - T_c) + \psi_2(t) \\ E_3(0, t) &= \psi_3(t)\end{aligned}\quad (5.70)$$

where  $P(t) = P(t + T_R)$  is the pump profile, assumed to be periodic with period  $T_R$ . In particular in [8, 9] they consider a Gaussian pump profile:

$$P(t) = \begin{cases} P_a e^{(-t^2/\tau_p)} & -T_R \leq t < T_R \\ P(t + T_R) & = P(t) \end{cases} \quad (5.71)$$

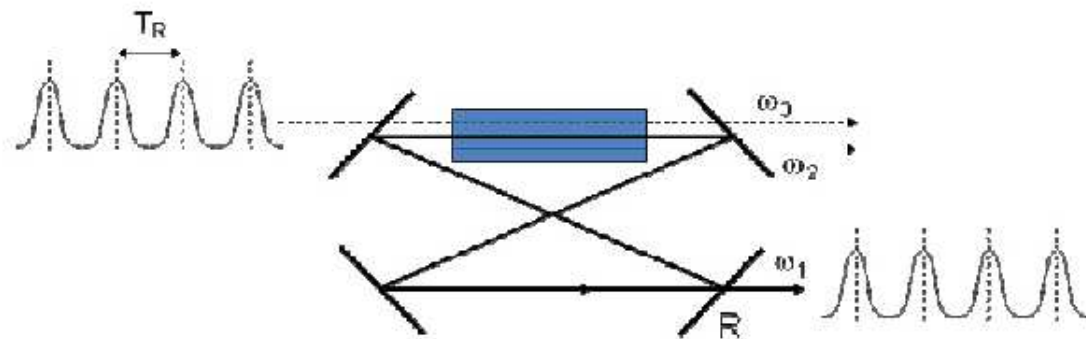


Figure 5.5.1: Singly resonant SPOPO

of amplitude  $P_a$  and width  $\tau_p \ll T_R$ .  $T_c$  is the signal cavity round trip time,  $R$  is the total intensity reflection coefficient of the cavity,  $\theta$  is the phase shift acquired per pass by the signal field if its carrier frequency does not coincide with the cavity resonance,  $\psi_j(t)$  is a delta correlated Gaussian noise of amplitude  $B_j$  that represent external (classical) noise sources on the field  $E_j$ .

The crucial point is that the SPOPO equations can be seen as a mathematical map which expresses the pulses at one round trip in terms of the pulses at a previous one.

In absence of noise ( $A_j = B_j = 0$ ) the SPOPO map with initial condition  $E_1^{(n)} = P(\tau)$  and with  $E_1^{(n)}(z, \tau)$  given at each round trip by the solution of the first of eqs. (5.68), admits a zero signal-idler solution,  $E_2^{(n)} = E_3^{(n)} = 0$ . The condition for the stability of this solution can be investigated by linearization of eqs. (5.68) around the zero signal-idler solution. The linearization procedure has the effect to decouple the perturbation of the pump,  $e_1^{(n)}(z, \tau)$ , from those of the other fields,  $e_j^{(n)}(z, \tau)$ , which are then driven by the unperturbed pump field. In this way the equations for the perturbations of the signal field from one round trip to another can be recast using a linear operator  $L$  into:

$$e_2^{(n)}(0, \tau) = L e_2^{(n-1)}(0, \tau) \quad (5.72)$$

The stability properties are given by the study of the spectrum of the operator  $L$ . In particular it is well know that the solution will be stable if the spectral radius,  $\rho(L)$ , of the operator  $L$  is smaller than one. In other words, if the largest eigenvalue of the operator  $L$  is smaller than one, the SPOPO is below threshold and the steady state is stable. Otherwise the SPOPO is above threshold and the steady state is unstable.

The study of the spectrum of  $L$  does not give us information about the noise sensitivity of the SPOPO system, which can still amplify random noise and produce macroscopic pulses even if it is below threshold of oscillation. This is the case when the system is strongly non-normal and the boundaries of the pseudospectrum are sufficiently far from the unitary circle (corresponding to threshold).

The presence of a pulsed pump field makes it impossible to solve the eqs. (5.68) and their linearization in an analytic form. In [8, 9] the equations of the SPOPO dynamics have been solved in a numerical way by using a split-step method, with a Fourier transform in the time domain and a second-order Runge-Kutta in the longitudinal coordinate.

In performing a linear stability analysis below threshold of the equations (5.68), (5.72) and a correlated study of the pseudospectrum can tell us if perturbations of certain magnitude and phase can grow exponentially or not. Fig. 5.5.2 shows the stability eigenvalues and the pseudospectra for perturbations of amplitude  $10^q$  and generic phases. The dots represent the eigenvalues of the

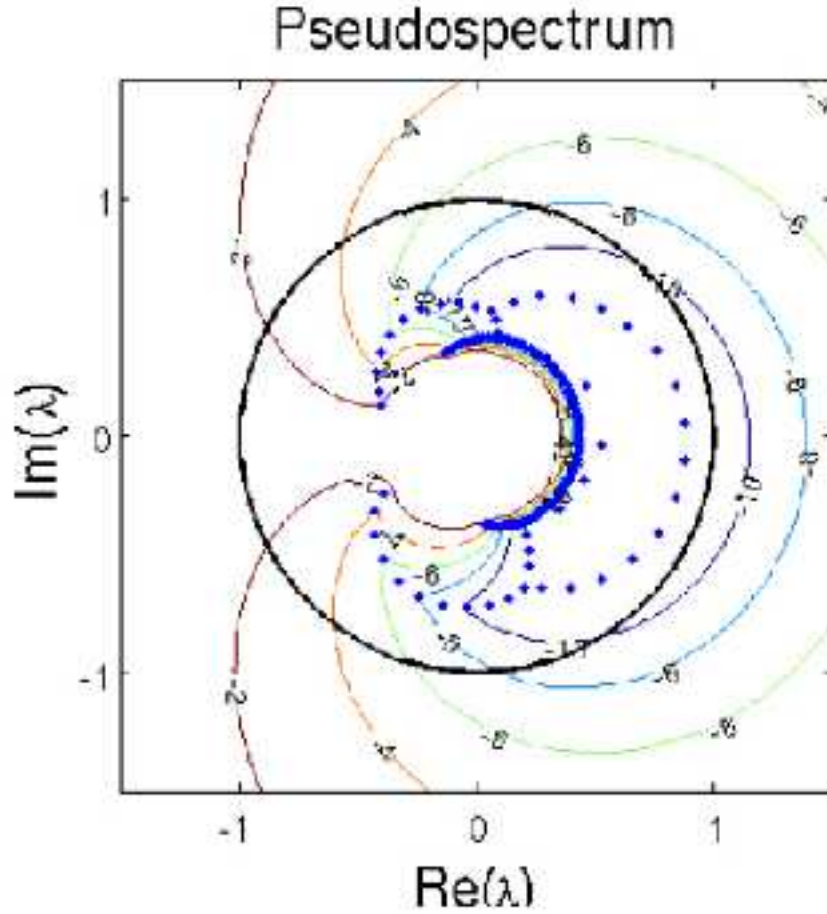


Figure 5.5.2: Stability analysis of a singly resonant SPOPO. The dots are the stability eigenvalues of the solution below threshold. The stability threshold is the unit circle. The contour curves correspond to the growth of the perturbations with initial magnitude  $10^q$  where  $q$  is the number reported close to the curves. Parameters are:  $B_j = 0$ ,  $A_j = 10^{-8}$ ,  $\rho_i = 0$ ,  $\Delta k = \theta = 0$ ,  $\gamma_i = \{0, 0.0166, -0.0117\}$   $R = 0.137$ ,  $T_c - T_R = -0.0173$  and normalized input peak pump of  $P = 3.6$ .

linear stability analysis and the fact that they are all inside the unit circle in the complex plane means that the system is below threshold. If a given curve is outside the unit circle, perturbations of that size and phase are exponentially amplified. In this light Fig. 5.5.2 shows that for the given parameters values, the stationary solution is stable (below threshold) while noise fluctuations of amplitude as small as  $10^{-10}$  can be amplified. The pseudospectra have been computed using the singular value decomposition routine in Matlab.

Upper panel of Fig. 5.5.3 shows the signal intensity as a function of time via the round trip number for the same parameters setting of Fig. 5.5.2. Noise amplitudes  $B_j$  in the cavity are  $10^{-8}$  in normalized units. It is important to point out that self sustained noisy oscillations occur in spite of the system working below threshold. The time jitter in the generation of the pulses is a signature of noise amplification instead of deterministic signal generation. Lower-left and lower-right panels of Fig. 5.5.3 show the last two signal pulses of the numerical simulation and the amplitudes of pump and signal fields averaged over the duration of the simulation, respectively. The generation of signal pulses below threshold due to noise amplification and non-orthogonality is enormous and depletes the pump pulse.

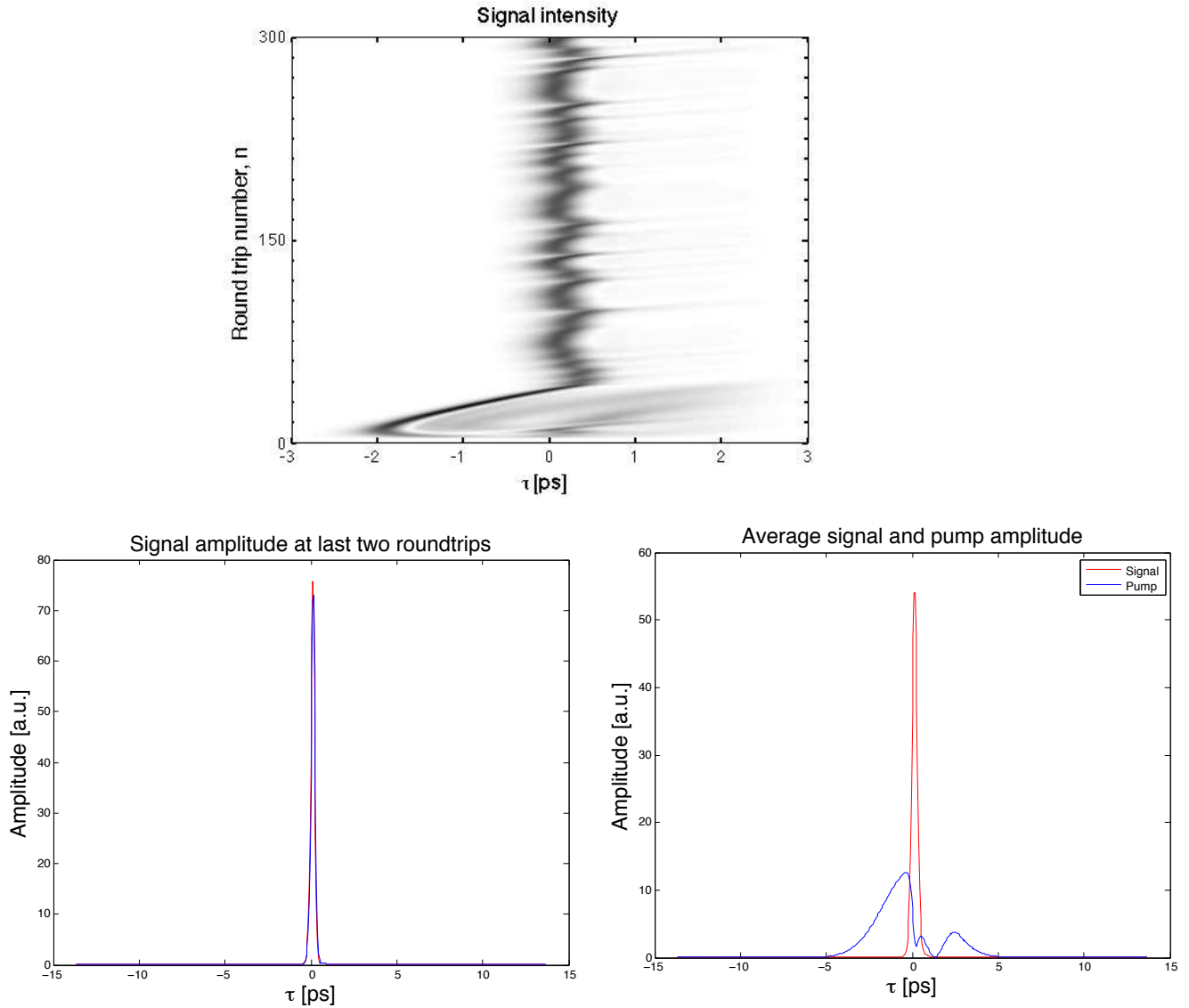


Figure 5.5.3: (upper panel) Signal intensity as function of time via the round trip number. (lower-left) The last two pulses of the giant noise amplification of the signal field presented in the upper panel. (right panel) The averaged pump (blue line) and signal (red line) during signal noise amplification. Parameters are as in Fig. 5.5.2.

### 5.5.2 High finesse singly resonant case

Previous work [9] has focused on giant noise amplification in cavities with low mirror reflectivities and classical noise sources (see the value of  $R = 0.137$  in the simulations presented in Figs. 5.5.2 and 5.5.3). Treatments of quantum fluctuations in optical cavities are however performed within the limit of validity of mean-field models with high mirror reflectivities (high cavity finesse). For this reason we have written new codes for the numerical integration of the SPOPO equations and the evaluation of the pseudospectra in this regime. We have then progressively increased the mirror reflectivity  $R$  from 0.137 to 0.9 while maintaining the conditions of giant noise amplification. The transients to reach stationary pulse generation due to noise amplification increase in duration with the mirror reflectivity making it unpractical to use values of  $R$  above 0.9. Fig. 5.5.4 shows the stability eigenvalues and the pseudospectrum for  $R = 0.9$ . Although the phase range of the growing perturbations is reduced with respect to the low reflectivity case, giant pulses driven by fluctuations are predicted in the high finesse cavity case too. Upper panel of Fig. 5.5.5 shows the signal intensity as a function of time via the round trip number for the same parameters setting of Fig. 5.5.4. Noise amplitudes  $B_j$  in the cavity are  $10^{-8}$  in normalized units. Again, self sustained noisy oscillations occur in spite of the system working below threshold. The time jitter in the generation of the pulses is a signature of noise amplification instead of deterministic signal generation. Lower-left and lower-right panels of Fig. 5.5.5 show the last two signal pulses of the numerical simulation and the amplitudes of pump and signal fields averaged over the duration of the simulation, respectively. Even for high-finesse cavities ( $R = 0.9$ ) the generation of signal pulses below threshold due to noise amplification and non-orthogonality is enormous and fully depletes the pump pulse.

### 5.5.3 The Doubly Resonant and Degenerate Cases

We have also tried to identify a regime of giant pulse generation from noise for high cavity finesse, at equal group velocities for signal and idler and at frequency degeneracy for Type-I OPOs where the signal and idler fields have the same polarization. Fig. 5.5.6 shows that at equal group velocities of the signal and idler fields, the stability spectrum of eigenvalues develops horns that are well above the threshold line. The situation is even worse at frequency degeneracy (see Fig. 5.5.7) where one observes a shift of the pseudospectrum of exponential growth of fluctuations to much larger amplitudes than the singly resonant case of the previous subsection. Similar situations have been observed in the equal group velocity and equal frequency cases for decreasing values of the reflectivity  $R$ . This means that at present we have not been able to observe the phenomenon of giant sub-threshold pulses at degeneracy. The non-degenerate, singly resonant configuration appears to offer far more flexibility of operation than the degenerate setup for the observation of noise induced pulses in parametric oscillators.

### 5.5.4 Conditions for Giant Noise Amplification in SPOPO

In conclusion we can say that three main conditions are preferential for giant noise amplification in SPOPOs below threshold:

- Large Non-Degeneracy. Non degeneracy of the signal-idler frequencies is of fundamental importance since the phenomenon does not appear to survive in the degenerate case. In a SPOPO experiment performed at University of Southampton with a periodically poled lithium niobate crystal, short SPOPO pulses have been observed [15]. For one sign of the

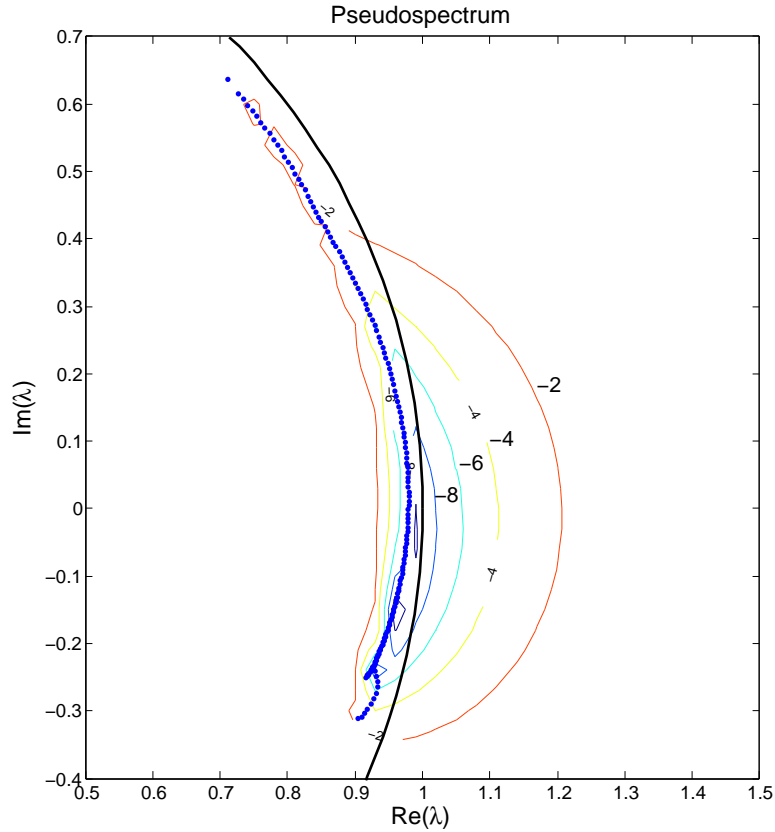


Figure 5.5.4: The blue dots are the stability eigenvalues of the solution below threshold. The stability threshold is the unit circle (in black). The contour curves correspond to the growth of the perturbations with initial magnitude  $10^q$  where  $q$  is the number reported close to the curves. Parameters are:  $B_j = 0$ ,  $A_j = 10^{-8}$ ,  $\rho_i = 0$ ,  $\Delta k = \theta = 0$ ,  $\gamma_i = \{0, 0.014, -0.01\}$ ,  $R = 0.9$ ,  $T_c - T_R = -0.0002$  and normalized input peak pump of  $P = 0.84$ .

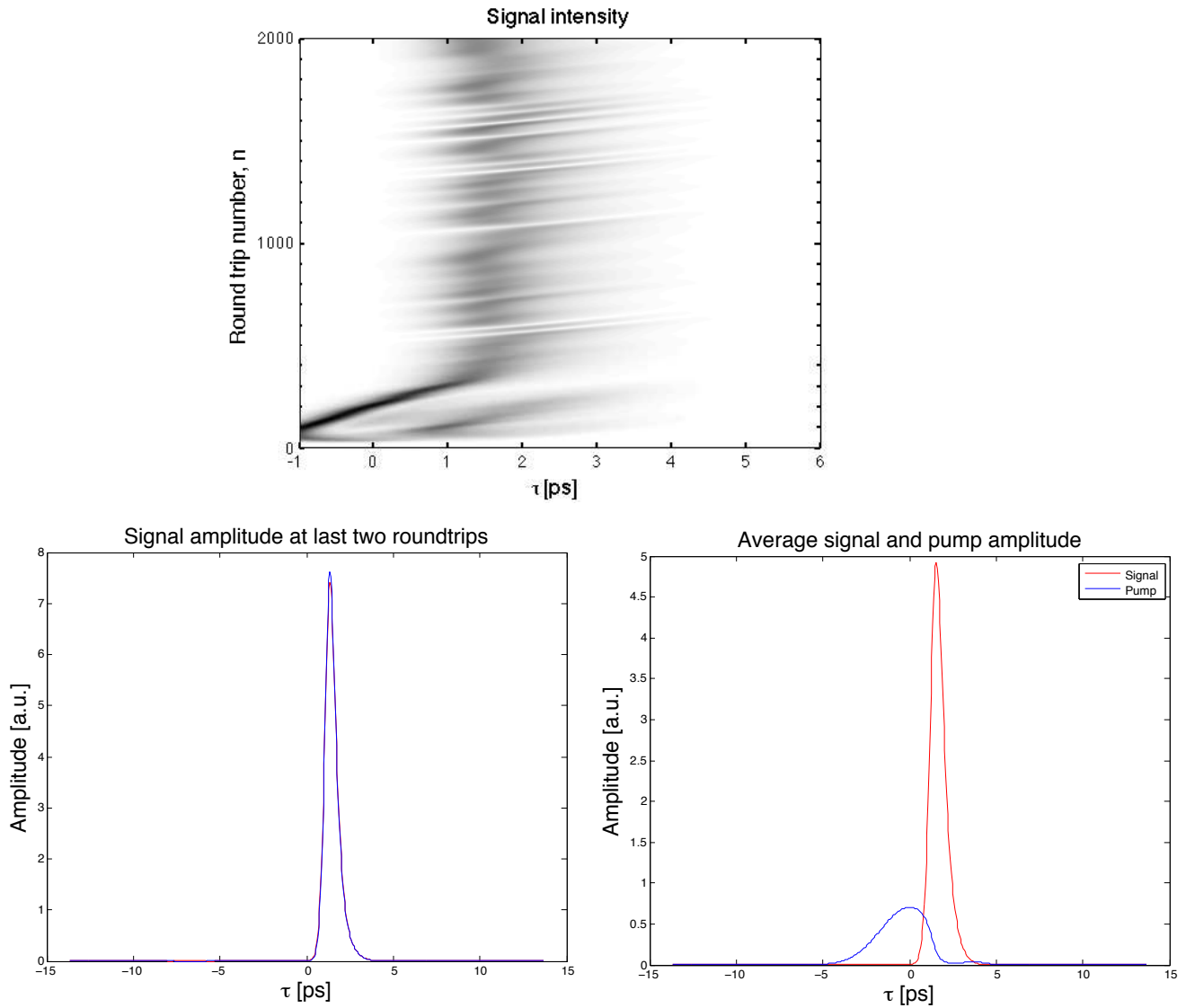


Figure 5.5.5: (upper panel) Signal intensity as function of time via the round trip number. (lower-left) The last two pulses of the giant noise amplification of the signal field presented in the upper panel. (lower-right) The averaged pump (blue line) and signal (red line) during signal noise amplification. Parameters are as in Fig. 5.5.4.

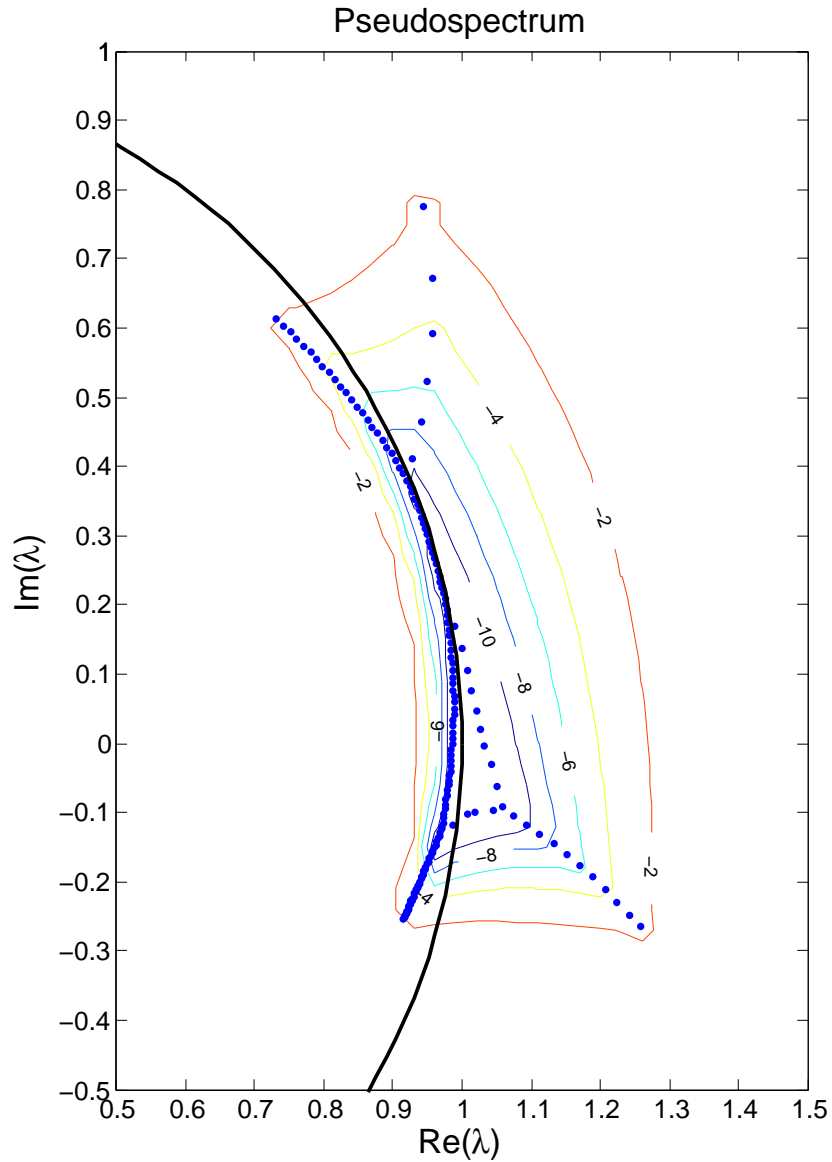


Figure 5.5.6: The dots are the stability eigenvalues of the solution below threshold. The stability threshold is the unit circle. The contour curves correspond to the growth of the perturbations with initial magnitude  $10^q$  where  $q$  is the number reported close to the curves. In this case we have equal group velocity and parameters:  $B_j = 0$ ,  $A_j = 10^{-8}$ ,  $\rho_i = 0$ ,  $\Delta k = \theta = 0$ ,  $\gamma_i = \{0, -0.01, -0.01\}$ ,  $R = 0.9$ ,  $T_c - T_R = -0.0002$  and normalized input peak pump of  $P = 0.85$

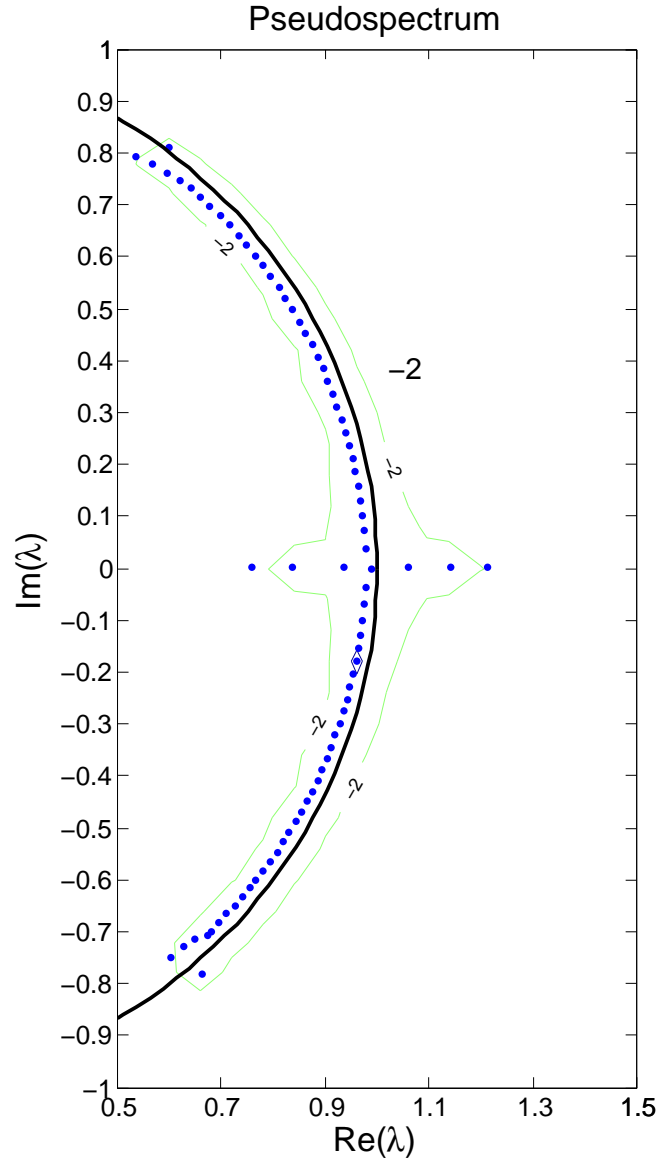


Figure 5.5.7: The dots are the stability eigenvalues of the solution below threshold. The stability threshold is the unit circle. The contour curves correspond to the growth of the perturbations with initial magnitude  $10^q$  where  $q$  is the number reported close to the curves. In this case we have equal frequency and parameters:  $B_j = 0$ ,  $A_j = 10^{-8}$ ,  $\rho_i = 0$ ,  $\Delta k = \theta = 0$ ,  $\gamma_i = \{0, -0.064, -0.064\}$ ,  $R = 0.9$ ,  $T_c - T_R = -0.0008$  and normalized input peak pump of  $P = 0.8$ .

pump-signal detuning the SPOPO pulses were shortened but appeared to be jittery. This may be a precursor of the Giant-Pulse Amplification described theoretically earlier. In the experiment of [15] the idler and signal frequencies are hugely different, of the order of  $10^{13} Hz$ .

$$\begin{aligned}\lambda_p &= 1.047\mu m & \nu_p &= 2.86 \times 10^{14} Hz \\ \lambda_s &= 1.700\mu m & \nu_s &= 1.76 \times 10^{14} Hz \\ \lambda_i &= 2.726\mu m & \nu_i &= 1.10 \times 10^{14} Hz\end{aligned}$$

$$\nu_s - \nu_i = 6.6 \times 10^{13} Hz$$

- Large loss asymmetry. In fact in the experiment of [15] the signal field is resonated while the idler field is not. The singly resonant configuration studied in this thesis appears to be the optimal for the observation of giant noise amplification.
- Different group velocities. Finally, non-orthogonality and non-normality appear to be associated with different speed of propagation of the signal and idler pulses in the crystal.

## 5.6 Giant Amplification of Quantum Noise

The theoretical approach described above assumes that the noise in the cavity has a classical origin (thermal fluctuations). In quantum optics, however, it is important to assess if noise induced phenomena can be driven by quantum fluctuations. In this section we provide the theory and simulations of SPOPOs under the action of quantum noise.

### 5.6.1 Nondegenerate OPO in the time domain

We consider a unidirectional ring cavity with a non-degenerate OPO with only the signal resonant to the cavity [9]. We consider pulses on a single transverse mode; the total length of the cavity is  $L$ , the crystal is between  $z = 0$  and  $z = L_{cr}$ , the empty part of the cavity is between  $z = L_{cr}$  and  $z = L$ . We do not repeat the derivation of the commutation relations that are assumed to be those found in [10]. We then write a Hamiltonian that is consistent with the classical equations and find the noise terms for the corresponding Langevin equations.

### 5.6.2 Propagation inside the crystal

The classical equations in dimensional units are:

$$\begin{aligned}\partial_t A'_1 &= [-\gamma_1 + i\Delta k - v_1(\partial_z - ib_1\partial_{tt})] A'_1 - v_1 g' A'_2 A'_{23} \\ \partial_t A'_2 &= [-\gamma_2 - v_2(\partial_z - ib_2\partial_{tt})] A'_2 - v_2 g' A'_1 \overline{A'_3} \\ \partial_t A'_3 &= [-\gamma_3 - v_3(\partial_z - ib_3\partial_{tt})] A'_3 - v_3 g' A'_1 \overline{A'_2}\end{aligned}\tag{5.73}$$

where 1, 2, 3 refer to pump, signal and idler, respectively,  $A'_i = (n_i/\omega_i)^{1/2} E_i$ , with  $n_i$  being the refractive indices and  $\omega_i$  the group frequencies,  $\gamma_i$  are the overall loss for the  $i$ -field in the material due to scattering and partial reflection at the ends of the crystal,  $v_i$  are the group velocities, and

$\Delta k$  is the phase mismatch. Note that although we use the same Greek letters,  $\gamma_i$  and  $\Delta k$  have now different dimensions and in particular different sizes from those of the previous notes since they have been multiplied by  $v_i$ . In order to have the nonlinear terms multiplied by the same constant, we introduce the transformation  $A_i = A'_i/\sqrt{v_i}$ :

$$\begin{aligned}\partial_t A_1 &= [-\gamma_1 + i\Delta k - v_1(\partial_z - ib_1\partial_{tt})] A_1 - \sqrt{v_1 v_2 v_3} g' A_2 A_3 \\ \partial_t A_2 &= [-\gamma_2 - v_1(\partial_z - ib_1\partial_{tt})] A_1 - \sqrt{v_1 v_2 v_3} g' A_1 \bar{A}_3 \\ \partial_t A_3 &= [-\gamma_3 - v_3(\partial_z - ib_{23}\partial_{tt})] A_3 - \sqrt{v_1 v_2 v_3} g' A_1 \bar{A}_2\end{aligned}\quad (5.74)$$

In the following we neglect dispersion, i.e.  $b_i = 0$ . We consider the pump as a classical field, while we use the approach of Ref. [10] for signal and idler, i.e. continuous mode quantized fields for the traveling waves instead of discrete cavity modes. In particular, we use the narrow bandwidth approximation to reduce eq. (5.7) of [10] as follows

$$\hat{E}_i(z, t) = \int d\omega \left[ \frac{\hbar\omega}{4\pi\epsilon_0 c S n_i(\omega)} \right]^{1/2} \hat{a}_i(\omega) \exp[-i\omega(t - \frac{n_i(\omega)z}{c})] \rightarrow \left[ \frac{\hbar\omega_i}{2\epsilon_0 c S n_i} \right]^{1/2} \hat{a}_i(v_i t - z), \quad (5.75)$$

where  $c$  is the speed of light in vacuum and  $S$  is the section of the beam.

The commutation relation should be

$$\left[ \hat{a}_i(v_i t - z), \hat{a}_i^\dagger(v_i t' - z') \right] = \delta(v_i t - z - v_i t' + z'). \quad (5.76)$$

Note that the creation and destruction operators are dimensional, with  $[\hat{a}_i(v_i t - z)] = z^{-1/2}$ . In order to find the correct scaling for the noise terms, we introduce variables  $a_i$  as follows

$$A_i = \left( \frac{n_i}{\omega_i} \right)^{1/2} \left( \frac{\hbar\omega_i}{4\pi\epsilon_0 c S n_i} \right)^{1/2} a_i = \left( \frac{\hbar}{2v_i\epsilon_0 c S} \right)^{1/2} a_i. \quad (5.77)$$

The dynamical equations for the variables  $a_i$  are:

$$\begin{aligned}\partial_t a_1 &= [-\gamma_1 + i\Delta k - v_1\partial_z] a_{01} - g a_2 a_3 \\ \partial_t a_2 &= [-\gamma_2 - v_2\partial_z] a_2 - g a_1 \bar{a}_3 \\ \partial_t a_{23} &= [-\gamma_3 - v_{23}\partial_z] a_3 - g a_1 \bar{a}_2\end{aligned}\quad (5.78)$$

where

$$g = \left( \frac{\hbar v_1 v_2 v_3}{2\epsilon_0 c S} \right)^{1/2} g'. \quad (5.79)$$

At this point, we write the Hamiltonian for the operators  $a_i$ , see ref. [11, 12] with transverse derivatives replaced by the longitudinal one :

$$H = H_0 + H_{int} \quad (5.80)$$

$$H_0 = -\hbar \int dz a_i^\dagger (v_i \partial_z) a_i \quad (5.81)$$

$$H_{int} = i\hbar g \int dz \left( a_1 a_2^\dagger a_3^\dagger - \bar{a}_1 a_2 a_3 \right) \quad (5.82)$$

and the Lindblad irreversible terms of the density matrix as:

$$\Lambda\rho = \int dz \gamma_i \left( 2a_i\rho a_i^\dagger - \rho a_i^\dagger a_i - a_i^\dagger a_i \rho \right) \quad (5.83)$$

with  $i = 1, 2$  and sum over repeated indexes.

### 5.6.3 The Langevin Equation

The equation for the density matrix is:

$$\partial_t \rho = -\frac{i}{\hbar} [H_0 + H_{int}, \rho] + \Lambda\rho \quad (5.84)$$

For the derivation of the drift terms in the Fokker-Plank equation, one defines

$$\eta(\alpha_i, \bar{\alpha}_i) = \exp \int dz (\zeta_i a_i^\dagger - \bar{\zeta}_i a_i) \quad (5.85)$$

and uses the following correspondences

$$Tr \left[ \int dz a^\dagger a \rho \eta \right] = \int dz \left( \bar{\alpha} - \frac{1}{2} \partial_\alpha \right) \left( \alpha + \frac{1}{2} \partial_{\bar{\alpha}} \right) W \quad (5.86)$$

$$Tr \left[ \int dz \rho a^\dagger a \eta \right] = \int dz \left( \alpha - \frac{1}{2} \partial_{\bar{\alpha}} \right) \left( \bar{\alpha} + \frac{1}{2} \partial_\alpha \right) W \quad (5.87)$$

$$Tr \left[ \int dz (a^\dagger a \rho - \rho a^\dagger a) \eta \right] = \int dz (\partial_{\bar{\alpha}} \bar{\alpha} - \partial_\alpha \alpha) W \quad (5.88)$$

where the identity

$$\partial_\alpha \alpha W - \alpha \partial_\alpha W = W \quad (5.89)$$

has been used and where  $W$  is the Wigner distribution defined as:

$$W(\zeta_i, \bar{\zeta}_i) = \frac{1}{\pi^2} \int d^2 \zeta_i e^{-i(\zeta_i \bar{\alpha}_i + \bar{\zeta}_i a)} \eta(\alpha_i, \bar{\alpha}_i) \quad (5.90)$$

For the equations containing space derivatives, we assume that all functions vanish at the extrema of the integration range, which should be true for pulses that are well separated from one another. Putting all of these together, one gets

$$-\frac{i}{\hbar} [H_0, \rho] \rightarrow - \int dz (\partial_{\alpha_i} (v_i \partial_z) \alpha_i + c.c.) W. \quad (5.91)$$

For the interaction Hamiltonian we get

$$-\frac{i}{\hbar} [H_{int}, \rho] \rightarrow - \int dz (\partial_{\alpha_1} a_0 \bar{\alpha}_2 + \partial_{\alpha_2} a_0 \bar{\alpha}_1 + c.c.) W. \quad (5.92)$$

with  $i, j = 1, 2$ ,  $i \neq j$ . For the Liouvillian, one gets

$$\int dz a_i \rho a_i^\dagger \eta \rightarrow \int dz \left( \alpha_i \bar{\alpha}_i + \frac{1}{2} \partial_{\alpha_i} \alpha_i + \frac{1}{2} \partial_{\bar{\alpha}_i} \bar{\alpha}_i - \frac{1}{2} + \frac{1}{4} \partial_{\alpha_i \bar{\alpha}_i} \right) W, \quad (5.93)$$

that gives

$$\int dz \Lambda \rho \eta \rightarrow \int dz \gamma_i (\partial_{\alpha_i \bar{\alpha}_i} + \partial_{\alpha_i} \alpha_i + \partial_{\bar{\alpha}_i} \bar{\alpha}_i) W. \quad (5.94)$$

Using Ito calculus, the Langevin equation and its corresponding Fokker-Planck equation are given by the formulae (4.3.21) and (4.3.22) in [13], which are

$$d\mathbf{x} = A dt + B dw \quad (5.95)$$

$$\partial_t p = - \sum_i \partial_i [A_i p] + \frac{1}{2} \sum_{i,j} \partial_i \partial_j D_{ij} p \quad (5.96)$$

where  $\mathbf{x} = (\alpha, \bar{\alpha})^T$ ,  $A(\mathbf{x}, t)$  is a vector of so called drift terms,  $B(\mathbf{x}, t)$  is a matrix,  $D = BB^T$ ,  $w(\mathbf{x}, t)$  is a multivariable Wiener process and the sums are over  $\alpha$  and  $\bar{\alpha}$ . In order to have  $\alpha$  and  $\bar{\alpha}$  the complex conjugated of one another, it must be

$$\bar{A}_\alpha = A_{\bar{\alpha}} \quad (5.97)$$

$$\bar{B}_{\alpha, \alpha} = B_{\bar{\alpha}, \bar{\alpha}} \quad (5.98)$$

$$\bar{B}_{\bar{\alpha}, \alpha} = B_{\alpha, \bar{\alpha}} \quad (5.99)$$

We get

$$D_{\alpha, \alpha} = B_{\alpha, \alpha}^2 + B_{\alpha, \bar{\alpha}}^2 = 0 \quad (5.100)$$

$$D_{\bar{\alpha}, \bar{\alpha}} = B_{\bar{\alpha}, \bar{\alpha}}^2 + B_{\bar{\alpha}, \alpha}^2 = 0 \quad (5.101)$$

$$D_{\alpha, \bar{\alpha}} = B_{\alpha, \alpha} B_{\bar{\alpha}, \alpha} + B_{\bar{\alpha}, \bar{\alpha}} B_{\alpha, \bar{\alpha}} = \gamma \quad (5.102)$$

These equations are solved by

$$Re \{B_{\alpha, \alpha}\} = -Im \{B_{\alpha, \bar{\alpha}}\} \quad (5.103)$$

$$Im \{B_{\alpha, \alpha}\} = Re \{B_{\alpha, \bar{\alpha}}\} \quad (5.104)$$

$$Re \{B_{\alpha, \alpha}\} = Im \{B_{\alpha, \alpha}\} = \frac{\sqrt{\gamma}}{2} \quad (5.105)$$

From these relations we get the Langevin equations

$$\begin{aligned} \partial_t \alpha_1 &= [-\gamma_1 + i\Delta k - v_1 \partial_z] \alpha_1 - g \alpha_2 \alpha_3 \\ \partial_t \alpha_2 &= [-\gamma_2 - v_2 \partial_z] \alpha_2 - g \alpha_1 \bar{\alpha}_3 + \sqrt{\gamma_2} \chi_2 \\ \partial_t \alpha_3 &= [-\gamma_3 - v_3 \partial_z] \alpha_3 - g \alpha_1 \bar{\alpha}_2 + \sqrt{\gamma_3} \chi_3 \end{aligned} \quad (5.106)$$

where  $\chi_i$  are noise terms *with dimension*  $(tl)^{-1/2}$  and correlation

$$\langle \bar{\chi}_i(z, t) \chi_j(z', t') \rangle = \delta_{ij} \delta(z - z') \delta(t - t') \quad (5.107)$$

Finally one can exchange the role of the space and time derivatives for computational convenience by introducing the new variables  $a'_1 = \sqrt{v_1} \alpha_1$  and  $a'_i = \sqrt{v_i} \alpha_i$ :

$$\begin{aligned}
\partial_z \alpha'_1 &= \frac{1}{v_1} [-\gamma_1 + i\Delta k - \partial_t] \alpha_1 - \frac{g\alpha_2\alpha_3}{\sqrt{v_1v_2v_3}} \\
\partial_z \alpha'_2 &= \frac{1}{v_2} [-\gamma_2 - \partial_t] \alpha_2 - \frac{g\alpha_1\bar{\alpha}_3}{\sqrt{v_1v_2v_3}} + \sqrt{\frac{\gamma_2}{v_2}} \chi_2 \\
\partial_z \alpha'_3 &= \frac{1}{v_3} [-\gamma_3 - \partial_t] \alpha_3 - \frac{g\alpha_1\bar{\alpha}_2}{\sqrt{v_1v_2v_3}} + \sqrt{\frac{\gamma_3}{v_3}} \chi_3
\end{aligned} \tag{5.108}$$

Note that in this case there is no difference between the equation in the Ito calculus and in the Stratonovich calculus because the diffusion coefficients do not depend on the variables  $\alpha, \bar{\alpha}$ .

#### 5.6.4 Propagation in the empty part of the cavity

From [9], the initial condition for the signal in dimensional units is

$$A_2(0, t) = \exp(i\theta) \sqrt{R} A_2(L_{cr}, t_0 = t - \frac{L - L_{cr}}{c}), \tag{5.109}$$

with  $R$  the reflectivity of the mirror. By distributing outside the crystal the dissipation caused by the mirror, we can replace the boundary condition in eq. (5.109) with the equation

$$\partial_t A_2 = \left( c \frac{i\theta + \ln \sqrt{R}}{L - L_{cr}} - c\partial_z \right) A_2. \tag{5.110}$$

The formal solution of eq. (5.110) is

$$A_2(z, t) = \exp \left[ c(t - t_0) \frac{i\theta + \ln \sqrt{R}}{L - L_{cr}} \right] A_2(z - c(t - t_0), t_0), \tag{5.111}$$

which, for  $z = L$  and  $t = L/c$  such that  $t_0 = L_{cr}/c$ , corresponds to eq. (5.109) (note that  $z = L$  and  $z = 0$  coincide with each other in a ring cavity). By using the narrow bandwidth approximation of eq. (2.8) of [14],

$$\hat{E}_i(z, t) = \int d\omega \left[ \frac{\hbar\omega}{4\pi\epsilon_0 cS} \right]^{1/2} \hat{a}_i(\omega) \exp[-i\omega(t - \frac{z}{c})] \rightarrow \left[ \frac{\hbar\omega_i}{2\epsilon_0 cS} \right]^{1/2} \hat{a}_i(ct - z), \tag{5.112}$$

eq. (5.110) can be transformed into the Langevin equation

$$\partial_t \alpha_2 = \left( c \frac{i\theta + \ln \sqrt{R}}{L - L_{cr}} - c\partial_z \right) \alpha_2 + \sqrt{c \frac{|\ln \sqrt{R}|}{L - L_{cr}}} \chi(z, t), \tag{5.113}$$

where  $\chi$  is a noise term *with dimension*  $(tl)^{-1/2}$  and correlation as in eq. (5.107). Again, one needs to enter a final renormalization of the variable  $\alpha'_2 = \sqrt{c}\alpha_2$  when transforming these equations into those with the space differentials for numerical integration to obtain:

$$\partial_z \alpha'_2 = \left( \frac{i\theta + \ln \sqrt{R}}{L - L_{cr}} - c^{-1}\partial_t \right) \alpha'_2 + \sqrt{\frac{|\ln \sqrt{R}|}{L - L_{cr}}} \chi(z, t), \tag{5.114}$$

### 5.6.5 Application of Ito calculus

This last equation can be integrated using Ito's calculus [16]. We can rewrite it as an Ornstein-Uhlenbeck process for a stochastic process  $X_z$ ,

$$dX_z = \mu X_z dz + \sigma dB_z \quad (5.115)$$

with

$$\begin{aligned} \mu &= \frac{\ln(\sqrt{R})}{L-1} - i \frac{\theta}{L-1} = \mu_R + i\mu_I \\ \sigma &= \sqrt{\frac{|\ln(\sqrt{R})|}{L-1}}. \end{aligned} \quad (5.116)$$

In writing these equations we have assumed that the longitudinal variable  $z$  is non-dimensional and scaled to the crystal length  $L_{cr}$ .

The solution of (5.115) is given by the stochastic integral

$$X_L = e^{\mu(L-1)} X_2 + \sigma \int_0^{L-1} e^{\mu(z-s)} dB_s. \quad (5.117)$$

The integral is a stochastic variable with normal distribution (it is the limit of the sum of normally distributed random variables). Hence we need to compute only the expectation value and variance of  $X_L$  to have a complete description of its distribution. The expectation value of the integral is zero (the integral is a random walk starting from the origin). Hence

$$E(X_L) = e^{\mu(L-1)} X_2. \quad (5.118)$$

The real and imaginary parts of  $X_z = R_z + iI_z$  are independent random variables with the same distribution. We can compute their variance using Ito's isometry. This states that

$$E \left[ \left( \int_0^T f(t, \omega) dB_t \right)^2 \right] = E \left[ \int_0^T f^2(t, \omega) dt \right] \quad (5.119)$$

where  $f(t, \omega)$  is a function of the parameter  $t$  and the stochastic variable  $\omega$ . In other words, for the purpose of computing the variance we can replace the stochastic integral over the Brownian motion  $B_t$  with a standard time dependent integral.

We now apply the Ito isometry to the variance of (5.115) keeping in mind that  $B_z$  is a complex Brownian motion with independent real and imaginary parts,

$$B_z = B_{1z} + iB_{2z}. \quad (5.120)$$

Therefore,

$$\begin{aligned} \text{Var}(R_L) &= \text{Var}(I_L) = E [R_L^2] \\ &= \sigma^2 E \left[ \left( \int_0^{L-1} e^{\mu_R(z-s)} \cos [\mu_I(z-s)] dB_{1z} \right)^2 \right] + \sigma^2 E \left[ \left( \int_0^{L-1} e^{\mu_R(z-s)} \sin [\mu_I(z-s)] dB_{2z} \right)^2 \right] \\ &= \sigma^2 \int_0^{L-1} e^{2\mu_R(z-s)} dz = -\frac{\sigma^2}{2\mu_R} (1 - e^{2\mu_R(L-1)}) = \frac{1-R}{2}. \end{aligned} \quad (5.121)$$

By normalizing the variables we are led to consider quantum fluctuation as Gaussian noise of amplitude around  $10^{-9} \sim 10^{-8}$ . One can now note that the quantum Langevin equations (5.108) are mathematically equivalent to the classical equations integrated earlier (see eqs.5.68) in the case of high-finesse (the narrow bandwidth approximation). The important result is that the quantum fluctuations correspond to noise of magnitude  $10^{-9} \sim 10^{-8}$ . This means that quantum fluctuations can induce giant noise amplifications in SPOPO in the singly resonant case with reflectivities of order  $R = 0.9$ , as reported in Fig. 5.5.4 and Fig. 5.5.5.

## 5.7 Conclusions

In this Chapter model equations for the evolution of signal and idler pulses in a SPOPO are derived and numerically integrated. A novel regime of giant sub-threshold pulses driven by quantum fluctuations is described through the analysis of stability eigenvalues, growth factors and pseudospectra. Sub-threshold pulses driven by quantum fluctuations are found at various mirror reflectivities in the non-degenerate regime where signal and idler have different group velocities. As a matter of fact we have shown that quantum fluctuations, which are of amplitude around around  $10^{-9} \sim 10^{-8}$ , can induce giant noise amplifications in SPOPO in the singly resonant case with reflectivities of order  $R = 0.9$ . Now the question that remains to be addressed is if giant sub-threshold pulses, driven by quantum fluctuations, still retain the non classical features typical of below threshold SPOPOs. In other words, if we want to move towards the realization of macroscopic continuous variable entanglement in SPOPOs we need to understand if quantum entanglement in OPOs below threshold survives the necessary conditions for Giant Pulse Amplification.

A positive answer to this question, which we have not fully investigated, would be very useful for practical implementation in which strong entangled beams are required, besides the obvious theoretical importance of such a phenomenon.

## Bibliography

- [1] A. E. Siegman, *Lasers* (University Science Books, Mill Valley, 1986).
- [2] A. E. Siegman, Phys. Rev. A **39**, 1253 (1989).
- [3] A. E. Siegman, Phys. Rev. A **39**, 1264 (1989).
- [4] S. H. Strogatz *Nonlinear Dynamics and Chaos* (Westview Press, 2000).
- [5] L. N. Trefethen, SIAM Review **39**, 383 (1997).
- [6] L. N. Trefethen and M. Embree, *Spectra and Pseudospectra* (Princeton University Press, 2005).
- [7] R. W. Boyd, *Nonlinear Optics* (Academic Press, 1992)
- [8] A. J. Scroggie, G.-L. Oppo and G. D'Alessandro, J. Opt. Soc. Am. B **17**, 84 (2000).
- [9] G. D' Alessandro and C. Brent Laforet, Opt. Lett. **34**, 614 (2009); G. D' Alessandro and F. Papoff, Phys. Rev. A **80**, 023804 (2009).
- [10] K. J. Blow, R. Loudon, S. J. D. Phoenix, and T. J. Shepherd Phys. Rev. A **42**, 4102 (1990).
- [11] A. Gatti, H. Wiedemann, L. A. Lugiato, I. Marzoli, G.-L. Oppo and S. M. Barnett, Phys. Rev. A **56**, 877 (1997).
- [12] R. Zambrini, S. M. Barnett, P. Colet, and M. San Miguel, Phys. Rev. A **65**, 023813 (2002).
- [13] C. Gardiner, *Handbook of Stochastic Methods* (Springer-Verlag, Berlin, 2004).
- [14] K.J. Blow, R. Loudon, S.J.D. Phoenix and T.J. Shepherd, Phys. Rev. A **65**, 023813 (2002).
- [15] L. Lefort, K. Peuch, S. D. Butterworth, Y. P. Svirko and D. C. Hanna, Opt. Lett. **24**, 28 (1999).
- [16] B. Oksendal, *Stochastic Differential Equations: An Introduction with Applications* (Springer-Verlag, Berlin, 2003).

## Self-organization, Pattern Formation, Cavity Solitons and Rogue Waves in SROPOs

### 6.1 Introduction.

In the last two chapters we have seen and investigated quantum and stochastic properties of singly resonant optical parametric oscillators (SROPO) below threshold of operation. To complete this thesis, we analyse in this chapter novel and somewhat unexpected properties of SROPOs above the threshold of operation. In particular we study the formation of spatial transverse patterns, cavity solitons and even optical turbulence in these optical systems. Optical turbulence, being a form of noise amplification, closes the circle of the investigations of the stochastic properties of SROPOs.

Transverse pattern formation, autosolitons and cavity solitons have been the subject of intense research in nonlinear optics in the last two decades since their original predictions [1, 2, 3, 4, 5]. Unlike in other fields of science, transverse patterns and dissipative solitons find useful applications in photonics such as optical memories, delay lines and optical registers [6]. Cavity solitons counterparts in the propagation direction have also been shown to generate passive mode-locking in fiber lasers [7].

Formation of transverse spatial structures in quadratic nonlinear cavities was predicted first in optical parametric oscillators (OPOs) [8, 9] and later extended to second harmonic generation [10, 11]. Early predictions in OPOs were confined to the degenerate case where signal and idler fields have the same frequency. Experimental evidence of pattern formation was indeed found in triply resonant degenerate OPOs close to the confocal cavity configuration [12] and via conical emissions [13, 14]. Confirmation of the predictions of [8] was provided in a broad-aperture degenerate OPOs in a plane-mirror mini-cavity [15]. Degenerate OPOs also display phase domain dynamics and dark-ring cavity solitons [17]. Finally, OPO models for non-degenerate Type-II cases in doubly or triply resonant cavity configurations have also been shown to display self-organization and pattern formation [16, 18, 19, 20, 21].

Transverse instabilities in the case of non-degenerate, singly resonant OPOs (SROPOs), where the signal field is the only resonated field in an optical cavity, have been less discussed in the literature. On the theoretical side pattern formation in SROPOs is expected to replicate results of the complex Ginzburg-Landau laser case [18]. On the experimental side cw SROPO configurations are notoriously difficult to operate because of high oscillation thresholds (typically several watts) in common birefringent crystals [22]. Quasi-phase matching in periodically poled materials has, however, considerably reduced operation thresholds of cw SROPOs [23] allowing for diode [24] and

fiber [25] laser pumping for spectroscopy applications. A major advantage of cw SROPOs is that their wide tunability is monotonic and not affected by mode jumps typical of doubly or triply resonant configurations.

In this chapter we investigate the formation and dynamics of transverse structures in SROPOs. We first derive a mean-field model in section 6.2 where the nonlinearity is of  $\text{sinc}^2$  form in agreement with early studies of SROPO steady states emissions [26, 27, 28]. The analysis builds on approaches that describe and integrate the propagation equations inside the OPO crystal [29, 30] by considering transverse effects and by carefully separating the mean-field and close-to-threshold approximations. The final model equations are capable of describing transverse pattern formation in the presence of pump depletion, signal-idler recombination and external seeding close to the signal frequency. External seeding proves to be of fundamental importance for transverse structures in SROPOs since, in its absence, changes of the cavity length are compensated by changes in the signal (and idler) frequency thus nullifying the common mechanism of Turing pattern formation in off-resonant optical systems [1, 31].

In section 6.3 plane-wave steady states and their stability are analyzed in the SROPO models with external seeding, close to and far from threshold. These studies confirm that no pattern formation should be expected without a detuned external seed. Analytical expressions for the location in the parameter space of the loss of stability of homogeneous solutions to spatially modulated structures are then provided in section 6.4. The thresholds for pattern formation when changing the seeding intensity are then compared with those obtained from numerical integration of the SROPO dynamical equations with excellent agreement. Section 6.5 investigates when spatially periodic spatial structures break down to either optical turbulence for small seeding intensities or to cavity solitons for large pump and seeding intensities. Optical turbulence is demonstrated to be the mechanism which generates rogue waves in the spatio-temporal evolution of the output fields. Finally, bright and dark cavity solitons are found in multistable configurations with localized hexagonal and honeycomb patterns.

## 6.2 Mean-field models.

We consider parametric down conversion in a  $\chi^{(2)}$  crystal of length  $L$  at perfect phase matching, a condition that can also describe the average effect of quasi-phase matching in periodically poled crystals. In this case the propagation of the pump, signal and idler fields in the crystal along the  $z$  direction are described by [32]:

$$\begin{aligned} \partial_z E_0 + \frac{n_0}{c} \partial_t E_0 &= \frac{i}{2k_0} \nabla^2 E_0 - \alpha E_1 E_2 \\ \partial_z E_1 + \frac{n_1}{c} \partial_t E_1 &= \frac{i}{2k_1} \nabla^2 E_1 + \mu \alpha E_0 E_2^* \\ \partial_z E_2 + \frac{n_2}{c} \partial_t E_2 &= \frac{i}{2k_2} \nabla^2 E_2 + \nu \alpha E_0 E_1^*. \end{aligned} \quad (6.1)$$

where  $E_j$  with  $j = 0, 1, 2$  are the slowly varying amplitudes of pump, signal and idler fields, respectively, with wave-numbers  $k_j = n_j \Omega_j / c$  and  $\nabla^2$  is the transverse Laplacian operator along the  $x$  and  $y$  directions perpendicular to the propagation axis  $z$ . The frequency constraint  $\Omega_0 = \Omega_1 + \Omega_2$  is rewritten as  $\mu + \nu = 1$  where  $\Omega_1 = \mu \Omega_0$ ,  $\Omega_2 = \nu \Omega_0$  and the effective coupling parameter  $\alpha$  is given by

$$\alpha = \frac{4\pi \Omega_0 \chi^{(2)}}{nc} \quad (6.2)$$

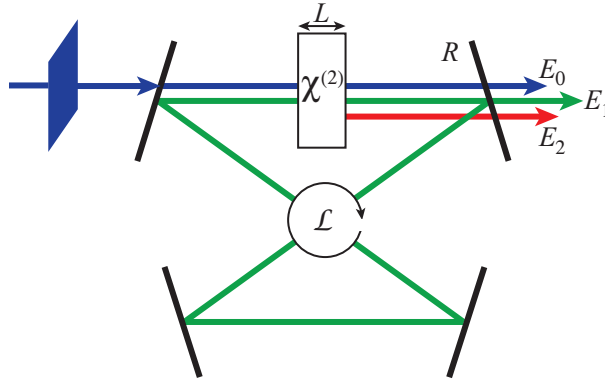


Figure 6.2.1: Schematic diagram of a SROPO cavity of length  $\mathcal{L}$  with a single partially reflecting mirror  $R$  and containing a parametric down-conversion crystal of length  $L$ .

where  $\chi^{(2)}$  is the second order susceptibility of the crystal,  $n = n_0 = n_1 = n_2$  is the common refractive index of the three waves that guarantees phase matching and  $c$  is the speed of light in vacuum.

We assume that the parametric down conversion crystal is contained in an optical cavity of length  $\mathcal{L}$  where the signal field is the only one to be resonated (see Figure 6.2.1). The steps involved in taking the mean-field approximation are the same as those reported in [21] although in the SROPO case there is only one resonated field. Hence we will consider only the following equation:

$$\partial_z E_1 + \frac{n_1}{c} \partial_t E_1 = \frac{i}{2k_1} \nabla^2 E_1 + \mu \alpha E_0 E_2^* \quad (6.3)$$

We set  $z = 0$  at the entrance of the crystal and write the longitudinal boundary condition as :

$$E_1(x, y, 0, t) = e^{\mathcal{D}} E_1 \left( x, y, L, t - \frac{\mathcal{L} - L}{c} \right) + \sqrt{T} E_{IN}(x, y); \quad (6.4)$$

$$\mathcal{D} = \ln \sqrt{R} - i\delta + (\mathcal{L} - L) \frac{i}{2k} \nabla^2; \quad (6.5)$$

$$\delta = \frac{\omega_c - \Omega_1}{c} \mathcal{L}; \quad T = 1 - R, \quad (6.6)$$

where  $R(T)$  is the mirror reflectivity (transmittivity) for the signal field,  $E_{IN}$  is a complex input field of frequency  $\omega_{IN}$  close to  $\Omega_1$ , normally known as the seeding., while  $\omega_c$  is the frequency of the longitudinal cavity mode closest to  $\Omega_1$ . Note that if the seeding is zero, the detuning is also zero since the frequency  $\Omega_1$  shifts to the cavity mode by changing the idler frequency while maintaining the relation  $\Omega_0 = \Omega_1 + \Omega_2$ . In the following we use the transmittivity  $T$  of the output mirror as a small parameter, i.e.

$$\sqrt{T} = \varepsilon \ll 1. \quad (6.7)$$

In order to impose the boundary condition (6.4) on the propagation equation (6.3), the usual Mean Field Limit (MFL) transformation is entered:

$$\begin{aligned} z' &= z \\ t' &= t + \left[ \frac{\mathcal{L} - L}{c} \right] \frac{z}{L}. \end{aligned} \quad (6.8)$$

Under condition (6.8), we obtain

$$\partial_z = \partial_{z'} + \left[ \frac{\mathcal{L} - L}{cL} \right] \partial_{t'}; \quad \partial_t = \partial_{t'}; \quad (6.9)$$

$$\partial_z + \frac{n}{c} \partial_t = \partial_{z'} + \left[ \frac{\mathcal{L} - L}{cL} \right] \partial_{t'} + \frac{n}{c} \partial_{t'} = \partial_{z'} + \left[ \frac{\mathcal{L} + (n-1)L}{cL} \right] \partial_{t'}. \quad (6.10)$$

By introducing the new field variable  $F$  such that

$$F = \Gamma E_1 + \sqrt{T} E_{IN} \frac{z}{L} \quad \text{with} \quad \Gamma = \exp\left(\mathcal{D} \frac{z}{L}\right) \quad (6.11)$$

we obtain

$$\begin{aligned} \partial_{t'} F &+ \frac{cL}{\mathcal{L} + (n-1)L} \partial_{z'} F \\ &= \frac{cL}{\mathcal{L} + (n-1)L} \left[ \frac{\mathcal{D}}{L} \left( F - \sqrt{T} E_{IN} \frac{z}{L} \right) + \Gamma \left( \partial_z E_1 + \frac{n}{c} \partial_t E_1 \right) + \sqrt{T} E_{IN} \frac{1}{L} \right] \\ &= \frac{cL}{\mathcal{L} + (n-1)L} \left[ \frac{\mathcal{D}}{L} \left( F - \sqrt{T} E_{IN} \frac{z}{L} \right) + \Gamma \left( \frac{i}{2k_1} \nabla^2 E_1 + \mu \alpha E_0 E_2^* \right) \right. \\ &\quad \left. + \sqrt{T} E_{IN} \frac{1}{L} \right]. \end{aligned} \quad (6.12)$$

The longitudinal boundary conditions (6.4) are now transformed into

$$F(x, y, 0, t') = F(x, y, L, t') \quad (6.13)$$

i.e. the field is periodic at the same time  $t'$ . The standard MFL conditions are:

$$\begin{aligned} \varepsilon &\ll 1; & \delta &= O(\varepsilon) \ll 1; \\ \alpha L &= O(\varepsilon) \ll 1; & (\mathcal{L} - L)/2k_1 &= O(\varepsilon) \ll 1 \end{aligned} \quad (6.14)$$

One then obtains:

$$\mathcal{D} \approx -\frac{T}{2} - i\delta + i \frac{\mathcal{L} - L}{2k_1} \nabla^2; \quad \Gamma \approx 1 + \frac{\mathcal{D}}{L} z, \quad (6.15)$$

since

$$\ln \sqrt{R} = \ln \sqrt{1 - T} \approx \ln \left( 1 - \frac{T}{2} \right) \approx -\frac{T}{2}. \quad (6.16)$$

At the first order in  $\varepsilon$  eq. (6.12) becomes:

$$\begin{aligned} \partial_{t'} F &+ \frac{cL}{\mathcal{L} + (n-1)L} \partial_{z'} F \\ &= -\frac{cT/2}{\mathcal{L} + (n-1)L} F - i \frac{c\delta}{\mathcal{L} + (n-1)L} F + i \frac{c\mathcal{L}}{2k_1[\mathcal{L} + (n-1)L]} \nabla^2 F \\ &\quad + \frac{c\sqrt{T}}{\mathcal{L} + (n-1)L} E_{IN} + \frac{cL}{\mathcal{L} + (n-1)L} \mu \alpha E_0 E_2^*. \end{aligned} \quad (6.17)$$

For convenience, we introduce the parameters

$$\tau = \frac{\mathcal{L} + (n-1)L}{c}; \quad \gamma = \frac{T}{2}; \quad a = \frac{\mathcal{L}}{2k_1}. \quad (6.18)$$

One then obtains:

$$\tau \partial_{t'} F + L \partial_{z'} F = -\gamma F - i\delta F + ia\nabla^2 F + \mu\alpha L E_0 E_2^* + \sqrt{2\gamma} E_{IN}. \quad (6.19)$$

Since the new longitudinal boundary condition (6.13) is now synchronous and periodic, one can use an expansion in longitudinal Fourier modes.

The final equation for the normalized signal field reads as:

$$\begin{aligned} \tau \partial_{t'} E_1 + L \partial_z E_1 &= -\gamma E_1 - i\delta E_1 + ia\nabla^2 E_1 \\ &+ \mu\alpha L E_0 E_2^* + \sqrt{2\gamma} E_{IN}. \end{aligned} \quad (6.20)$$

Under the MFL conditions, however, only the longitudinal mode closest to  $\Omega_1$  has components different from zero if all the terms on the right hand side of equation (6.17) are independent of  $z'$ . However, the term that contains  $E_0 E_2^*$  is, in principle, a function of  $z'$ . The requirement for consistency with  $F$ , i.e.  $E_1$ , independent of  $z'$  is that the nonlinear term is also required to be independent of  $z'$ . There are two possibilities to accomplish this: 1) both  $E_0$  and  $E_2$  are also independent of the propagation direction and 2) the signal is affected by the average of the propagation of the pump and wave fields along the crystal. The  $z$ -variation per pass of the resonated signal field,  $E_1$ , hence can be neglected when it is affected by the average of the propagation of the pump and idler waves along the crystal [30], i.e.

$$E_1 = \frac{1}{L} \int_0^L E_0(z) E_2^*(z) dz. \quad (6.21)$$

To obtain an explicit dependence of pump and idler fields along the direction of propagation we consider the first and third equations of the system (6.1) and neglect diffraction in the crystal:

$$d_z E_0(z) = -\alpha E_1 E_2(z) \quad (6.22)$$

$$d_z E_2(z) = \nu\alpha E_0(z) E_1^* \quad (6.23)$$

where the signal amplitude  $E_1$  is now independent of  $z$ . By taking the second derivative of (6.22) and using (6.23), one obtains

$$d_z^2 E_0(z) = -(\nu\alpha^2 I_1) E_0(z) \quad (6.24)$$

which shows that the pump field oscillates along the propagation direction with a frequency that depends on the signal intensity  $I_1$ . Integrating this equation we find

$$E_0(z) = A_0 \cos\left(\alpha\sqrt{\nu I_1} z\right), \quad (6.25)$$

where  $A_0$  is the amplitude of the pump field at the entrance of the crystal [30]. From (6.22),

$$E_2(z) = -\frac{1}{\alpha E_1} d_z E_0 = A_0 E_1^* \sqrt{\frac{\nu}{I_1}} \sin\left(\alpha\sqrt{\nu I_1} z\right) \quad (6.26)$$

in agreement again with [30].

We can now calculate the spatial average (6.21):

$$\frac{1}{L} \int_0^L E_0(z) E_2^*(z) dz = |A_0|^2 \frac{E_1}{2\alpha L I_1} \sin^2 \left( \alpha L \sqrt{\nu I_1} \right) \quad (6.27)$$

and insert it into (6.19):

$$\begin{aligned} \tau \partial_{t'} E_1 + L \partial_z E_1 &= -\gamma E_1 - i\delta E_1 + ia \nabla^2 E_1 \\ &+ \mu |A_0|^2 \frac{E_1}{2I_1} \sin^2 \left( \alpha L \sqrt{\nu I_1} \right) + \sqrt{2\gamma} E_{IN}. \end{aligned} \quad (6.28)$$

By expanding in longitudinal Fourier modes and retaining only the longitudinal mode closest to  $\Omega_1$ , corresponding to  $\partial_{z'} E_1 = 0$ , we finally obtain:

$$\begin{aligned} \partial_{t'} E_1 &= \kappa [-(1+i\theta) E_1 + i\hat{a} \nabla^2 E_1 \\ &+ \mu |A_0|^2 \frac{E_1}{2\gamma I_1} \sin^2 \left( \alpha L \sqrt{\nu I_1} \right) + \hat{E}_{IN}] \end{aligned} \quad (6.29)$$

where

$$\begin{aligned} \kappa &= \frac{\gamma}{\tau} = \frac{\gamma c}{\mathcal{L} + (n-1)L}; & \hat{a} &= \frac{a}{\gamma} = \frac{\mathcal{L}}{2k_1 \gamma}; \\ \theta &= \frac{\delta}{\gamma} = \frac{(\omega_c - \Omega_1) \mathcal{L}}{c\gamma}; & \hat{E}_{IN} &= \sqrt{\frac{2}{\gamma}} E_{IN}. \end{aligned} \quad (6.30)$$

Finally, we renormalize the transverse space variables  $x$  and  $y$  by dividing them by  $\sqrt{\hat{a}}$ , the time variable by multiplying it by  $\kappa$  and the field amplitudes according to

$$\begin{aligned} E &= \alpha L \sqrt{\nu} E_1; & |E_0|^2 &= |A_0|^2 \frac{\mu \nu \alpha^2 L^2}{2\gamma} \\ E_{IN} &= \alpha L \sqrt{\nu} \hat{E}_{IN} \end{aligned} \quad (6.31)$$

to obtain

$$\begin{aligned} \partial_\tau E = \partial_{\kappa t'} E &= E_{IN} - (1+i\theta) E \\ &+ |E_0|^2 \frac{E}{I} \sin^2 \left( \sqrt{I} \right) + i \nabla^2 E. \end{aligned} \quad (6.32)$$

The analysis of eq. (6.32) is the main focus of the research presented here. It will be referred to as the *sinc*<sup>2</sup> model since  $\sin^2(\sqrt{I})/I = \text{sinc}^2(\sqrt{I})$ .

We note that in SROPO configurations the frequency of the signal field,  $\Omega_1$ , is tuneable by corresponding changes of the idler frequency,  $\Omega_2$ , while maintaining the energy conservation condition  $\Omega_0 = \Omega_1 + \Omega_2$ . This means that with no external seeding ( $E_{IN} = 0$ ) the detuning  $\theta$  is also zero since the SROPO tunes its signal frequency to the closest longitudinal cavity mode  $\omega_c$ . With an external seeding different from zero and detuned with respect to the cavity, it is advantageous to consider the external frequency  $\omega_{IN}$  as reference and introduce

$$\theta = \frac{(\omega_{IN} - \Omega_1) \mathcal{L}}{c\gamma}. \quad (6.33)$$

Under these conditions  $E_{IN}$  should be considered to be real and equation (6.32) remains unchanged.

It is interesting to investigate the behaviour of the pump and idler fields inside the OPO crystal as provided by Eqs. (6.25) and (6.26). Figure 6.2.2 shows the pump and idler intensities during propagation for three sample values of  $|E_0|^2$ , namely 1.2, 2.0 and 8.0. While at  $|E_0|^2 = 1.2$  (black lines) the changes of pump and idler per pass are limited, for  $|E_0|^2 = 2.0$  (red lines) and  $|E_0|^2 = 8.0$  (blue lines) they are substantial. In particular, full pump depletion and substantial back-conversion of signal and idler fields into the pump are clearly visible in Figure 6.2.2 for  $|E_0|^2 = 8.0$ . In the SROPO case these phenomena are not incompatible with the mean field approximation and are at the base of the  $\text{sinc}^2$  nonlinearity of model (6.32). The mean field approximation implies that the signal intensity remains almost constant with respect to its input value during propagation in the  $\chi^{(2)}$  medium with large changes taking place over several cavity round-trips. No such constraints apply to pump and idler fields as shown in Fig. 6.2.2.

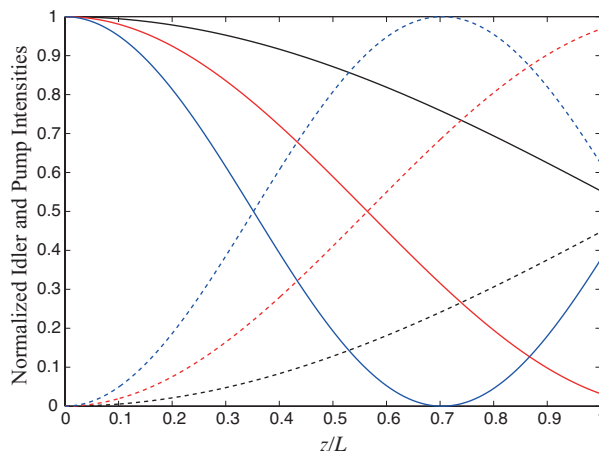


Figure 6.2.2: Pump intensity (solid lines) and idler intensity (dashed lines) in the SROPO crystal for  $|E_0|^2 = 1.2$  (black lines),  $|E_0|^2 = 2.0$  (red lines) and  $|E_0|^2 = 8.0$  (blue lines). The intensities are normalized to the input pump values  $|E_0|^2$ . The propagation distance is normalized to the crystal length.

Note that the  $\cos^2$  and  $\sin^2$  nature of the pump and idler intensities, respectively, guarantees conservation of the energy density in every point along the SROPO crystal. Energy conservation in turn guarantees the validity of the Manley-Rowe relations about the variations of the energy densities  $N_i$  per field along the crystal:

$$\frac{dN_0}{dz} = -\frac{dN_1}{dz} - \frac{dN_2}{dz} \quad (6.34)$$

since  $dN_1/dz = 0$ . These facts are a-posteriori confirmations that the physical processes described in Eqs. (6.1) are compatible with the application of the mean-field limit to the signal field even for large values of the pump and seeding intensities.

### 6.2.1 The close-to-threshold approximation.

Close to the signal generation threshold it is possible to obtain partial differential equations in the mean-field limit where the nonlinear terms are in a polynomial form and thus easier to analyze. The scaling of the mean field limit requires that the nonlinear coefficient per pass,  $\alpha L$ , has to be of the order of the mirror transmittivity,  $1 - R$ . This implies that the argument of the  $\sin^2$  term

in equation (6.27) may become large for large signal intensities without breaking the mean-field conditions. Close to threshold, however, the signal intensity satisfies  $I_1 < 1$  and the  $\sin^2$  term can be approximated by a power expansion. In this case pump and idler display small changes per pass across the crystal meaning that pump depletion and back-conversion do not take place in a single pass. Equations (6.25) and (6.26), however, tell us that while the pump can be approximated to first order to a constant value  $A_0$ , the idler has to grow along  $z$  from its initial value. This is in agreement with previous analysis below threshold where the important noise term is associated with the idler fluctuations at the entrance of the crystal [33]. In the case of SROPOs close to threshold, we can approximate  $E_0$  and  $E_2$  in (6.25) and (6.26) with

$$E_0(z) \approx A_0 \left( 1 - \frac{\nu I_1 \alpha^2 z^2}{2} \right) \quad (6.35)$$

$$E_2(z) \approx A_0 E_1^* \left( \nu \alpha z - \frac{\nu^2 I_1 \alpha^3 z^3}{6} \right). \quad (6.36)$$

By using these expressions to evaluate the average (6.21) one obtains:

$$\frac{1}{L} \int_0^L E_0(z') E_2^*(z') dz' \approx \frac{\nu \alpha L |A_0|^2 E_1}{2} \left( 1 - \frac{\nu \alpha^2 L^2 I_1}{3} \right).$$

By repeating the same steps of the mean-field limit as described in the previous subsection we obtain:

$$\partial_\tau E = E_{IN} - (1 + i\theta)E + |E_0|^2 \left( E - \frac{EI}{3} \right) + i\nabla^2 E \quad (6.37)$$

which describes the spatio-temporal behaviour of the SROPO close to threshold in the presence of an external seeding  $E_{IN}$  and will be referred to as the *cubic model*.

## 6.3 Plane wave steady-states

As mentioned in section 6.2, when there is no external seeding,  $E_{IN} = 0$ , the detuning is zero since the SROPO automatically adjusts its frequency to the closest cavity resonance. The plane wave steady-state intensities,  $I_s$ , are implicit for the  $\text{sinc}^2$  model (see [26, 27, 28]) and explicit for the cubic model:

$$\begin{aligned} I_s &= |E_0|^2 \sin^2 \left( \sqrt{I_s} \right) \\ I_s &= 3(|E_0|^2 - 1)/|E_0|^2 \end{aligned} \quad (6.38)$$

The steady-state signal intensity of the SROPO as a function of the pump intensity,  $|E_0|^2$ , is shown in Figure 6.3.1 for the  $\text{sinc}^2$  model (solid line) and the cubic approximation (dashed line). These are trivially complemented by the zero-intensity state that is stable below threshold,  $|E_0|^2 < 1$ , and unstable above. In the cubic case the stationary intensity above threshold asymptotes to the value 3 for large pump intensities and is always stable. The steady-state curve for the  $\text{sinc}^2$  model, on the other hand, becomes multivalued at large values of the input pump intensity ( $|E_0|^2 > 20$ , not shown here) [27, 28]. Here, however, we are interested in values of the pump intensity below 10, as these are more realistic with respect to present state-of-the-art of broad area SROPO realisations. In adimensional units for the amplitude and remembering that the threshold for oscillation is attained for  $|E_0|^2 = 1$  (see the second of eqs. 6.38), a value of  $|E_0|^2 = 10$  means 10 times above threshold. In

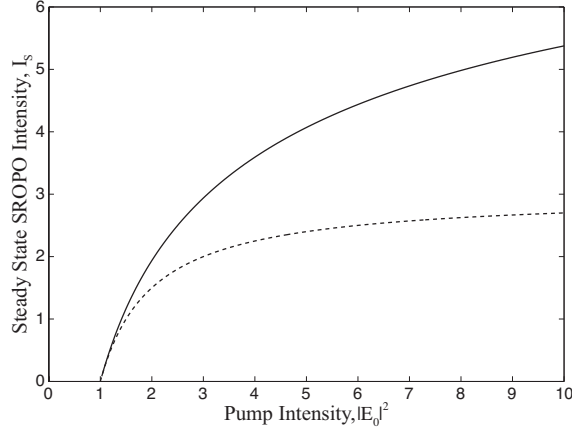


Figure 6.3.1: Intensity of the SROPO steady-state for the  $\text{sinc}^2$  model (solid line) and the cubic approximation (dashed line) with increasing pump intensities for  $E_{IN} = 0$  and  $\theta = 0$ . All variables are dimensionless.

this regime it is possible to prove that, above threshold, the non-zero steady-state intensities in the  $\text{sinc}^2$  model are also stable [28]. Note that when comparing the  $\text{sinc}^2$  and the cubic models, there is a substantial difference between their steady-state intensities even below  $|E_0|^2 = 2$ . At twice above threshold this difference becomes considerable and the close to threshold (cubic) model has to be discarded.

Analogously to lasers, the field phase is decoupled from the steady-state equations and is affected by fluctuations and drift processes. When there is external seeding,  $E_{IN} > 0$ , the phase of the SROPO locks to that of the external beam, depending on the magnitude of the detuning  $\theta$  and the input intensity. Such behaviour strongly differs from that of  $E_{IN} = 0$ . In the case of  $E_{IN} \neq 0$  the steady-state intensities are given by

$$E_{IN}^2 = I_s \left[ (1 - |E_0|^2 f(I_s))^2 + \theta^2 \right] \quad (6.39)$$

where

$$f(I_s) = \text{sinc}^2(\sqrt{I_s}) \quad (6.40)$$

$$f(I_s) = 1 - I_s/3 \quad (6.41)$$

for the  $\text{sinc}^2$  and cubic models, respectively. The steady-state curves of the SROPO intensity versus the input intensity become S-shaped, a behaviour typical of injected optical systems, as shown in section 6.4.

For the cubic model without diffraction it is possible to obtain analytical results. For example, for  $|\theta| < (|E_0|^2 - 1)/\sqrt{3}$  the plane-wave steady-state curves are S-shaped, and the positions of the turning points  $[(E_{IN}^2)^-, I_s^-]$  and  $[(E_{IN}^2)^+, I_s^+]$  can be determined by finding the maxima and minima of (6.39):

$$I_s^\pm = \frac{2(|E_0|^2 - 1) \pm ((|E_0|^2 - 1)^2 - 3\theta^2)^{1/2}}{|E_0|^2} \quad (6.42)$$

and then using these values in (6.39). At resonance,  $\theta = 0$ , the turning points are located at:

$$\begin{aligned} [(E_{IN}^2)^+, I_s^+] &= [0, 3(|E_0|^2 - 1)/|E_0|^2] \\ [(E_{IN}^2)^-, I_s^-] &= [4(|E_0|^2 - 1)^3/(9|E_0|^2), \\ &\quad (|E_0|^2 - 1)/(3|E_0|^2)] . \end{aligned} \quad (6.43)$$

Note that the + turning point at resonance corresponds to the zero seeding case of SROPO intensity given by eq. (6.38).

### 6.3.1 Linear stability analysis of the SROPO with seeding.

The linear stability analysis of the steady-states given in the previous section produces two stability eigenvalues:

$$\lambda_{\pm} = \xi \pm \sqrt{\beta^2 - \theta^2} \quad (6.44)$$

where for the sinc<sup>2</sup> model

$$\xi = |E_0|^2 \text{sinc}(2\sqrt{I_s}) - 1 \quad (6.45)$$

$$\beta = |E_0|^2 \frac{\cos(2\sqrt{I_s}) + \sqrt{I_s} \sin(2\sqrt{I_s}) - 1}{2I_s} \quad (6.46)$$

and for the cubic model

$$\begin{aligned} \xi &= |E_0|^2 - 1 - 2|E_0|^2 I_s/3 \\ \beta &= -|E_0|^2 I_s/3. \end{aligned} \quad (6.47)$$

For the sinc<sup>2</sup> model, the stability eigenvalues are implicit functions of the steady-state intensity,  $I_s$ . It is, however, easy to display the stability of the stationary states graphically along the S-shaped curves by picking increasing values of  $I_s$ , evaluating  $\lambda_{\pm}$  and reporting the stability result on the diagram, as displayed in Figures 6.3.2 and 6.4.1. Here black solid lines correspond to two negative real eigenvalues (sinks), turquoise solid lines to stable complex eigenvalues (foci), dot-dashed blue lines to at least one positive real eigenvalue (saddles or sources) and red dashed lines to complex eigenvalues with positive real part (unstable foci). In terms of bifurcations, the intersection of a black solid line and a blue dot-dashed line signals a saddle-node bifurcation, while the transition of a turquoise solid line into a red dashed line signals a Hopf bifurcation.

We find that the turning points of the S-shaped curves always correspond to either saddle-node (the  $[(E_{IN}^2)^+, I_s^+]$  points) or saddle-source (the  $[(E_{IN}^2)^-, I_s^-]$  points) bifurcations corresponding to a change of sign of one real eigenvalue. For the cubic model this fact can be demonstrated analytically. In the lowest branch of the S-curve, the two real eigenvalues turn complex (see the red dashed line in Figures 6.3.2 and 6.4.1). This means that the lowermost part of the S-curve is Hopf unstable.

## 6.4 Turing instabilities and pattern formation

In this section we describe instabilities of the stationary states of the SROPO to transverse perturbations due to diffraction with and without external seeding. By moving to the spatial Fourier

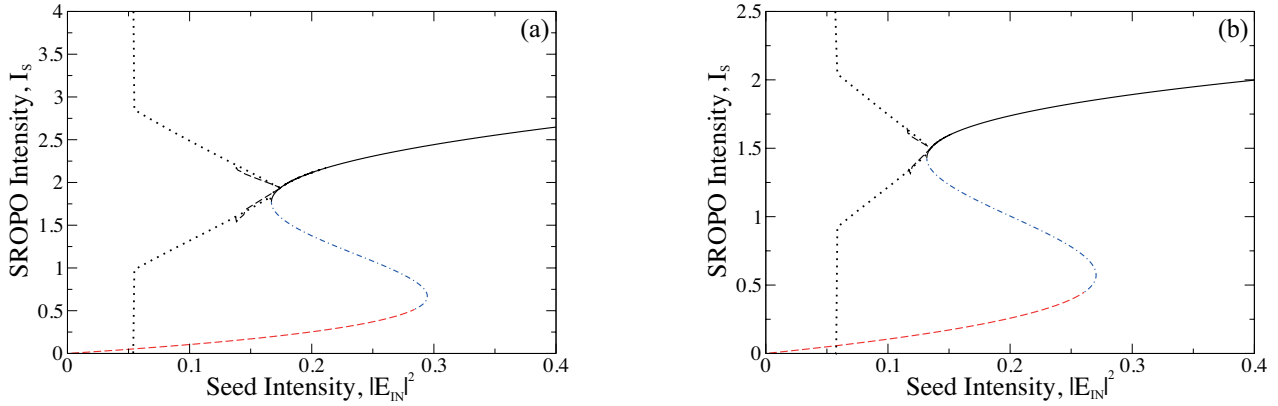


Figure 6.3.2: Plane wave steady-state stability and pattern formation for (a) the sinc<sup>2</sup> model (6.32) of a SROPO and (b) the cubic model (6.37) of a SROPO close to threshold. The solid (black), dot-dashed (blue) and dashed (red) lines correspond to stable, unstable and Hopf unstable plane wave steady states, respectively. The black dotted (black dashed) lines correspond to the minimum and maximum of the intensity of stationary hexagonal (roll) patterns. The vertical dotted line corresponds to the instability of hexagons leading to optical turbulence. Parameters are  $|E_0|^2 = 2$  and  $\theta = -0.3$ . All variables are dimensionless.

space of the transverse wave-vector  $k$  and repeating the linear stability steps of the previous section, we obtain the two stability eigenvalues of (6.44) but with the detuning  $\theta$  replaced by

$$\theta_k = \theta + k^2 \quad (6.48)$$

which introduces an explicit dependence on the transverse spatial scale. Note that since both  $\theta$  and  $k$  have no physical dimensions, also  $\theta_k$  is an adimensional quantity.

We start with the analysis of possible Turing instabilities without external seeding ( $E_{IN} = 0$ ) and with zero detuning  $\theta = 0$ . In this case, the evaluation of the stability eigenvalues with the appropriate factor (6.48) is done only at the values of  $I_s$  given by (6.38). In the cubic case the eigenvalues reduce to:

$$\lambda_{\pm} = -(|E_0|^2 - 1) \pm \sqrt{(|E_0|^2 - 1)^2 - k^4}. \quad (6.49)$$

The largest eigenvalue has a zero value for the plane-wave case,  $k = 0$ , corresponding to the uncoupled phase of the SROPO models without seeding as studied in the previous section. For large wave-vectors the eigenvalues can become complex, i.e. one may observe damped oscillations. However, the presence of diffraction cannot make the real part of the eigenvalues positive which means that, for the SROPO alone, there are no spatio-temporal instabilities and hence no pattern formation. We obtain the same result for the sinc<sup>2</sup> model within the pump intensity ranges studied here although the implicit nature of the steady-state (6.38) requires straightforward numerical evaluations of the stability eigenvalues for given wave-vectors  $k$ .

We now consider the case of external seeding where the detuning,  $\theta$ , can be non-zero. By using the expressions (6.44) with  $\theta$  replaced by  $\theta_k$  (6.48) one observes that the transverse wave-vector can destabilise the system only when it counterbalances the detuning and that this is most effective when

$$k^2 = -\theta \quad (6.50)$$

i.e. the off-resonance mechanism for pattern formation typical of optical systems [1, 8]. We refer to the off-resonance mechanism as Turing pattern formation since it has been demonstrated that all the requirements of Turing instabilities are fully satisfied [31].

The condition (6.50) provides us with the value along the steady-state curves at which we expect pattern formation to occur,  $I_s^c$ . This value simply corresponds to the steady-state value of the plane wave solution at zero detuning (6.38) since for  $\theta_k = 0$  the stability eigenvalues (6.44) reduce to  $\lambda_{\pm} = \xi \pm \beta$ , where  $\xi$  and  $\beta$  are given by (6.45) for the  $\text{sinc}^2$  model and (6.47) for the cubic model. By tracing a horizontal line at the  $I_s^c$  value on the diagrams of Figures 6.3.2 and 6.4.1 one obtains the corresponding value of  $|E_{in}^c|^2$  of the seeding intensity where the Turing instability takes place. The bifurcation from the homogeneous states to steady transverse patterns is obtained when decreasing the seeded amplitude  $E_{IN}$  so that the locked plane wave state progressively approaches the upper turning point of the S-shaped steady-state curve (the  $[(E_{IN}^2)^+, I_s^+]$  point). Before reaching it, the stationary plane wave intensity reaches the value  $I_s^c$  and a stationary roll pattern is formed supercritically while a hexagonal pattern is formed subcritically in agreement with [35]. This bifurcation scenario is in agreement with early analysis of complex Ginzburg-Landau models in the presence of injection [36, 37]) although our cubic model does not contain diffusion or purely imaginary nonlinearities. It is also in remarkable agreement with numerical simulations, as demonstrated in section 6.4.1.

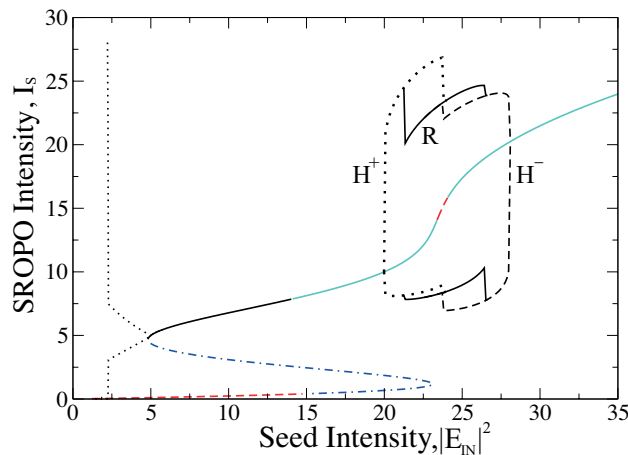


Figure 6.4.1: Same as Fig. 6.3.2 but for parameter values  $|E_0|^2 = 8$  and  $\theta = -1$  (all variables are dimensionless). The solid turquoise lines correspond to stable plane wave steady states with complex stability eigenvalues. For seed intensities above 20, minima and maxima of the intensity of stable hexagonal patterns  $H^+$  (dotted lines), of stable roll patterns  $R$  (solid lines) and of stable honeycomb patterns  $H^-$  (dashed lines) are displayed.

We have also investigated instabilities of the plane wave to pattern structures for large values of both the input pump and the seeding intensity as shown in Fig. 6.4.1. These instabilities have no counterpart in the close-to-threshold regime and can be estimated analytically by using the stability eigenvalues (6.44) with (6.45) and  $\theta_k = 0$  for the most unstable wave-vector (6.50). Figure 6.4.2 shows the instability eigenvalue  $\lambda_+$  versus the stationary SROPO intensity for different values of the input pump  $|E_0|^2$ . Above a threshold value of  $|E_0|^2 \sim 4.37$  (corresponding to a critical value

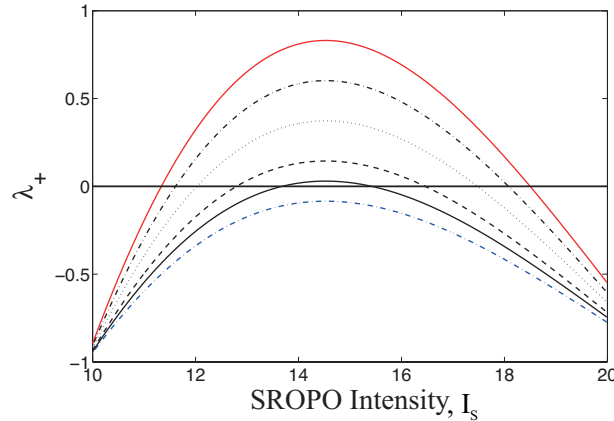


Figure 6.4.2: Stability eigenvalue  $\lambda_+$  versus the SROPO stationary intensity. Parameters are  $\theta = -1$ ,  $|E_0|^2 = 4$  (lowermost dashed-dotted blue line),  $|E_0|^2 = 4.5$  (solid black line),  $|E_0|^2 = 5$  (dashed black line),  $|E_0|^2 = 6$  (dotted black line),  $|E_0|^2 = 7$  (uppermost dashed-dotted black line) and  $|E_0|^2 = 8$  (uppermost solid red line). All variables are dimensionless.

of  $I_s = 14.5$ ), there is a range of values of the SROPO intensity where the plane wave solution is unstable to spatial patterns. The limit values of the SROPO intensity are the zeroes of the  $\lambda_+$  curve shown in Figure 6.4.2 with the lower (upper) intersection corresponding to an instability when increasing (decreasing) the seeding intensity.

In Figure 6.4.3 we show the plane-wave instability range in the parameter space of the SROPO intensity versus the seed intensity for different values of the pump intensity. In section 6.4.1 we show that the bifurcations at the boundaries of the instability ranges are subcritical in nature and that there are extended regions of bistability between patterns and stable plane waves to support cavity solitons. The ranges displayed in Fig. 6.4.3 provide a minimum size of the parameter region where pattern formation is expected. For example, the plane-wave instability range for  $|E_0|^2 = 8$  evaluated analytically from the stability eigenvalues is approximately between  $|E_{IN}|^2 = 22$  and  $|E_{IN}|^2 = 26$  (see Fig. 6.4.3) while the numerical simulations find stable patterns between  $|E_{IN}|^2 = 20$  and  $|E_{IN}|^2 = 28$  because of subcriticality (see Fig. 6.4.1).

### 6.4.1 Numerical patterns

We have first numerically integrated the sinc<sup>2</sup> (6.32) and cubic (6.37) models for  $|E_0|^2 = 2$  and  $\theta = -0.3$ . We have started with relatively large values of the seeding amplitude,  $E_{IN} = 0.45$ , where the stable plane-wave solution has been recovered. By progressively decreasing  $E_{IN}$ , a supercritical roll pattern is observed to appear at around  $E_{IN} = 0.424$ ,  $I_s^c = 1.9$  for the sinc<sup>2</sup> model and  $E_{IN} = 0.374$ ,  $I_s^c = 1.5$  for the cubic model, in excellent agreement with the theoretical predictions given in section 6.4. By further decreasing the seeding intensity, the amplitude of the roll pattern increases (see black dashed lines in Fig. 6.3.2 until it merges into a hexagonal structure. Having located the hexagonal pattern (see Fig. 6.4.4 (a) for its transverse intensity structure), we have traced it with increasing and decreasing values of the external seeding intensity. Note the period of the patterns in fig. (6.4.4) is of the order of  $10^{-6}$ m. For small seeding intensities, Figures 6.3.2 and 6.4.1 show the maximum and minimum intensity of the hexagonal pattern (dotted lines) and show that these change linearly with decreasing seeding intensity. The bifurcation back to the steady plane-wave solution is subcritical although the regime of sub-critical bistability is very

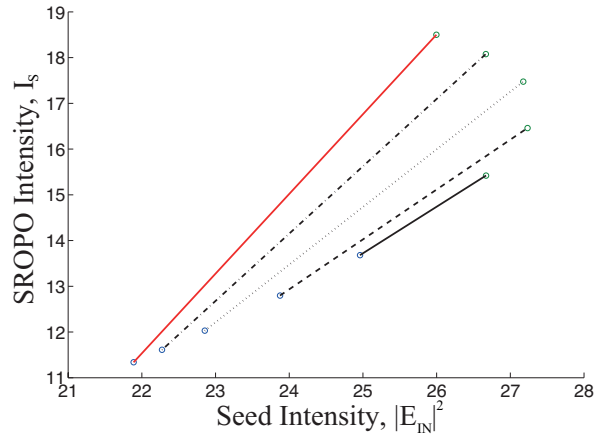


Figure 6.4.3: Plane wave instability regions to spatial patterns in the (seed intensity, SROPO intensity) parameter space. Parameters are  $\theta = -1$ ,  $|E_0|^2 = 4.5$  (solid black line),  $|E_0|^2 = 5$  (dashed black line),  $|E_0|^2 = 6$  (dotted black line),  $|E_0|^2 = 7$  (uppermost dashed-dotted black line) and  $|E_0|^2 = 8$  (uppermost solid red line). All variables are dimensionless.

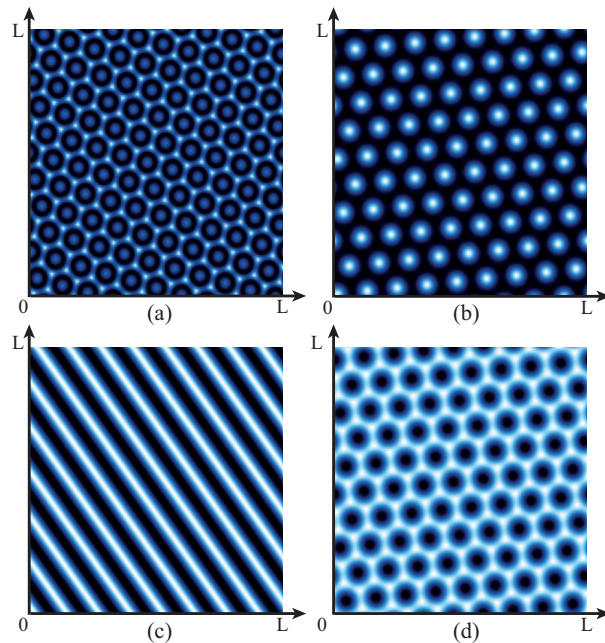


Figure 6.4.4: Intensity of transverse patterns in a SROPO. (a) Hexagons for  $|E_{IN}|^2 = 3$ . (b) Hexagons for  $|E_{IN}|^2 = 22$ . (c) Rolls for  $|E_{IN}|^2 = 24$ . (d) Honeycombs for  $|E_{IN}|^2 = 27$ . Parameters are  $|E_0|^2 = 8$  and  $\theta = -1$ . All variables are dimensionless. The period of the patterns is of the order of  $10^{-6}\text{m}$ .

small and difficult to detect on the scales of the diagrams. When further decreasing the external seeding, one observes a sudden destabilisation of the hexagonal pattern into a region of optical turbulence. The abrupt transition from stable patterns to turbulence is clearly displayed in Figures 6.3.2 and 6.4.1 by the almost vertical line on the left hand side of these diagrams that corresponds to a sudden jump in the values of the minima and maxima intensities observed in the transverse section during the turbulent evolution.

For larger values of the input pump,  $|E_0|^2$ , new regions of pattern formation arise in the SROPO with seeding in a way similar to what has been described for nascent optical bistability [4]. These new regions can only be observed in the sinc<sup>2</sup> model since the cubic model can only display stable plane wave solutions for large  $|E_0|^2$  and large  $E_{IN}^2$ . Moreover, the cubic model is not accurate away from threshold. For the numerical simulations presented here we have selected the value of  $|E_0|^2 = 8$  where the minimum size of the pattern region is more than 15% of the maximum value of the seed intensity in order to guarantee relevance to possible experimental realizations. In Fig. 6.4.1 we present the intensities of the observed patterns together with the steady-state plane wave curves for the selected value of  $|E_0|^2 = 8$ . At low seed intensities the phenomenology is similar to that described for  $|E_0|^2 = 2$  above. However, at larger seeding intensities the upper branch of the S-shaped plane-wave steady-state curve suddenly increases. The steady-state first develops damped oscillations and then becomes unstable to a Hopf bifurcation (see dashed red lines around the seed intensity of 23 in Figure 6.4.1). Around such bifurcation, a new region of stationary patterns develops. We have identified rolls R (solid lines), hexagons H<sup>+</sup> (dotted lines) and honeycombs H<sup>-</sup> (dashed lines). The intensities of the different transverse patterns are displayed in Figure 6.4.4. We note that none of the patterns observed at large input pumps and seeding intensities are present in the cubic model. Finally, pattern bistability is observed between rolls and hexagons and rolls and honeycombs.

## 6.5 Optical turbulence, rogue waves and cavity solitons

When the seeding is small, the input energy is not sufficient to lock the SROPO to the external laser. These unlocked regimes are typical of lasers with injected signals [38]. The larger the detuning,  $\theta$ , between the external laser and the SROPO cavity, the larger the seed intensity necessary for locking. Since the lower branch of the S-shaped steady-state curves is always Hopf unstable for small seeding, one expects to observe dynamical regimes where locking and unlocking alternate in space and time. In comparison with purely temporal systems, the presence of transverse degrees of freedom elongates the locking region to lower values of the seeding intensity, as displayed in Figures 6.3.2 and 6.4.1 where stable hexagons are observed well into the region where plane wave solutions are unstable. As the seeding intensity is decreased, unlocking eventually takes place and stable patterns develop defects [39, 37] that induce first phase and then amplitude instabilities. The resulting regime corresponds to optical turbulence since one observes a sudden (exponential) decrease of the spatio-temporal correlation function [40]

$$C(\rho) = \frac{\text{Re}[\langle E(\mathbf{r}, t)E^*(\mathbf{r}', t) \rangle - \langle E(\mathbf{r}, t) \rangle \langle E^*(\mathbf{r}, t) \rangle]}{\text{Re}[\langle E(\mathbf{r}, t)E^*(\mathbf{r}, t) \rangle - \langle E(\mathbf{r}, t) \rangle \langle E^*(\mathbf{r}, t) \rangle]} \quad (6.51)$$

where  $\mathbf{r}$  and  $\mathbf{r}'$  identify separate positions on the transverse plane,  $\rho = |\mathbf{r} - \mathbf{r}'|$ , Re denotes the real part and  $\langle \cdot \rangle$  corresponds to temporal averages. Such behaviour is demonstrated in Figure 6.5.1 where the correlation function  $C(\rho)$  is calculated for the hexagonal pattern (dashed line), the turbulent regimes for  $|E_0|^2 = 2$  (solid line) and  $|E_0|^2 = 8$  (dot-dashed line). Fitting exponentials to the correlation functions shows that in the turbulent regimes the correlation length is reduced by at least a factor of six.

In the regime of optical turbulence, large variations of the SROPO intensity are observed in both space and time. In Figures 6.3.2 and 6.4.1 we display the range of variation of the SROPO intensity at a given time  $t$  at the onset of optical turbulence. The wide increase in the maximum SROPO intensity when changing the seed strength below the hexagon instability is clearly visible.

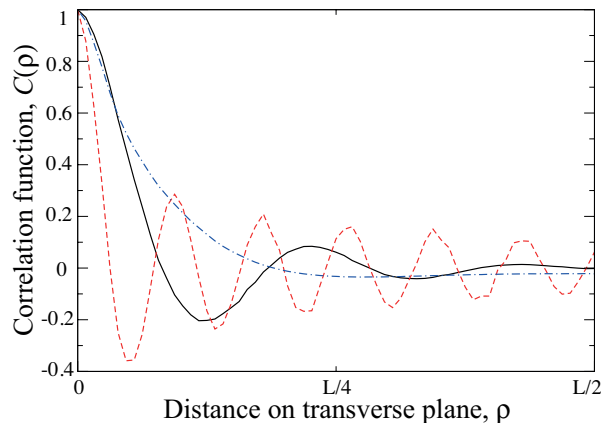


Figure 6.5.1: Spatial correlation function  $C(\rho)$  as in (6.51) for the hexagonal pattern (red dashed line,  $|E_0|^2 = 2$ ,  $\theta = -0.3$ ,  $|E_{IN}|^2 = 0.09$ ), optical turbulence close to threshold (black solid line,  $|E_0|^2 = 2$ ,  $\theta = -0.3$ ,  $|E_{IN}|^2 = 0.04$ ) and away from threshold (blue dot-dashed line,  $|E_0|^2 = 8$ ,  $\theta = -1.0$ ,  $|E_{IN}|^2 = 2.19$ ). All variables are dimensionless.

To characterize the regime of optical turbulence we have considered the temporal evolutions of the maximum SROPO intensity, the spatial average of the SROPO intensity and its standard deviation. As displayed in Figure 6.5.2, the spatial statistics is large enough to guarantee probability distributions of well defined averages and deviations. Larger values of the pump power increase the size of the probability distribution of the SROPO intensity and that of the fluctuations of its maximum value (compare Figures 6.5.2(a) and (b)). Such an increase results in the occurrence and propagation of transverse rogue waves.

Following the generally accepted definition of rogue waves in systems with injection [41], we plot the temporal evolution of

$$q(\tau) = I_{x,y}^{Max}(\tau) - \langle\langle I \rangle\rangle_{x,y,\tau} - 8\langle\langle \sigma \rangle\rangle_{x,y,\tau} \quad (6.52)$$

corresponding to transverse pulse maxima,  $I_{x,y}^{Max}$ , above or below a threshold given by the average value of the intensity,  $\langle\langle I \rangle\rangle_{x,y}$ , plus eight times the standard deviation,  $\sigma_{\tau,x,y}$ , of the SROPO intensity for the sinc<sup>2</sup> model in the dashed-dotted red lines of Figures 6.5.2(a) and (b). The presence of peaks of a rogue wave is signalled by positive values of  $q(\tau)$  [41]. With pump intensities a few times above threshold (Figure 6.5.2(a)), the rogue wave test fails ( $q(\tau)$  remains negative) and the optical turbulence generated by the unlocking of the seed laser and the SROPO is relatively mild. With larger values of the pump power, however, rogue waves are commonplace and affect the spatio-temporal evolution of the SROPO field for long durations of the temporal evolution (see Figure 6.5.2(b)). When comparing these results with those related to lasers with injections [41], we note that our simulations are fully spatio-temporal and show that the material dynamics, typical of semiconductor media, is not essential in the generation and maintenance of rogue waves during optical turbulence. The main mechanism underlying rogue waves in SROPOs is the absence of locking between master and slave devices leading to intermittent phase jumps. Full investigations of optical turbulence in injected (seeded) optical devices will be presented elsewhere.

Finally, we have studied the presence and stability of cavity solitons (CS) in SROPOs with a particular focus on localised structures induced by the sinc<sup>2</sup> nonlinearity, i.e. away from threshold

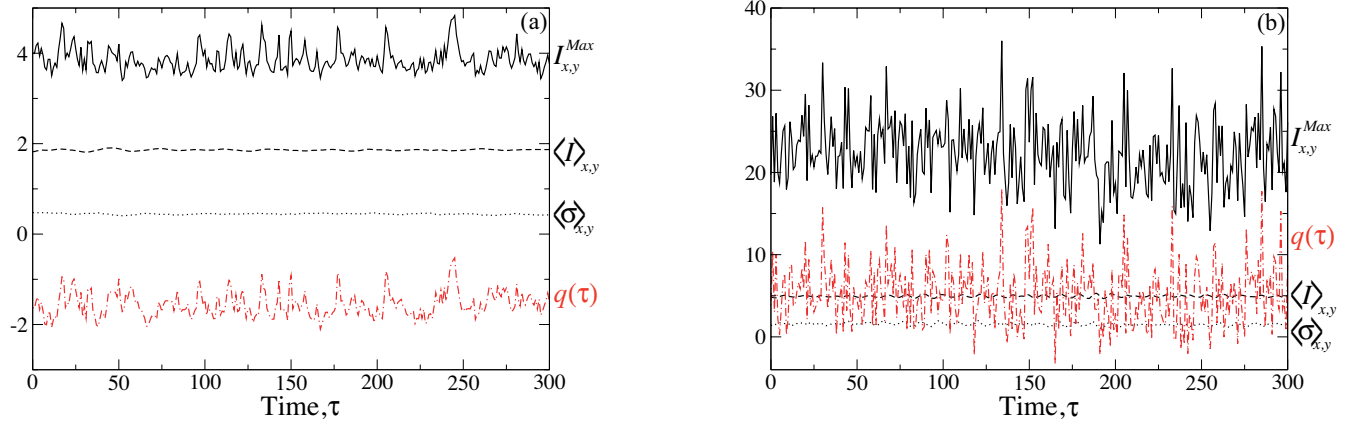


Figure 6.5.2: Temporal evolution of the maximum SROPO intensity (solid black line), the spatially averaged SROPO intensity (dashed black line), its standard deviation (dotted black line) and  $q(\tau)$  for the sinc<sup>2</sup> model (6.32). Parameters are (a)  $|E_0|^2 = 2$ ,  $\theta = -0.3$ ,  $|E_{IN}|^2 = 0.04$  and (b)  $|E_0|^2 = 8$ ,  $\theta = -1$ ,  $|E_{IN}|^2 = 2.19$ . All variables are dimensionless.

and with large seeding from an external laser. CS have been described in a variety of OPO devices without seeding from degenerate [42, 43, 44, 17] to non-degenerate triply resonant configurations [20, 45, 46]. CS in degenerate OPOs have also been numerically extended to include the presence of seeding [47]. In the case of the non-degenerate SROPOs investigated here, the resonance condition of SROPO operation rules out any CS in the absence of seeding. It is then important to stress that all CS solutions described in this section are due to the external seeding field and have no counterpart in the case of  $E_{IN} = 0$ .

Since we have introduced the sinc<sup>2</sup> nonlinearity in spatio-temporal models of SROPOs to describe self-organization when pump depletion and back-conversion take place, we focus here on CS in the limit of large pump powers. From Figures 6.4.1 and 6.4.3 we see that there are broad ranges of the parameter space where bistability between the plane wave solution and pattern structures is observed. For example, we find coexistent hexagons and homogeneous solutions for  $|E_{IN}|^2$  between 19.98 and 21.90 and coexistent honeycombs and homogeneous solutions for  $|E_{IN}|^2$  between 26.00 and 28.09. Note that we even observe tri-stability among plane waves, hexagons and rolls for  $|E_{IN}|^2$  between 21.25 and 21.90 and among plane waves, honeycombs and rolls for  $|E_{IN}|^2$  between 26.00 and 26.52. In the two wide regions of homogeneous-pattern bistability we have been able to locate single peak (bright) and single trough (dark) CS as shown for example in Figure 6.5.3 (a) and (d), respectively. The onset and nature of these CS are again similar to those observed in nascent optical bistability [4]. Together with the single unit bright and dark CS we have also found many multi-peak [48] and multi-trough localized structures that correspond to clusters of CS (also referred to as localized patterns [49]). A few examples of these bright and dark clusters are displayed in Figure 6.5.3. The range of existence of single unit CS and CS clusters is displayed in Figure 6.5.4. Snaking of both bright and dark CS is observed with stability branches of larger and larger clusters approaching the pattern stability lines in the parameter space (see Figure 6.5.4). The details of the bifurcations and of the number of branches of bright and dark CS for changing

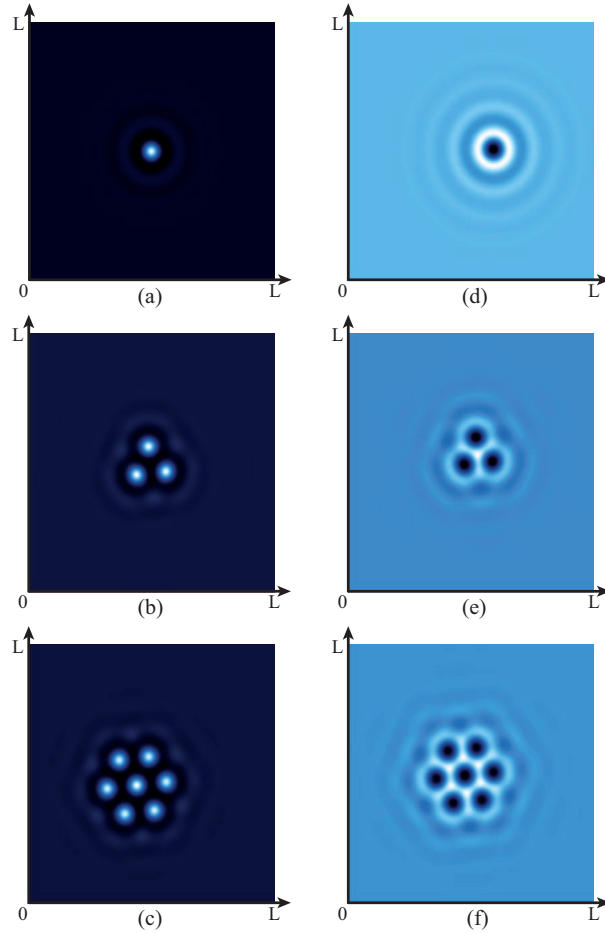


Figure 6.5.3: Stable bright (a)-(c) and dark (d)-(f) CS configurations of the SROPO model (6.32). Parameters are  $|E_0|^2 = 8$ ,  $\theta = -1$ ,  $|E_{IN}|^2 = 20.8$  for (a)-(c),  $|E_{IN}|^2 = 26.5$  for (d) and  $|E_{IN}|^2 = 27.1$  for (e)-(f). All variables are dimensionless.

$|E_0|^2$  are too long to be described here and will be the subject of future work.

## 6.6 Conclusions.

Self-organization and pattern formation in OPOs has been known for a number of years in degenerate [8] or doubly or triply resonant non-degenerate configurations [19, 20, 21]. The case of a widely non-degenerate SROPO has, however, been overlooked because of experimental limitations, now overcome, and the fact that off-resonance operation is inhibited because of its intrinsic tuneability. Here we have shown that under the action of a detuned injection close to the signal frequency, one can find an extremely rich variety of self-organized structures, from regular co-existing patterns to clusters of CS and even optical turbulence. In particular, we have derived mean field models for SROPOs with external seeding and shown that, away from threshold, cubic nonlinearities should be replaced by  $\text{sinc}^2$  terms. The  $\text{sinc}^2$  nonlinearity is capable of describing regimes of pump depletion and back-conversion. In these regimes, the external seeding generates hexagonal, roll and honeycomb patterns as well as bright and dark CS. Note that CS in SROPOs offer positional control associated to the generation of entangled photons with vastly different frequencies.

In contrast to laser systems, the fast material dynamics of  $\chi^{(2)}$  media makes a SROPO with

external seeding an ideal candidate for comparisons between theory and experiments of optical self-organization. The fast material dynamics is also beneficial to the investigation of spatio-temporal structures in the regime of short pulse generation where many of the results presented here can find useful extensions. These investigations together with the full characterization of the turbulent regimes are the subject of present research.

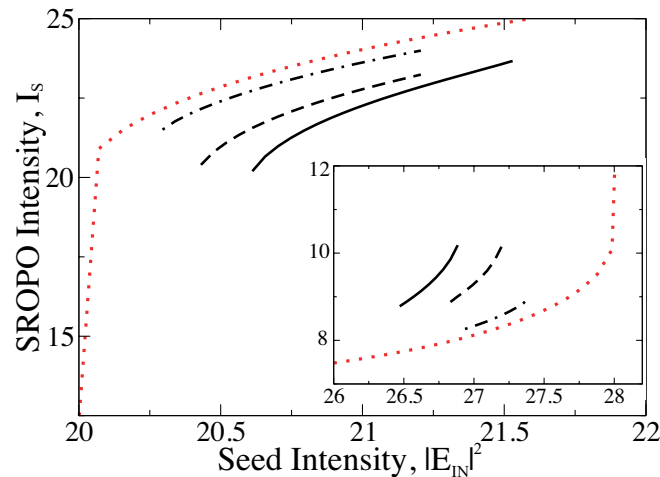


Figure 6.5.4: Stability range of clusters of CS for bright (main figure) and dark (inset) CS. Solid, dashed and dot-dashed black lines correspond to the maximum SROPO intensity in clusters of one, three and seven CS. The red dotted line corresponds to the maximum (minimum) intensity of the stable hexagonal (honeycomb) pattern in the main figure (inset). Parameters are  $|E_0|^2 = 8$  and  $\theta = -1$ . All variables are dimensionless.

## Bibliography

- [1] L. A. Lugiato and R. Lefever, Phys. Rev. Lett. **58**, 2209 (1987)
- [2] G. D'Alessandro and W. J. Firth, Phys. Rev. Lett. **66**, 2597 (1991)
- [3] N. N. Rosanov, A. V. Fedorov and G. V. Khodova, Phys. Stat. Sol. B **150**, 545 (1988); N. N. Rosanov, *Spatial Hysteresis and Optical Patterns* (Springer, Berlin, 2002)
- [4] M. Tlidi, P. Mandel and R. Lefever, Phys. Rev. Lett. **73**, 640 (1994)
- [5] W. J. Firth and A. J. Scroggie, Phys. Rev. Lett. **76**, 1623 (1996)
- [6] T. Ackemann, W. J. Firth and G.-L. Oppo, Adv. Atom. Mol. Opt. Phys. **57**, 323 (2009)
- [7] P. Grelu and N. Akhmediev, Nature Photonics **6**, 84 (2012)
- [8] G.-L. Oppo, M. Brambilla and L. A. Lugiato, Phys. Rev. A **49**, 2028 (1994)
- [9] G. J. de Valcarcel, K. Staliunas, E. Roldan and V. J. Sanchez-Morcillo, Phys. Rev. A **54**, 1609 (1996)
- [10] C. Etrich, U. Peschel and F. Lederer, Phys. Rev. E **56**, 4803 (1997)
- [11] P. Lodahl and M. Saffman, Phys. Rev. A **60**, 3251 (1999)
- [12] S. Ducci, N. Treps, A. Maitre and C. Fabre, Phys. Rev. A **64**, 023803 (2001).
- [13] M. Shelton and D. P. West, Opt. Express **9**, 16 (2001).
- [14] M. Peckus, K. Staliunas, M. Saffman, G. Sleky, V. Sirutkaitis, V. Smilgevicius and R. Grigonis, Opt. Commun. **251**, 165 (2005).
- [15] M. Peckus, K. Staliunas, Z. Nizauskaite and V. Sirutkaitis, Opt. Lett. **32**, 3014 (2007)
- [16] G.-L. Oppo, M. Brambilla, D. Camesasca, A. Gatti and L. A. Lugiato, J. Mod. Opt. **41**, 1151 (1994)
- [17] G.-L. Oppo, A. J. Scroggie and W. J. Firth, Phys. Rev. E **63**, 066209 (2001)

- 
- [18] K. Staliunas, J. Mod. Opt. **42**, 1261 (1995)
- [19] S. Longhi and A. Geraci, Phys. Rev. A **54**, 4581 (1996)
- [20] V. J. Sanchez-Morcillo, E. Roldan, G. J. de Valcarcel and K. Staliunas Phys. Rev. A **56**, 3237 (1997)
- [21] M. Santagiustina, E. Hernandez-Garcia, M. San-Miguel, A. J. Scroggie and G.-L. Oppo, Phys. Rev. E **65**, 036610 (2002)
- [22] S. T. Yang, R. C. Eckardt and R. L. Byer, Opt. Lett. **18**, 971 (1993)
- [23] W. R. Bosenberg, A. Drobshoff, J. I. Alexander, L. E. Meyers and R. L. Byer, Opt. Lett. **21**, 1336 (1996)
- [24] M. E. Klein, C. K. Laue, D.-H. Lee, K.-J. Boller and R. Wallenstein, Opt. Lett. **25**, 490 (2000)
- [25] A. Henderson and R. Stafford, Opt. Express **14**, 767 (2006)
- [26] L. B. Kreuzer, in Proceedings of the Joint Conference on Lasers and Opto-Electronics (Institution of Electrical and Radio Engineers, London, 1969), page 52
- [27] W. Brunner, R. Fischer and H. Paul, Ann. Phys. (Leipzig) **30**, 299 (1973).
- [28] W. Brunner and H. Paul, Prog. Opt. **15**, 1 (1977).
- [29] E. Rosencher and C. Fabre, J. Opt. Soc. Am. B **19**, 1107 (2002)
- [30] C. R. Phillips and M. M. Fejer, J. Opt. Soc. Am. B **27**, 2687 (2010)
- [31] G.-L. Oppo, J. Math. Chem. **45**, 95 (2009)
- [32] R. W. Boyd, *Nonlinear Optics*, (Academic Press, New York, 2008)
- [33] D. Cuozzo and G.-L. Oppo, Phys. Rev. A **84**, 043810 (2011)
- [34] F. Prati, G. Tissoni, C. McIntyre and G.-L. Oppo, Eur. Phys. J. D **59**, 139 (2010)
- [35] S. Ciliberto, P. Coulet, J. Lega, E. Pampaloni and C. Perez-Garcia, Phys. Rev. Lett. **65**, 2370 (1990)
- [36] P. Coulet and K. Emilsson, Physica A **188**, 190 (1992)
- [37] P. Coulet and K. Emilsson, Physica D **61**, 119 (1992)
- [38] G.-L. Oppo, A. Politi, G. L. Lippi and F. T. Arecchi, Phys. Rev. A **34**, 4000 (1986)
- [39] Q. Ouyang and H. L. Swinney, Chaos **1**, 411 (1991)
- [40] G. K. Harkness, J. C. Lega and G.-L. Oppo, Chaos, Solitons and Fractals **4**, 1519 (1994)
- [41] C. Bonatto, M. Feyereisen, S. Barland, M. Giudici, C. Masoller, J. R. Rios Leite and J. R. Tredicce, Phys. Rev. Lett. **107**, 053901 (2011); J. Zamora-Munt, B. Garbin, S. Barland, M. Giudici, J. R. Rios Leite, C. Masoller and J. R. Tredicce, Phys. Rev. A **87**, 035802 (2013).

- 
- [42] S. Longhi, Phys. Scr. **56**, 611 (1997)
  - [43] K. Staliunas and V. J. Sanchez-Morcillo Opt. Comm. **139**, 306 (1997)
  - [44] G.-L. Oppo, A. J. Scroggie and W. J. Firth J. Opt. B **1**, 133 (1999)
  - [45] S. Longhi, Opt. Comm. **149**, 335 (1998)
  - [46] G. J. de Valcarcel, E. Roldan and K. Staliunas Opt. Comm. **181**, 207 (2000)
  - [47] K. Staliunas and V. J. Sanchez-Morcillo, arXiv:nlin /0002029 (2000)
  - [48] J. M. McSloy, W. J. Firth, G. K. Harkness and G.-L. Oppo, Phys. Rev. E **66**, 046606 (2002)
  - [49] D. J. B. Lloyd, B. Sandstede, D. Avitabile and A. R. Champneys, SIAM J. App. Dyn. Syst. **7**, 1049 (2008)

### 7.0.1 Achievements of the thesis

The subject matter of this Thesis is the study of Singly Resonant Optical Parametric Oscillators in both the below-threshold and above-threshold regimes (Chapters 4-6) as sources of non classical radiation and as sources of complex spatial structures via self-organization. In Chapter 4 we have applied the input output theory of [1] to the study of quantum fluctuations of singly resonant optical parametric oscillators. The model has been used to calculate intensity and quadrature squeezing spectra. We have shown that below the threshold of oscillation the fluctuations in the light outside the cavity at the frequencies of the signal and the idler fields are squeezed below the shot noise as much as in the doubly resonant case. We have also shown that the signal and the idler fields are entangled over a wide range of pump parameter values in the SROPO by using the Simon-Duan *et al.* criterion of state separability.

One major difference of the SROPO from the doubly resonant case is that we observe an unexpected dependence of the intensity-difference spectrum on the pump parameter, leading to a narrowing of the spectral lines as the threshold of oscillation is approached. An analogous dependence of the quadrature spectrum on the pump parameter is also found. A peculiar feature of singly resonant configurations is that the narrowing of the spectral lines does not affect the squeezing minimum, which can reach values similar to those of the doubly resonant case as threshold is approached. Since the singly resonant case is one of the simplest OPO configurations to realize, and since there is no difference in the squeezing properties of the light coming from this device respect to the doubly resonant cavity, we conclude that the singly resonant configuration could be an ideal candidate for the realization of two-color entangled light in quantum information processes.

In Chapter 5 we have introduced the phenomena of giant sub-threshold amplification in the contest of synchronously pumped parametric oscillator. We have shown that a crucial ingredient for giant amplification is that the device is making it operate in the singly resonant strongly non-degenerate configuration. As a matter of fact the phenomena do not survive the doubly resonant and frequency degenerate regime. We have derived a quantum picture of this situation and we have shown that quantum noise of the magnitude of  $(10^{-8} - 10^{-9}) V/m$  can be magnified of a factor of  $10^{10}$  thus becoming macroscopic even below the threshold of oscillation for the SPOPO. The question which remains unanswered is if this quantum noise-driven macroscopic signal keeps all the quantum properties typical of SPOPO below threshold, i.e. quantum squeezing and entanglement. In this case it would be possible to have a macroscopic quantum squeezing and entanglement using

this device in the giant amplification regime.

In Chapter 6 we have studied self-organization and pattern formation in OPOs which has been known for a number of years in degenerate [2] or doubly or triply resonant non-degenerate configurations [3, 4, 5]. The case of a widely non-degenerate SROPO has, however, been overlooked because of experimental limitations, now overcome, and the fact that off-resonance operation is inhibited because of its intrinsic tuneability. We have shown that under the action of a detuned injection close to the signal frequency, one can find an extremely rich variety of self-organized structures, from regular co-existing patterns to clusters of CS and even optical turbulence. In particular, we have derived mean field models for SROPOs with external seeding and shown that, away from threshold, cubic nonlinearities should be replaced by  $\text{sinc}^2$  terms. The  $\text{sinc}^2$  nonlinearity is capable of describing regimes of pump depletion and back-conversion. In these regimes, the external seeding generates hexagonal, roll and honeycomb patterns as well as bright and dark CS. Note that CS in SROPOs offer positional control associated to the generation of entangled photons with vastly different frequencies.

In contrast to laser systems, the fast material dynamics of  $\chi^{(2)}$  media makes a SROPO with external seeding an ideal candidate for comparisons between theory and experiments of optical self-organization. The fast material dynamics is also beneficial to the investigation of spatio-temporal structures in the regime of short pulse generation where many of the results presented here can find useful extensions. These investigations together with the full characterization of the turbulent regimes will be the subject of future communications.

## 7.0.2 Future work

The research work presented in this thesis has focused on SROPO configurations, both below and above threshold, when pumped with a homogeneous or single Gaussian mode pump field. A lot of work has been done in recent years about states of the electromagnetic field containing Optical Angular Momentum (OAM) [6]. One very interesting extension of our work would be to study the effect of OAM structures in OPOs. A first step in this direction was made in [7] where pumps with OAM were studied in the degenerate Type-I OPO case. It would be natural to see what happens to such configuration in the SROPO case. For example would the signal and idler field share the input OAM as in the degenerate case or would the OAM affect the two output field differently. In the latter case, what percentage of OAM would affect the signal and the idler fields, respectively? Is the process of OAM distribution a statistical process? If so, with what distribution?

The large variety of SROPO models introduced and investigated in this thesis allows also for novel and intriguing question. What happens when the SROPO is pumped and seeded with beams carrying OAM? What variations to the optical turbulence regimes would be observed? How the OAM beams interact in the down-conversion crystal when they affect different regions of the transverse space? What would happen to a SROPO pumped by pulsed beams carrying OAM?

These considerations can be successfully extended to the quantum regime where, for example, entanglement and squeezing with OAM has been recently observed [8] in a spatially non-degenerate, frequency-degenerate OPO. In these experiments small seeding at the signal frequency were used for stabilisation purposes. The first natural extension of our work would be to find out if squeezing and entanglement survive to the non-degenerate SROPO case. Secondly one would be able to use our results to investigate how OAM on the pump and/or seeding fields affects such quantum entanglement and how the control of the input OAM can be used in quantum information processes such as secure key distribution in quantum cryptography.

We believe that the re-discovered interest in the fundamentals and application of OPOs will

benefit from the achievements of the work presented in this thesis since SROPO configurations are becoming more and more commonplace due to the amazing developments of material science and quasi-phase matched crystals.

## Bibliography

- [1] M. J. Collett and C. W. Gardiner, *Phys. Rev. A* **30**, 1386 (1984).
- [2] G.-L. Oppo, M. Brambilla, D. Camesasca, A. Gatti and L. A. Lugiato, *J. Mod. Opt.* **41**, 1151 (1994).
- [3] S. Longhi and A. Geraci, *Phys. Rev. A* **54**, 4581 (1996).
- [4] V. J. Sanchez-Morcillo, E. Roldan, G. J. de Valcarcel and K. Staliunas *Phys. Rev. A* **56**, 3237 (1997).
- [5] M. Santagiustina, E. Hernandez-Garcia, M. San-Miguel, A. J. Scroggie and G.-L. Oppo, *Phys. Rev. E* **65**, 036610 (2002).
- [6] A. M. Yao and M. J. Padgett, *Adv. Opt. Phot.* **3**, 161 (2011).
- [7] G.-L. Oppo, A. J. Scroggie and W. J. Firth, *Phys. Rev. E* **63**, 066209 (2001).
- [8] M. Lassen, G. Leuchs, and U. L. Andersen, *Phys. Rev. Lett.* **102**, 163602 (2009).